Universität Zürich[UZH]

Department of Geography

Understanding diurnal changes in land surface temperature trends using MODIS and IMIS data

GEO 511 Master's Thesis

Author: Ali Sheib, 21-749-197

Supervised by: Dr. Hendrik Wulf

Faculty representative: Prof. Dr. Livia Piermattei

31.01.2025

University of Zurich[UZH]

GEO 511
Master Thesis
April 22, 2025

Understanding Diurnal Changes In Land Surface Temperature Using MODIS and IMIS Data

Ali SHEIB
21-749-197

Supervised by:
Dr. Hendrik WULF

Faculty representative:
Prof. Dr. Livia PIERMATTEI

Remote Sensing Laboratories
Department of Geography
University of Zurich

Abstract

This study investigates the credibility of using land surface temperature (LST) data retrieved from MODIS (Moderate Resolution Imaging Spectroradiometer) satellite images, and this requires comparing the acquired MODIS data with data from ground-based stations named as Intercantonal Measurement and Information System (IMIS). The study was applied for Swiss Alps covering the period between 2000 and 2023 including four MODIS observation times (i.e., MOD21A1D, MOD21A1N, MYD21A1D, and MYD21A1N). The comparative analysis based mainly on a Harmonic Regression Model which combines harmonic and linear regressions, and enables calculating the trends for both data sources. Therefore, analytical approaches were applied to support the comparison and data analysis. Five research questions were primarily identified as a reference for the achievement of the study. In order to compare the actual measurements, plots were created to determine the median absolute deviation "MAD-1", R-squared, slope and mean deviation values. While, comparison between the data means was made using the mean absolute difference "MAD-2" and Pearson's correlation values, and a compatibility was found between both data with a preference for nighttime. For the comparison of trends, it was performed by comparing the trends of the two data at each specific hour of the day during the four MODIS observation times using the MAD-2 and Pearson's correlation values. The comparison was also made between the mean of the trend data of both datasets using the mean absolute error (MAE) and standard deviation values. Determining the most representative observation time required to compare IMIS trend data at each of the MODIS observation times with the overall trends, the comparison was made using MAD-2 and Pearson's correlation values. It revealed that MOD21A1D observation time has the best representativeness of trends. In order to investigate factors resulting changes in data; however, changes in IMIS data was compared with the elevation and aspect of ground stations; while MODIS data was compared with the view angle of satellites' sensors. Therefore, elevation does not show any noticeable effect on IMIS data, except limited LST trend means which is almost low (< 0.05) at altitudes above 2000 m. This is also the case for the aspect where no relationship with IMIS trends has been reported. Besides, an effect of the view angle on MODIS measurements was noticed, but it differs between various observation times. In addition, Landsat 5, 7, and 8 observation times were utilized for comparison with the representativeness of MODIS observation times; especially that Landsat images are not acquired at nighttime which is a limitation effecting its accuracy. This study performed a comprehensive analytical approach that facilitates understanding the relation between MODIS LST and IMIS data and trends. It supports adopting MODIS data for calculating LST which is significant for future researches on hydroclimate analysis notably MODIS is a daily source of LST data.

Contents

Abbreviations

ACPs	Annual Cycle Parameters ATC Annual Temperature Cycle
AVHRR	Advanced Very High-Resolution Radiometer
ASTER	The Advanced Space borne Thermal Emission and Reflection Radiometer
AWV	Atmospheric Water Vapor
CF	Cloud Fraction
DEM	Digital Elevation Model
DSM	Digital Surface Model
EWSS	Early Warning Systems
FEWS NET	Famine Early Warning Systems Network
GCOS	Global Climate Observing System
GHGs	Greenhouse Gases
GEE	Google Earth Engine
IMIS	Intercantonal Measuring and Information System
IFOV	Instantaneous Field of View
IR	Infrared
LST	Land Surface Temperature
LCU	Land Cover/ Use
MAD-1	Median Absolute Deviation
MAD-2	Mean Absolute Difference
MODIS	Moderate Resolution Imaging Spectroradiometer
MAE	Mean Absolute Error
MW	Microwave
NASA	National Aeronautics and Space Administration
PC	Pearson's Comparison
RMSE	Root Mean Square Error
SLF	Swiss Federal Institute for Forest, Snow and Landscape Research WSL
SEVIRI	Spinning Enhanced Visible Infra-Red Imager
TES	Temperature Emissivity Separation
TIR	Thermal Infrared
Ta	Air Temperature
USGS	United States Geological Survey
WVS	Water Vapor Scaling

List of Figures

List of Tables

1 Introduction

1.1 Land Surface Temperature

Land Surface Temperature (LST) is the emission of thermal radiance from land surface as a result of the incoming solar energy that heats the ground surface or the canopy in vegetated areas. It is a major component of atmosphere and biosphere, and it relates to surface energy and water balance that affects the entire ecosystem at local and global scale. Even though, ground-based stations are used to measure the temperature of any single site, yet for a comprehensive assessment (i.e., large areal coverage), LST is measured by remote sensing where space-based thermal infrared (TIR) sensors are used. In this respect, LST is one of the most important Earth System Data Records by National Aeronautics and Space Administration (NASA) (King, 1999) and other space agencies (e.g., ESA, CSA, JAXA, etc.) especially LST is a key component of the Earth's energy balance system, affecting the energy exchange in the Earth's landscapes (Dimyati et al., 2024). Several studies utilized LST for integrated analysis of surface energy balance that extends to the study of urban heat islands, microclimate, surface soil moisture, evapotranspiration, climate change, etc. (Hidalgo and Arco, 2022). Studying LST has been recently involved in several research themes. For example, it predicts mortality due to chronic obstructive pulmonary disease (Mohammadi et al., 2025); the average LST increase in winter season poses a significant threat to winter agricultural productivity (Al-Faisal et al., 2021); LST also resulted bad effect on the land cover/use (LCU) in Central India with increased evapotranspiration and decreased green land and expansion of barren land (Moharir et al., 2025). In addition, LST is linked with the air temperature which is in turn increase the melting rate of snowpack and then increasing the runoff, sea level rise, and many other consequences. Land surface temperature has a wide relevance whether to urban and natural environments; and thus it is reversibly affected by Earth's surface components (e.g., urban areas water bodies, forests, etc.). In this respect, notably that urban areas are unique socio-economic and ecological environments with heterogeneous mixture of impervious surfaces and many other land use-land cover (LCU) classes (Dutta et al., 2022). For example, increased urban developments and LCU changes in Dammam Region, of Saudi Arabia, resulted short-and long-term consequences including increase in LST of urbanized cities in this region (Rahman et al., 2017). While, LST has less impact in natural environments with bare rocks and soil are dominant; and therefore, LST impact can extend to soil moistures, vegetation health, shallow groundwater, etc.; however, LST has less impact on soil moisture and canopy and wherever forests are dominant.

1.2 Satellite Thermal Sensors and Their Accuracy

Satellite thermal sensors measure the thermal radiation emitted from the Earth's surface and remote sensing techniques allow the estimation of LST at a spatially averaged pixel scale. Thus, spatial and temporal LST trends can be extracted using a number of satellite images with thermal bands (e.g., MODIS, Landsat, etc.), and this also enables studying their influencing factors such as elevation, cloud fraction (CF), atmospheric water vapor (AWV), and snowpack area. Thermal infrared data has been extensively used to retrieve LST products for a range of satellites, including for example AVHRR, MODIS, Landsat, ASTER, and SEVERI (Wang et al., 2015). The retrieval of LST from satellite data is a complex process influenced by a multitude of factors, from surface properties (e.g., emissivity, albedo, topography, etc.) to atmospheric conditions (e.g., water vapor, air temperature, etc.) and observation characteristics including viewing geometries and observations time (Owe et al., 2008)). However, most of these factors can be addressed to minimize error ratio; and then, they are validated using ground-based temperature data, such as in this study where MODIS LST measurements will be compared with Intercantonal Measurement and Information System (IMIS). Yet, there are many issues which are still questionable including mainly the representation of various MODIS LST trends to the overall trend for long time period and exact identification of the influencing (i.e., derivers) factors and their level of impact. To understand surface energy exchange, vegetation health, water stress, and urban heat island effects, it is important to improve the knowledge of diurnal LST spatial and temporal trends that capture the day-night variations that occur in the data. Recently, many studies have been performed to figure the impact of increased or decreased LST on physical processes and Earth's surface components, such as the variation of LST and wetlands (Muro et al., 2018), agricultural pastoral (Wei et al., 2021); mangrove forest (Thakur et al., 2021) and LCU changes (Nega and Balew, 2022). In this regard, diurnal LST trends are always established to figure out short-term changes on the environment and human life. Diurnal LST has been recently involved in the Early Warning Systems (EWSs), such as Famine Early Warning Systems Network (FEWS NET) extended by United States Geological Survey (USGS). It is also used for supporting climatic data where continuous records are lacking, or for regions with rugged topography and absent meteorological stations. Past and future trends of diurnal LST have been also correlated with vegetate cover (Wang et al., 2023).

For multiple acquisitions within a day, multiple sets of Annual Cycle Parameters (ACPs) can be generated, i.e., ACPs related to morning, noon, afternoon, or night hours (Sismanidis et al., 2016). Thus, estimations of regional temperature dynamics are provided by LST trends including heat waves and changes in diurnal temperature, making it a significant parameter in climate studies. Moreover, the LST is considered an essential climate variable by the Global Climate Observing System (GCOS) for the assessment of land surface and land-atmosphere exchange processes, as well as for providing observations of surface temperature changes at global and regional scales (Trenberth et al., 2013). In rugged topography areas and vulnerable ecosystems such as the Swiss Alps, there is usually a recognized response to temperature fluctuations that could be detected by LST trends, where warming and cooling clearly affect snow-melt rates and hydrological cycles.

The accuracy of measured LST remains a challenge; and thus, robust analyses are performed to improve the accuracy and reduce disparities of data derived from different thermal satellites images (Liu et al., 2007; Yao et al., 2021; Guo et al., 2022; Abunnasr and Mhawej, 2023; Roy et al., 2025). To address the problem of LST accuracy in the retrieved thermal data from satellite images, a comparative analysis with data obtained from ground-based stations will be applied, where the IMIS ground stations provide granular temperature data that is able to capture local variations missed by satellite observations. IMIS can serve as a reference data for quantification and validation of remote-sensing LST products. In particular, LST validation typically involves matching the retrieved LST datasets obtained from various remote sensing sensors with multiple years of in-situ data from distributed stations representing different land cover types (Martin et al., 2019). This represents the concept upon which the idea of this study has been built to quantify LST trends of the Swiss Alps using MODIS LST data. For Swiss Alps, there are several studies applied where they utilized satellite images for identifying different themes and calculate their variables. For example, Fontana et al., 2008 used AVHRR, VEGETATION, and MODIS NDVI time Series for grassland phenology in Swiss Alps where IMIS ground-based data were utilized for validation; while, Foppa and Seiz, 2012 processed MODIS data to determine the variations in snow cover on Swiss Alps. Besides, Tom et al., 2022 investigated the trends in Swiss Mountain Lakes using MODIS data. Moreover, Gök et al., 2024 investigated the LST in Swiss Alps using Landsat images. Even though, the first three studies used MODIS data, but they did not investigate LST, while the study elaborated by Gök et al., 2024; analyzed LST, but MODIS LST was not utilized. Therefore, the novelty of the current study implies the adoption of MODIS data for LST calculation.; especially that MODIS data can be retrieved on daily basis which is not the case for landsat images (i.e., 16 days' revisit time).

1.3 Detection of LST

LST is detected using either ground-based meteorological stations/or lately by the processing of satellite images for more comprehensive assessment. Each of LST measuring instruments has both advantages and disadvantages. Ground-based stations can precisely measure LST, but the measurements represent a unique site and the installation of several ground stations is necessary to create a uniform distribution and this is always a challenge notably in rugged and remote regions. Besides, LST derived from satellite images lack to the accuracy in many instances, plus the challenges created from cloud cover, fixed sensor characteristics and many other issues. Therefore, the integration of both datasets would be more reliable and useful. For ground-based, airborne and space borne remote sensing instruments, LST is the aggregated radiometric surface temperature of the ensemble of components within the sensor field of view. In both instruments, LST is determined from thermal emission at wavelengths in either infrared (IR) or microwave (MW) atmospheric windows. Yet, the advantages of using LST data are still confronting with many gaps which can be summarized as follows:

1. Confusion often exists between LST and air temperature and their impact on several land

processes (e.g., infiltration, evaporation, etc.) and the related sectors (e.g., water, agriculture, etc.); and this must be given concern by researchers.

2. Spatial resolution sometimes results imprecise measurements (e.g., MODIS with 250 m; AVHRR with 1.1 km); while higher spatial resolution images (e.g., Landsat with 30 m) do not acquire night LST data and this represents a limitation effecting the accuracy of LST.
3. Validation of datasets retrieved from LST is a must, but this is often hindered by the lack of ground-based stations.
4. Clouds sometimes create problem in retrieving complete scenes for LST. However, robust methods for filling the gaps in MODIS are applied (e.g., Yao et al., 2021).
5. Rugged topography may cause erroneous results, and this can be also resolved by applying topographic effect correction (Zhu et al., 2021).
6. There are various technical challenges (e.g., viewing angle) which also influences the accuracy of retrieved LST data.

1.4 Motivation and Research Objectives

Recently, measuring LST has been widely used in many studies and research projects to investigate the linkage between LST and other terrain and LCU components of such surface water bodies, etc. (Pal and Ziaul, 2017; Balas, 2023). LST has been lately adopted as a clue for evidencing climate change and to investigate the relationship between maximum thermal anomalies, heat waves (Toomey et al., 2011; Abbas et al., 2021), and LST is also tackled to determine the influenced terrestrial and marine ecosystems, and many hydrological processes such as evaporation, snowmelt rates (Yang et al., 2015), and it is used to study vegetation health, droughts and forest fires (Thakur et al., 2023; Zhao et al., 2021; Veraverbeke et al., 2012). The aforementioned applications of LST make it a major climatic variable that can be integrated in different themes, and this by itself a motivation to focus on investigation of LST retrieve from various instruments in order to reach the most creditable, accurate and validated results. Space-based instruments are significant to acquire consequent LST data (example in figure 1.1); however, there is uncertainty in quantifying LST, with a special emphasis to those obtained from remote sensing sensors, and this has led to errors in performing various assessments for the investigated climatic and hydrological processes and even for urban heat fluxes. Therefore, a precise quantification is needed to improve the accuracy of space-based LST-and validate it with LST measured by ground stations.

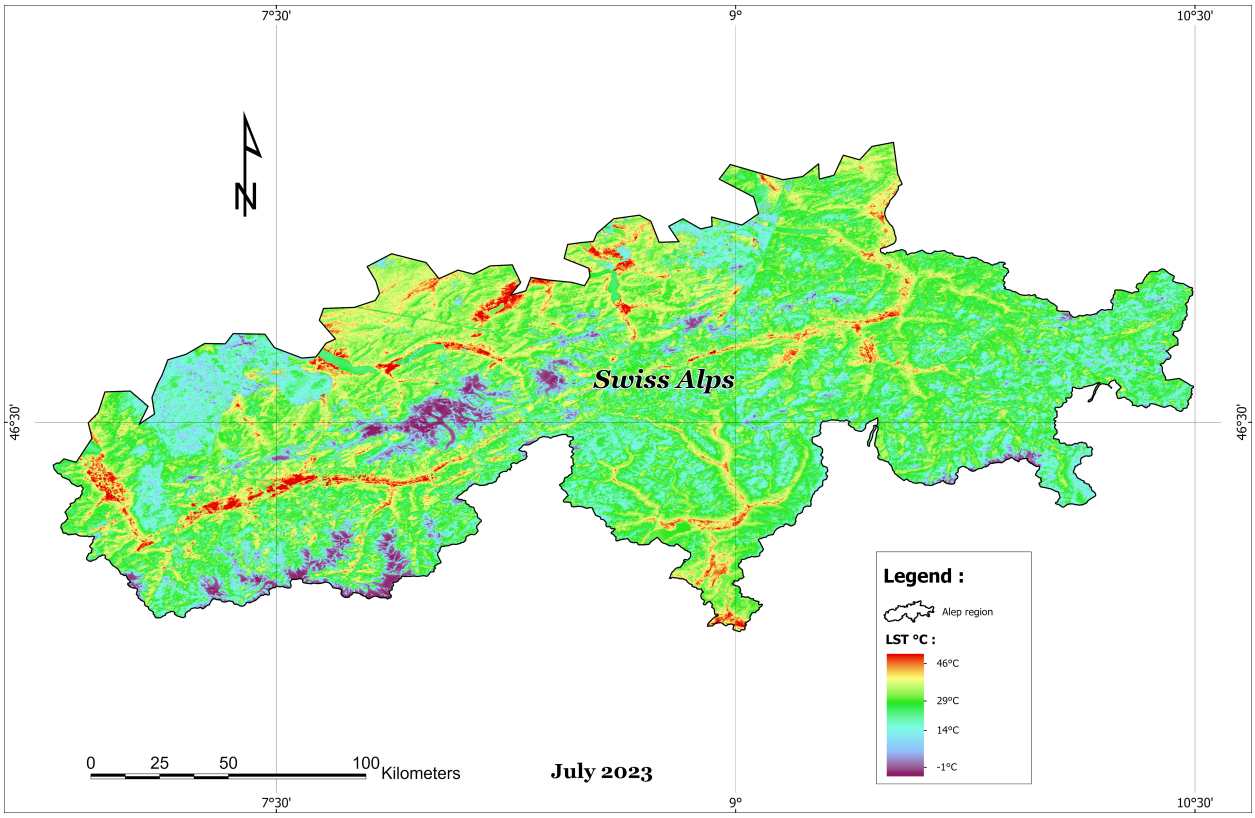

Figure 1.1: Example showing MODIS LST maps for Swiss Alps. It is a useful tool for monitoring and LST assessment, but the credibility of such maps can be reached if the results are compared with ground-based data (i.e., IMIS).

As per figure 1.1 with a comprehensive LST observation, it still requires to be validated by IMIS ground stations and this is the main objective of this study. It aims to understand if IMIS data can also validate MODIS LST trends and to what extent these trends at different times represent the overall trend in LST. The causes of the different LST trends at different time periods will be investigated. Finally, the implications of the MODIS validation results for the analysis of Landsat LST measurements will be analyzed. This study contributes to the understanding of the temporal aspect of LST trends in the Swiss Alpine Region. The context of this study implies with the following questions:

- RQ1: How well do MODIS LST measurements correspond to IMIS ground stations measurements at different observation times in the Swiss Alps?
- RQ2: How could IMIS ground station observations be used to validate MODIS LST trends at different observation times in the Swiss Alps?
- RQ3: To what extent do LST trends at different observation times represent the overall trend at all times?
- RQ4: What causes different LST trends at different observation times?
- RQ5: What are the implications of MODIS comparison results for the accuracy of Landsat LST observation times?

In order to answer these questions, this study will provide a comprehensive approach of data analysis that is capable of fulfilling the objectives of the study and suggest some implications responsible for the improvement of satellite LST data retrieval.

2 Study Area

The study area (Figure 2.1) represents the mountainous Alpine Region of Switzerland, referred to as the "Swiss Alps ", where it covers 2/3 of Switzerland territory with an area of about 27000 km^2. It is characterized by a mountainous and rugged topography that extends across the width of Switzerland from Lake Geneva in the west to the Austrian border in the east, with several mountain peaks such as Monte Rosa (4,634 m) and Liskamm (4,527 m).

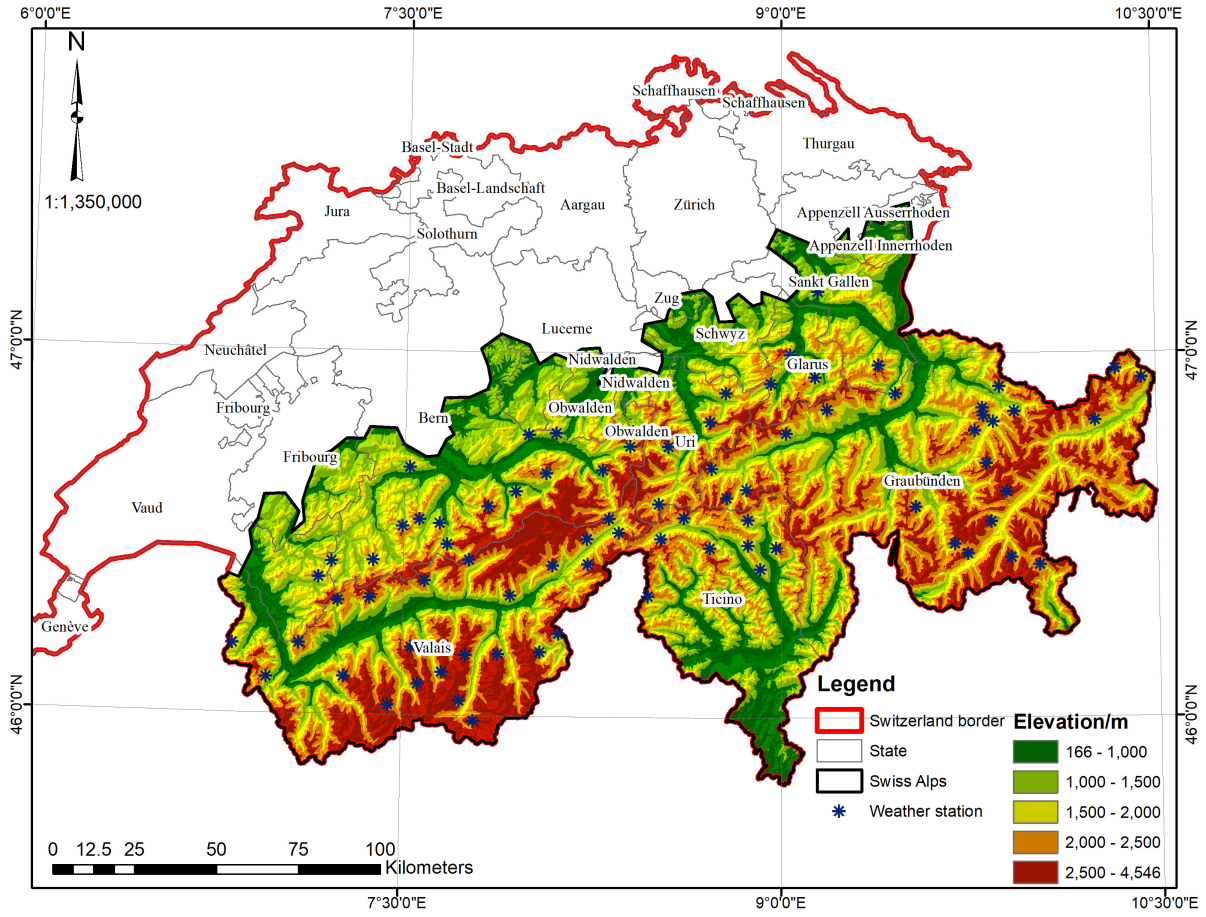

Figure 2.1: Map for the study area showing the variations in elevation in the Swiss Alps in addition to the locations of the 80 IMIS stations that are used for IMIS LST data retrieval

The availability of long time series data from ground-based meteorological stations (i.e., IMIS) for the Swiss Alps is the main reason for the selection of this area; in particular, it gives the opportu-

nity to benefit from the available data sets over long time periods (i.e., 2000-2023), which serves the objective of this study. Moreover, the terrain of the Swiss Alps motivated the selection of this area for study; especially that rugged terrain is considered as "topography effect", with high altitude mountains affects the accuracy of data acquired by satellite imagery. Therefore, the topographic effect creates ambiguity among the components of the satellite image scene, causing confusion in accurately determining the categories of LST, LCU, topographic orientation, etc.

3 Data Sources and Materials

In this study, data required for analysis includes two main sources; the ground-based stations and space-based instruments where the data retrieved from both sources will be compared in order to reach space-based validated data with optimal accuracy.

3.1 Inter-cantonal Measurement and Information System (IMIS) data

There are 198 stations that form the Intercantonal Measurement and Information System (IMIS). They are almost located on Jura Region and the Swiss Alps, and they are usually found above the tree line, mainly between 2000 and 3000 m. These stations are continuously recording every half hour. The majority of IMIS stations, which give local safety authorities vital information for public safety in communities and on roads, are situated close to avalanche-prone areas that could cause significant damage. Additionally, avalanche warning service of the Swiss Federal Institute for Forest, Snow and Landscape Research(WSL) utilizes these stations for research and snow-hydrological purposes. IMIS instruments also contain wind and snow dataset which are responsible for the weather measurements to determine the avalanche threat, are often located next to each other (Measurement and IMIS, 2023).

3.1.1 Main Data

For validation purpose between MODIS satellite and ground-based data, comprehensive records from meteorological ground stations must be available with a coverage for the entire period of the retrieved satellite images. For the Swiss Alps, not all (i.e., 198) IMIS stations are functional, and only 142 automatic stations have been consequently installed that cover a total of 28 year. They are producing data on a daily basis, and the measurements are taken every 30 minutes. However, there are only 80 considered stations (out of 142), since they cover the whole studied time span between 2000 and 2023 that coincide with the time-retrieval of MODIS images (Figure 3.1).

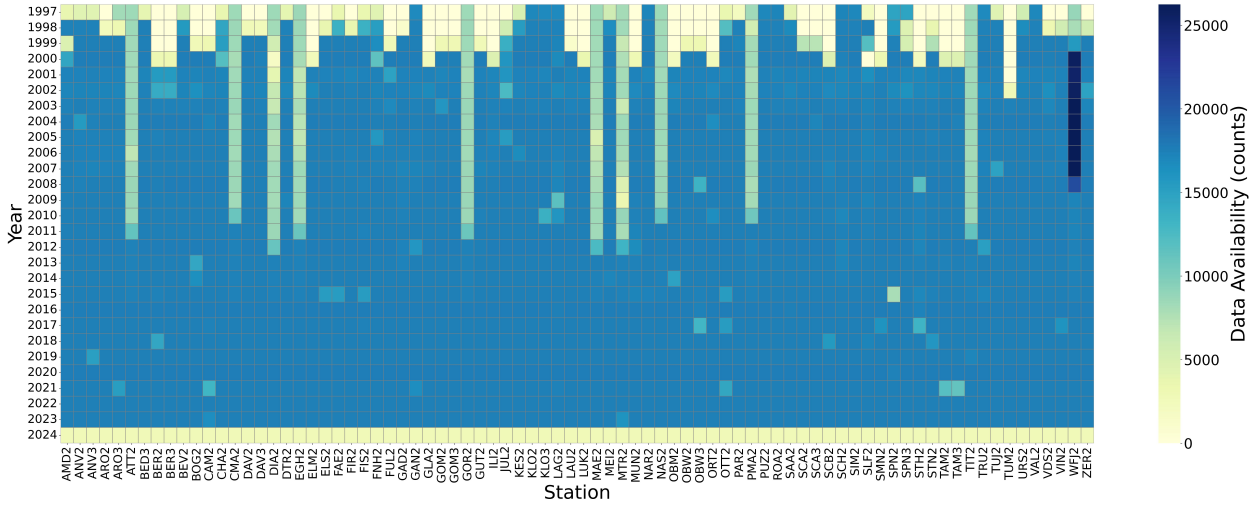

Figure 3.1: Color scale visualization showing the yearly availability of IMIS LST data covered the used stations.

3.1.2 Coordinates and Elevation Data

In order to characterize terrain variations of the 80 filtered stations, coordinates and elevation of the adopted 80 IMIS ground stations were graphically illustrated. The estimated average elevation of all stations is about 2288 m. This is also used for understanding the existed variations where LST data will be acquired. Thus, coordinates and elevation, in addition to other relevant information (e.g., climatic zone of each station, the real names and abbreviations of the stations) were provided by the SLF as metadata of the stations.

3.2 Satellite data

Daily MODIS LST datasets were retrieved at 1 km pixel resolution using the Temperature/Emissivity Separation (TES) algorithm, a physics-based algorithm that dynamically retrieves both LST and spectral emissivity simultaneously from MODIS TIR of bands 29, 31, and 32. The TES algorithm is combined with an improved Water Vapor Scaling (WVS) atmospheric correction scheme to stabilize the retrieval under warm and humid conditions. The Day/Night algorithm retrieves day and night LSTs and surface emissivities from pairs of day and night MODIS observations in seven TIR bands. The product consists of LSTs, quality assessment, observation time, view angle, and emissivities. There are two MODIS datasets retrieved for this study (Table 3.1). These are

1. MODIS/061/MOD21A1.V6.1 which is derived from MODIS-Terra satellite, which provides daily LST and emissivity values in a 1-kilometer spatial resolution.
2. MODIS/061/MYD21A1.V6.1, which is almost similar to the previous one, but it is retrieved by the MODIS-Aqua satellite.

MODIS-Terra satellite provides ascending data in the morning and descending data in the afternoon, while Aqua satellite provides descending data in the morning and ascending data in

the afternoon. Both products can be retrieved for free from Google Earth Engine (GEE) datasets (https://developers.google.com/earth-engine/datasets/catalog/modis).

Table 3.1: Characteristics of both MODIS products. Terra satellite provides ascending data in the morning and descending data in the afternoon, while Aqua satellite provides descending data in the morning and ascending data in the afternoon. Both products can be retrieved for free from Google Earth Engine (GEE) datasets (https://developers.google.com/earth-engine/datasets/catalog/modis).

Characteristic	**MOD21A1 (Terra)**	**MYD21A1 (Aqua)**
Satellite	Terra	Aqua
Spatial Resolution	1 km	1 km
Datatype	LST and Emissivity	LST and Emissivity
Observation Times	Ascending morning: 10:49 ± 0:29 Descending afternoon: 21:38 ± 0:29	Descending morning: 12:45 ± 0:28 Ascending afternoon: 1:57 ± 0:29
Bands	MODIS bands 29, 31, 32	MODIS bands 29, 31, 32

3.2.1 Optical Data Availability

For an easy understanding of the availability of the MODIS data, the time visualization has been divided into two different availability categories which enable explaining the detailed availability of data.

3.2.1.1 Yearly Availabilities

In this category, the time visualization (Figures 3.2,3.3,3.4,3.5) shows the availability of each MODIS dataset on yearly basis. The color of each square represents the number of observations (counts) of each specific stations in different years, and the number could be known by referring to color bar on the right side of each figure.

3.2.1.2 Daily Availabilities

In this category, the time visualization shows the availability of each MODIS dataset during each hour of the day, which enables visualizing the mean of the data during each hour. The color of each square represents the number of observations (counts) for each specific stations in different hours of the day, and the number could be known by referring to color bar on the right side (Figure 3.6).

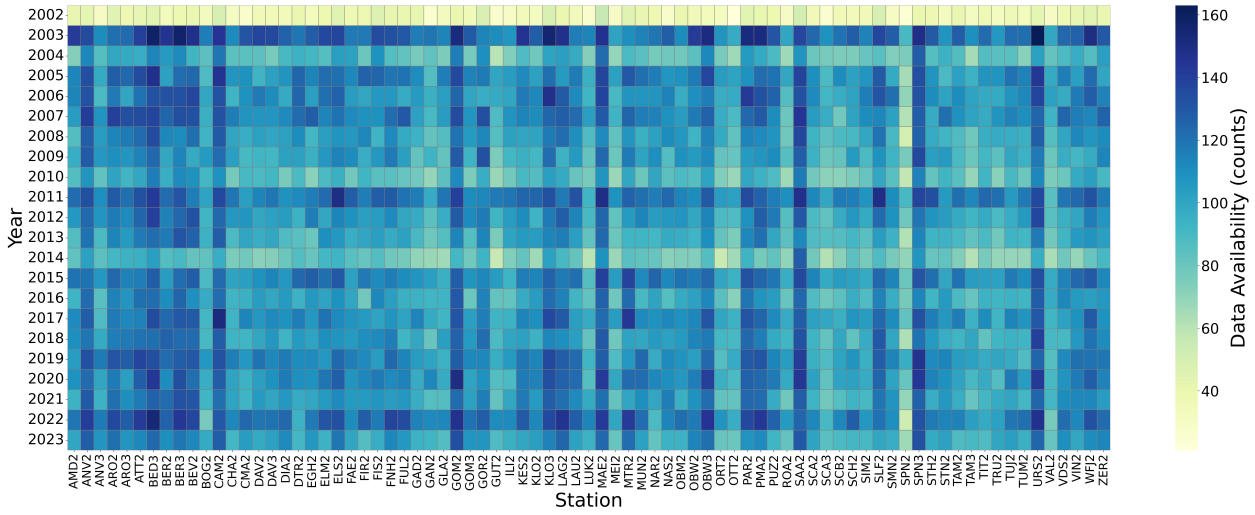

Figure 3.2: Color scale visualization of the availability of MYD21A1D dataset on yearly basis

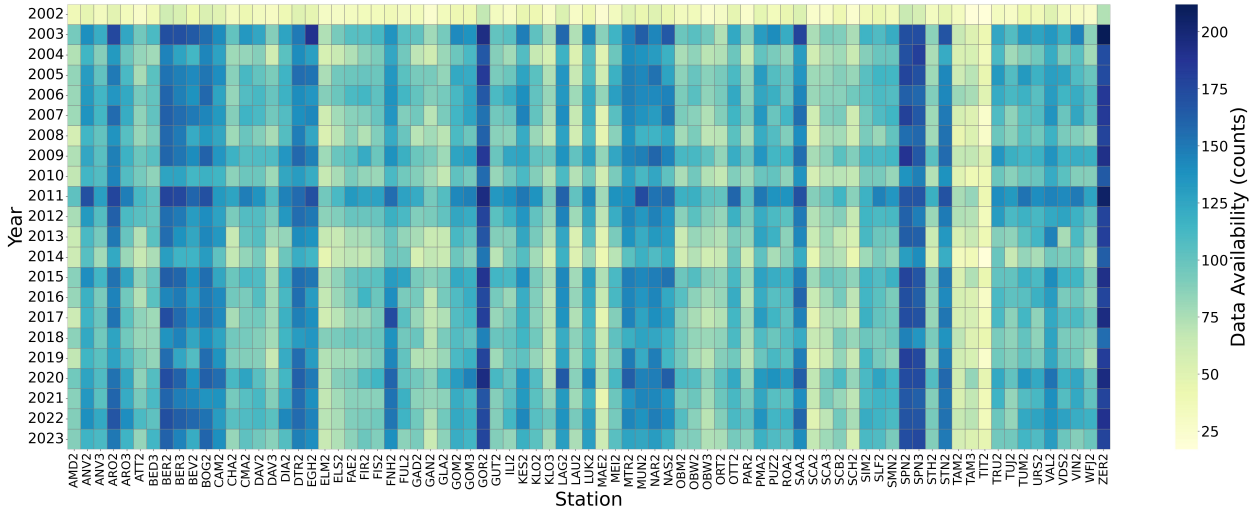

Figure 3.3: Color scale visualization of the availability of MYD21A1N dataset on yearly basis

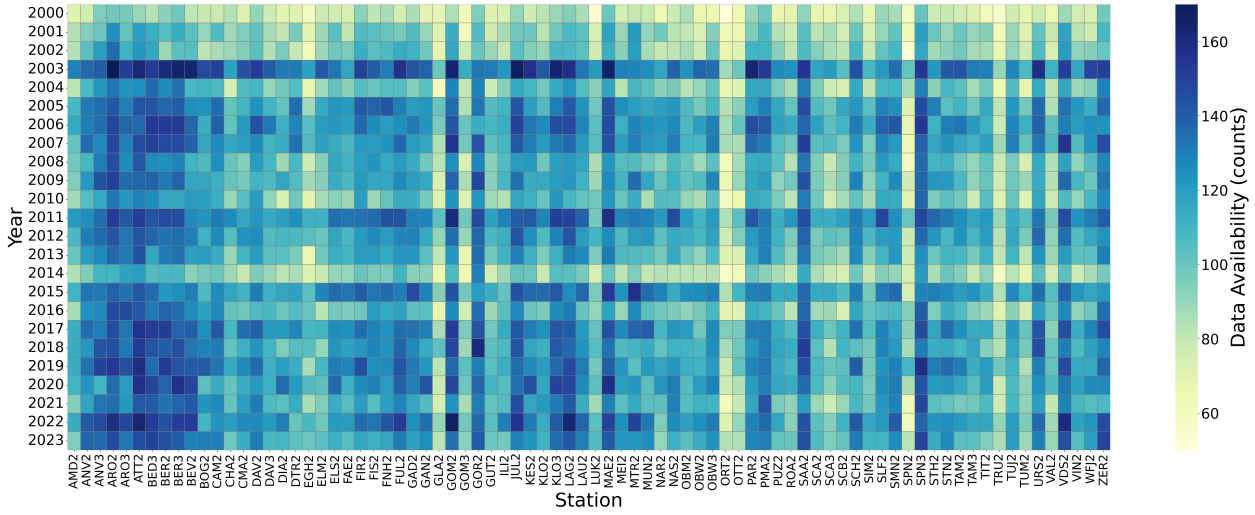

Figure 3.4: Color scale visualization of the availability of MOD21A1D dataset on yearly basis

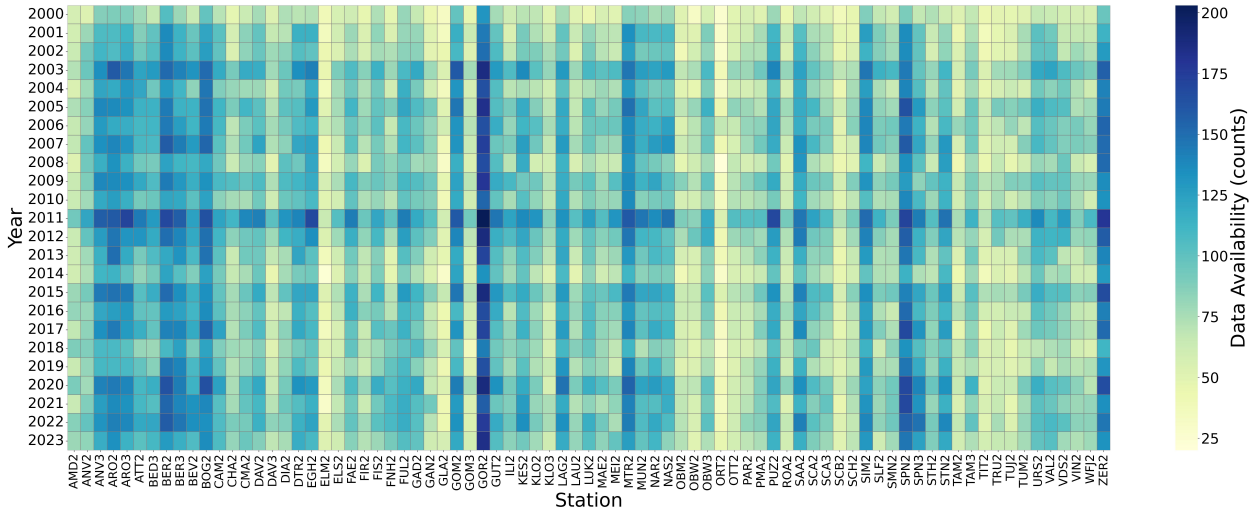

Figure 3.5: Color scale visualization of the availability of MOD21A1N dataset on yearly basis

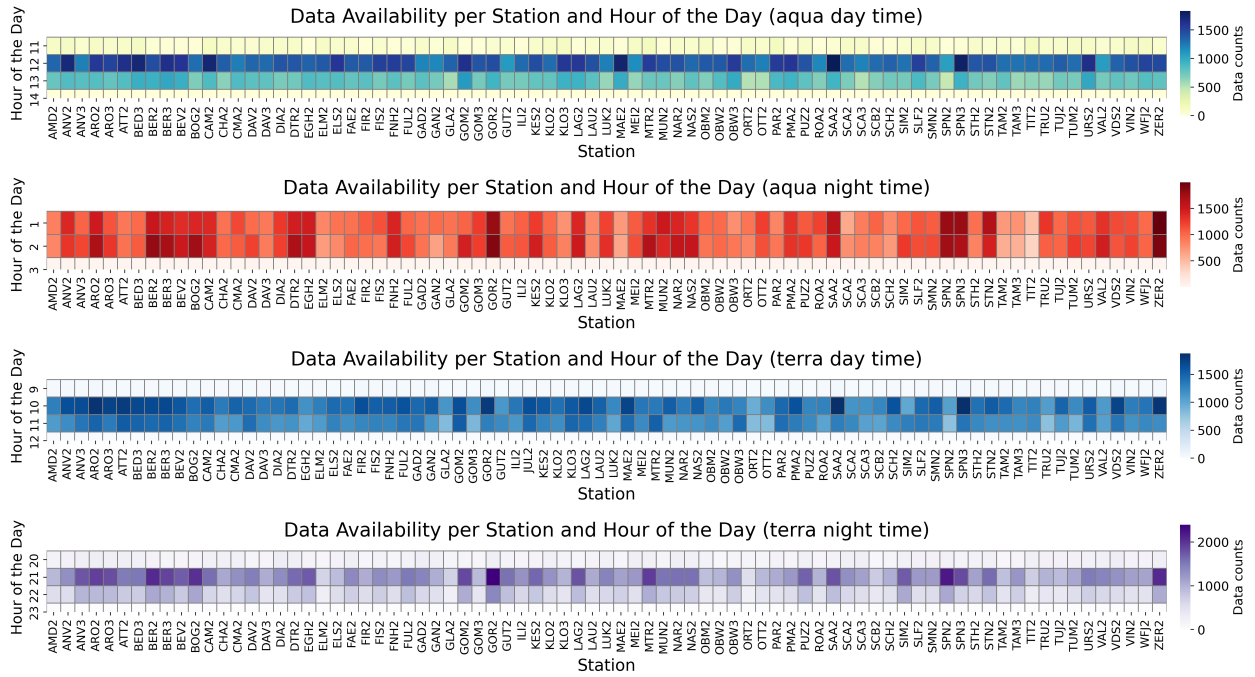

Figure 3.6: Color scale visualization of the availability of the four MODIS datasets during each hour of the day.

3.2.2 Aspect Data

Different acquisition times result geometric changes in the sun-target-sensor configuration, and such bias may additionally vary with slope and aspect of the topography (Gök et al., 2024). This makes it necessary to generate the aspects which represents the topographic slope face; and thus Copernicus DEM (Digital Elevation Model) GLO-30: Global 30m Digital Elevation Model dataset, which is a precise digital elevation model that describes the earth's surface including buildings, infrastructure, and vegetation is used. It is extracted from a modified DSM (Digital Surface Model) called World DEM&trade that is derived from radar satellite data during the TanDEM-X Mission. The extracted list clarifies the variation taking place in aspects of different stations' locations (Figure3.7).

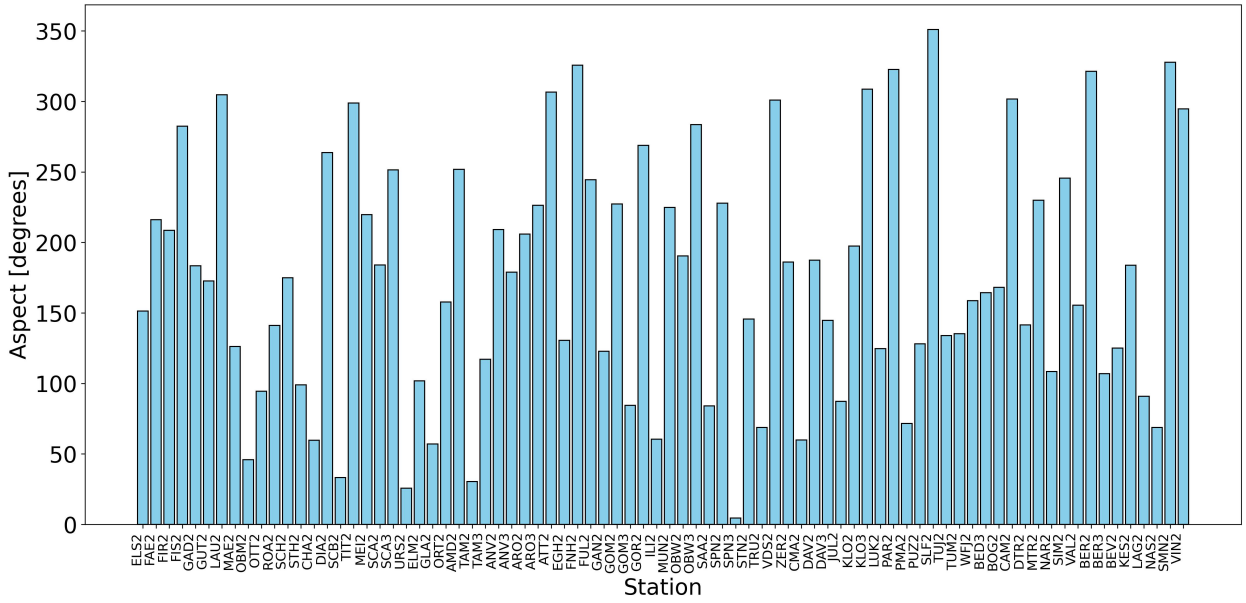

Figure 3.7: The variations in topographic aspects between the locations of different IMIS stations.

3.2.3 View Angle Data

View angle is one of the most critical factors of sensor accuracy, the quantity of light leakage in the oblique viewing angle changes with the surface pretilt angle, and the positional asymmetry of the light leakage becomes more erroneous as the pretilt angle grows (Oh et al., 2015). Thus, view angle must be investigated to deduce any relationship with the changing LST measurements. For this reason, the list of view angles of each observation at each location of the 80 stations was derived from the metadata of the four previously mentioned MODIS datasets.

4 Methods

The main concept upon which the methodology of this study was built includes: i) the preparation of the retrieve datasets from various sources with suitable (interpolated) data format for further analysis. ii) In addition, the validation of the prepared datasets retrieved from MODIS instruments by comparing it with datasets from ground-based stations (IMIS). Even though, both datasets (MODIS and IMIS) have different temporal coverage; however, the rational implies that IMIS data has been interpolated for better matching in the temporal resolution with MODIS LST.

4.1 Data preprocessing

4.1.1 IMIS Data Preparation and Interpolation

LST datasets from IMIS ground-based stations are large; especially when counting the existing 142 stations that cover a time span from 1996 to 2024 with 30 minutes measuring interval. However, the study focuses on the time span only between 2000 to 2023 as it was controlled by the availability of MODIS images; therefore, there has been a filtering to have only stations covering the whole time period (2000-2023) and with complete datasets.

In this respect, uncertainty exists due to the large time difference between MODIS and IMIS datasets; especially when comparing datasets that cover the same parameter but in different observation times. This uncertainty led to align the times of the two datasets in Python using a linear interpolation function from the SciPy library. The function considers the two LST sets, using the IMIS LST list as the main list with its time- span, while the MODIS dataset is considered to have a time-span that requires interpolated data. Thus, for computational purposes, the date/-time columns of both datasets were converted to numerical values and linear interpolation was applied according to the following equation:

$$y = y_1 + \frac{(x - x_1)}{(x_2 - x_1)} \times (y_2 - y_1) \tag{4.1}$$

The two time periods are explained by the 'Xs' 1 and 2, while the 'Ys' 1 and 2 represent the LST values. This means that x is the target time period for which y is the interpolated temperature value. It was assumed that successive points have a linear relationship; and thus, interpolation

function does the extrapolation for the outgoing time periods using fill_value'extrapolate'. Hence, data gaps, where the values might be out of the bounds of the main data, are filled after being calculated by the used equation, assuming there is a linear relationship between them. The new interpolated data were then stored in the new files, which contain a new edited date/time column (i.e., containing MODIS observation times) and a new edited IMIS LST column. This approach provides a solution for aligning data with different observation times while ensuring accurate interpolation.

For precise comparative analysis, the time and location must be strictly handled, and this leads to better consideration of the temporal compatibility between the two datasets to be compared. For this reason, the IMIS ground station data has been interpolated with the timing (day and night) of the MODIS observations, four new datasets were created. These are (Figure3.6):

- IMIS aqua daytime dataset covering the same times period as MYD21A1D.
- IMIS aqua nighttime dataset covering the same times period as MYD21A1N.
- IMIS terra daytime dataset covering the same time period as MOD21A1D.
- IMIS terra nighttime dataset covering the same time period as MOD21A1N.

These stations contain the measurements of IMIS ground stations during the same time periods covered by the MODIS datasets, making the comparison easier and more distinct.

4.1.2 Satellite Images Processing

As one of the major open sources for satellite data, MODIS satellite data used in the study was accessed and processed in Google Earth Engine (GEE), which is a cloud-based geospatial analytic platform that enables the usage of numerous satellite datasets, such as Landsat, MODIS, Sentinel, etc. with climate and socio-economic attributes. Using Java Script and Python APIs, GEE enables users to achieve many large scales themes using different satellite data. For example, land cover classification, environmental monitoring, climate studies, etc. Therefore, the steps were performed as follows

1. Data required was downloaded to the local desktop, and then processed using Python.
2. Data has been converted from Kelvins to °C.
3. Ground stations were plotted and MODIS data were downloaded for each location covering the entire study period 2000 - 2023.
4. A number of studies use Kriging methods that rely on spatial interpolation of the ground data along with satellite derived estimates (D'Agostino and Zelenka, 1992), (Journée et al., 2012). However, in this case, kriging was not applied to MODIS data at IMIS locations. This decision was based on factors such as the pre-processed nature of MODIS data, resolution compatibility concerns, and the specific objectives of the analysis.
5. Additionally, it was necessary to filter out redundant entries in the dataset, as they occur

frequently across most of the years under examination. Redundant data typically arises from repeated observations or overlapping records that do not contribute unique information to the analysis. Removing these duplications significantly reduced the total number of usable data points but ensured the integrity and reliability of the dataset for the intended analysis.

6. The obtained data was transformed into comma-separated value (csv) files, each representing a station location named with available LST MODIS data in °C for that location between 2000 and 2023.

Large MODIS data availability differences can significantly impact LST calculations due to temporal gaps, spatial inconsistencies, and missing data, and these differences could be addressed as follows

1. Temporal coverage gaps: Missing daily LST values due to cloud cover or atmospheric interference can be mitigated using interpolation techniques like kriging.
2. Spatial resolution challenges: MODIS provides coarse-resolution data that may not align with local measurement needs. Spatial interpolation methods can be used to refine and match resolutions for more accurate calculations. Ground observations (e.g., IMIS data) were integrated with MODIS LST values to complement and validate results.
3. Data quality control: Filtering redundant or low-quality observations ensures that the dataset is optimized for reliable calculations.

4.1.2.1 Time and View Angle Information

The orbital change experienced by both MODIS satellites instruments in a significant daily change in the timing of the observations, which is clearly shown in the time color scales in the data section. This means that the diversity in observation times requires time adjustment, which includes interpolation to the IMIS LST data to be consistent with the timing of the MODIS LST observations (Guo et al., 2021). However, by using the available metadata in GEE, the times of all available observations were exported in decimal form and then converted in Python to real-time data as 4 csv files, each specific to the times of a MODIS datasets, which were consequently used in the interpolation process.

In addition, MODIS is a cross-track scanning radiometer with a two-sided scan mirror that images the Earth with a total angular field of view of 110°, extending 55° on either side of the nadir (Xiong and Barnes, 2006). The topographical nature of the Swiss Alps has an impact on temperature patterns due to rugged topographic variations. This makes it necessary to take into account the variations in viewing angle which was also obtained from the MODIS metadata, in the same exported files with the LST measurements.

4.2 Harmonic Regression Model

The study of trends over the entire projected period requires a model for analyzing the complexity and variations that occur within the large amount of data used. For this reason, a Harmonic Regression Model was used notably it is capable of capturing the long-term linear trend (Gök et al., 2024); in addition, to the periodic seasonal variations of the LST, from both the IMIS and MODIS datasets.

4.2.1 Model Coefficients

The used Harmonic Regression Model in equation 4.2(Gök et al., 2024) was designed using the cosine and sine terms to detect the seasonal change by capturing the annual cycle:

$$y(t) = b_0 + b_1 \cdot t + b_2 \cdot \cos(\omega t) + b_3 \cdot \sin(\omega t) \tag{4.2}$$

where:

- $y(t)$ represents the LST at time t.
- b_0 is the intercept showing the mean LST baseline over the study period.
- b_1 is the linear trend coefficient showing the magnitude and direction of the long-term change taking place in the data.
- b_2 and b_3 are responsible for capturing the annual cycle of the data, reflecting its intensity and phase.
- ω is the angular frequency, defined as

$$\omega = \frac{2\pi}{T}, \tag{4.3}$$

  where:

$$T = 365.25 \cdot 24 \cdot 60 \cdot 60 \,\text{seconds (one year)}.$$

The harmonic terms, $\cos(\omega t)$ and $\sin(\omega t)$, account for ATCs, reflecting seasonal variations.

The four b coefficients represent the parameters of the model, which are determined by the nonlinear least squares optimization method in Python's $scipy.optimize.curve_fit$ function. This function is responsible for minimizing the residual sum of squares between the two data sets. Where it uses np.isfinite() function to capture the measurements that prevent the process of curve fitting, and it masks extreme LST values that might otherwise distort the LST trend (Weng and Fu, 2014). In addition, The threshold for detecting outliers in the data was established using Z-score analysis (Torres et al., 2017), where data points beyond ±2 standard deviations were excluded. This method ensures that extreme values, which may result from sensor anomalies, atmospheric interference, or data collection inconsistencies, do not distort the integrity of the analysis.

Setting the threshold at Z = ±2 removes data points that fall outside two standard deviations from the mean. This corresponds to approximately 95.4% of the data remaining, assuming a normal distribution. To validate whether the chosen threshold is appropriate, the following checks were applied: we generated a histogram and checked whether the data distribution closely follows a normal curve. Also, we compared results before and after outlier removal.

4.2.2 Model Substitute

Given that the used Harmonic Regression Model was the best fit to analyze the studied data, there are some other approaches that could be used for such analysis depending on the type of data and specific research goals such as the Polynomial Regression and the Fourier Series.

4.2.2.1 Polynomial Regression

A forecast or prediction can be made using a variety of techniques, including polynomial and linear regression. The linear regression model which is called polynomial regression is created by raising each predictor variable's (X) effect to the k-order. (Shaikh et al., 2021). It is typically applied when a polynomial function could be used to approximate the relationship between two data sets, which is not quite linear. Regarding the benefits of polynomial regression, it can capture different levels of data and is adaptable to non-linear trends. However, it may over fit the data, producing conclusions that are difficult to understand.

4.2.2.2 Fourier Series

The harmonic regression is a simple form of the Fourier Series method which also depends on sine and cosine terms with different frequencies representing a curve that shows the sine cosine function. The benefits of the Fourier Series implies the capability of capturing different cycles of the data (e.g., daily, seasonal, etc.), and it allows the detection of more detailed changes existed; and then, it will enable handling data characters that follow repeated patterns at certain trend intervals and have good statistical interpretations (Mariati et al., 2020). Besides, it is of higher complexity and costs, in addition to its high sensitivity in choosing the number of terms responsible for the over fit.

4.2.3 Model Limitations

Limitations often exit for the performance of models. In this respect, the harmonic regression model is an effective way for detecting seasonal fluctuations and long-term changes in temperature data, there are certain restrictions (i.e., expertise on how to run the model, software availability, etc.) and gaps (e.g., lack to sufficient data, etc.). These limitations are related to where the model might not represent all details of the data or where improvements could be made to create more accurate analyses.

4.2.3.1 Assumption of a Single Annual Cycle

A single annual cycle for the seasonal change in the data is considered as gap in the performed harmonic regression model. It depends of the sine and cosine in terms of a fixed frequency:

$$\omega = \frac{2\pi}{T} = \frac{2\pi}{365.25 \cdot 24 \cdot 60 \cdot 60} \approx 1.99 \times 10^{-7} \text{ radians/second} \tag{4.4}$$

This might not highly accurate knowing that temperature data passes through different seasonal cycles; and thus,, using these fixed terms is an obstacle in the path of capturing complex variations and periodic fluctuations among the data. Adoption of Fourier Series with different frequencies or higher order harmonics would be a better choice that has a better flexibility to deal with the complexity of the data.

4.2.3.2 Lack of Temperature Anomalies or Extremes

Within the used harmonic regression model, there might be a lot of deviations or outliers that are not captured by the model, and that appear due to sudden fluctuations and extreme events that may take place. The inability of the model to capture these changes is attributed to the overall trend and the periodic behavior of the temperature data. This misjudgment might lead to misunderstanding of occurring events such as heat waves and cold spells that results in sudden extreme LSTs. This can be solved by enriching the model with extra terms such as outliers' detection.

4.2.3.3 Linear Trend Assumption

As the $b1$ (equation 4.2) is the linear trend coefficient that is responsible for capturing the long term changes among data; thus, it is considered as a perfect indicator for any gradual change that might occur. However,this coefficient lacks to the accuracy in detecting the complex non-linear trends such as sudden changes that might take place during different time periods, and creates in bias in understanding LSTs over long periods, that resulted in misinterpretation of the data. Also in this case, addition of new non-linear terms may help in improving the abilities of the model in diving into complex trends' understanding.

4.3 LST Trends Calculation

Since the main objectives of this study are to validate the MODIS LST measurements and trends with respect to the IMIS data, and to understand the diurnal changes that occur in these trends, thus it was necessary to correctly calculate the trends of both datasets. In addition, two sides of the trends were considered, the overall trend and the hourly trend (e.g., Figure 8.4). In both cases, this investigation required an approach that tends to clean the data, detect outliers, fit the harmonic regression model used, and finally extract the trends.

4.3.1 Overall Trends

Following the previous approach, and after reading the csv files in the LST measurements and the date/time data, which were presented differently in different files (as date/time column in some files, and year, month, day,and time columns in other files), the used code filtered the data to obtain only the 2000-2023 period.The threshold for detecting outliers in the data was established using Z-score analysis (Torres et al., 2017), where data points beyond ±2 standard deviations were excluded. The aforementioned harmonic regression model with $b1$ coefficient (Linear Trend that was mainly calculated as change per second, and then converted to change per year) and its sinusoidal sine and cosine terms was applied for the data. The whole process was automated to produce a file containing the trend that occurred in the data of each station over the period 2000-2023 as the overall trend of each station. For further comparisons, the same methodology was applied for both IMIS and MODIS datasets.

4.3.2 Hourly Trends

For full understanding of the changes in data and to examine the diurnal changes, the same methodology used to obtain the overall trends was also used to obtain the hourly trends in data. The difference is that for the overall trends, the results were a single value for each station representing the overall trend over the entire time period examined. For the IMIS data, the process was automated done to obtain the average of the trends of each station with respect to the time of measurement, which is every 30 minutes. This means that each cell represents the average LST at a given time for a given station over the entire time span, and this is repeated every 30 minutes to cover all hours of the day. Given that MODIS measurements do not have this constant and complementary timing, the process was automated to obtain the mean LST of each station from the available MODIS observation times of each dataset. Due to the changes in the observation times (due to the existing orbital change), the observation times were rounded up, e.g., all observation times between 9:00 and 10:00 were considered as 9:00. This resulted in four different files for the four MODIS datasets of the projected time. These results provided a solid basis for later comparisons, analysis, and validation.

4.4 Analyzing Changes Between MODIS and IMIS Data

For better validation, precise analysis of the changes occurring in both MODIS and IMIS datasets is needed. To achieve this analysis, different methods were used to compare the changes occurring in both datasets and the changes in the trends.

4.4.1 MODIS Versus IMIS LST Measurements

Pivotal analysis and understanding requires a distinct comparison that explains the differences between the two datasets. For this purpose, comparison was performed between the actual measurements, and between the means of these measurements.

To compare the actual measurements, four comparison figures were created for the MODIS observation and IMIS datasets. By processing both datasets stored in csv files and extracting a sample of 10000 measurements from each dataset to manage memory and computational efficiency, a robust regression analysis was performed. The Theil-Sen Regressor from the Sklearn library, was used to model the relationship between IMIS data represented by the 'x' variable and the MODIS data represented by the 'y' variable. Three values were analyzed and then calculated to ensure a rigor analysis as follows:

1. R-squared value, which is responsible for estimating the proportion of variance explained by the model.
2. Slope value, which shows the rate of change between MODIS and IMIS measurements.
3. MAD-1 (Median absolute deviation) which is a measurement of accuracy that represents the median of the absolute difference between the two data sets, and it offers a direct and robust measure of the dispersion of a random variable, and it has many applications in different fields (Bassett and Koenker, 1978). It is more efficient than standard deviation in life-like situations where small errors may occur in observations and measurements (Huber and Ronchetti, 2009).

Consequently , a histogram illustrating the deviations between the two datasets was established to the main scatter plot, where the deviation of each point representing the difference between MODIS and IMIS data was calculated, with the x-axes constrained between -20 and 20 °C to reduce the effects of extremes and outliers. The y-axes represent the frequency of occurrence of each anomaly.

The analysis of this histogram helps understanding the symmetry of data, i.e. whether the occurring deviations were evenly distributed around zero. Then, the skewness of the deviation, which represents the asymmetry in the distribution of the deviation and shows any distortion, and the spread which shows the range of the spread of the deviation values of data.

In addition, the comparison of the means of MODIS and IMIS datasets was done differently. Therefore, after processing the time columns of both datasets and filtering the data, a statistical calculation was performed to calculate the annual mean and standard deviation of each dataset, summarizing the variability of its actual measurements in each year separately. The annual statistics of both datasets were merged into one dataset, which facilitates the comparison of mean LSTs.

The statistical analysis enables evaluating the agreement between the two datasets, and it was performed using PC (Pearson Comparison) and MAD-2. For the PC, it is responsible for quantifying the strength of the linear relationship between the two mean datasets. For any delay between the determining and the responding variables, it will be detected by this correlation (Andronis et al., 2022). On the other hand, the MAD-2 calculates the average absolute difference between the mean annual LST of the two datasets, showing the similarities between them. All these statistics were combined into four different plots, which are responsible for the comparison between the annual mean data of both MODIS and IMIS datasets during the four different MODIS observation times.

By comparing the actual measurements and the annual mean LSTs of MODIS and IMIS datasets, the above analysis can provide insight into their compatibility. The use of such statistical metrics and visualizations facilitated the understanding of the agreement between the satellite and ground station LST data.

4.4.2 MODIS Versus IMIS LST Trends

Since the comparison between MODIS and IMIS measurements was to validate the MODIS data with respect to the IMIS data, a comparison of the trends derived from both datasets was performed for the same purpose.

Using the previously described procedures for obtaining the hourly trends of both MODIS and IMIS data, the trends were derived and stored in the csv files. The spatial and temporal variations of the LST trends were then visualized using a heat map. The seaborn library, which is a Python library in Matplotlib, was created to produce nice rigor statistical visualization. It facilitates plotting with easy-to-use function and work with Pandas Data Frames. It also facilitates the visualization of the relationships, and trends in data in plots such as scatter plots, box plots, heat maps and regression plots). The heat map was created with stations on the x-axis and times of day on the y-axis. A custom color map transitioning from white (indicating lower trends) to green (indicating higher trends) was applied to highlight variations in temperature trends (°C/year), where each square represents the mean LST trend at each station and at each time of day for the IMIS data (Figure 4.1).

In addition, four other heat maps representing the means of the trends at each location at the four different observation times of the MODIS datasets were created in the same way to represent the MODIS trends variations (Figure 4.2).

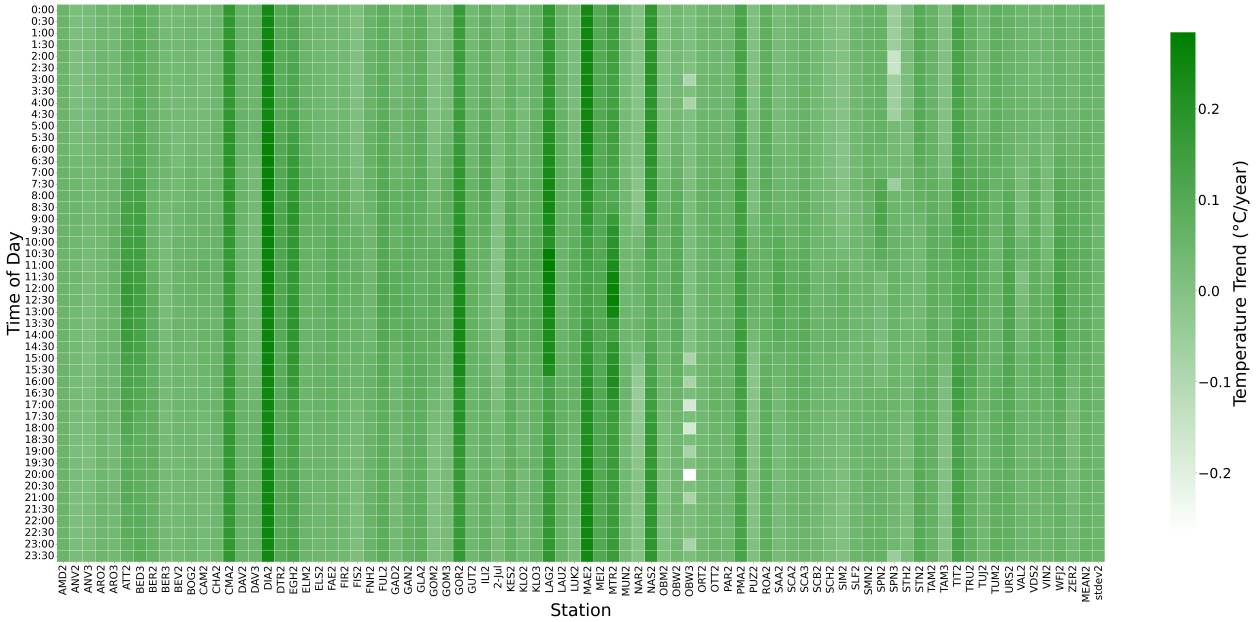

Figure 4.1: Color scale visualization of the variation of IMIS LST Trends variations as a function of stations and hours of the day

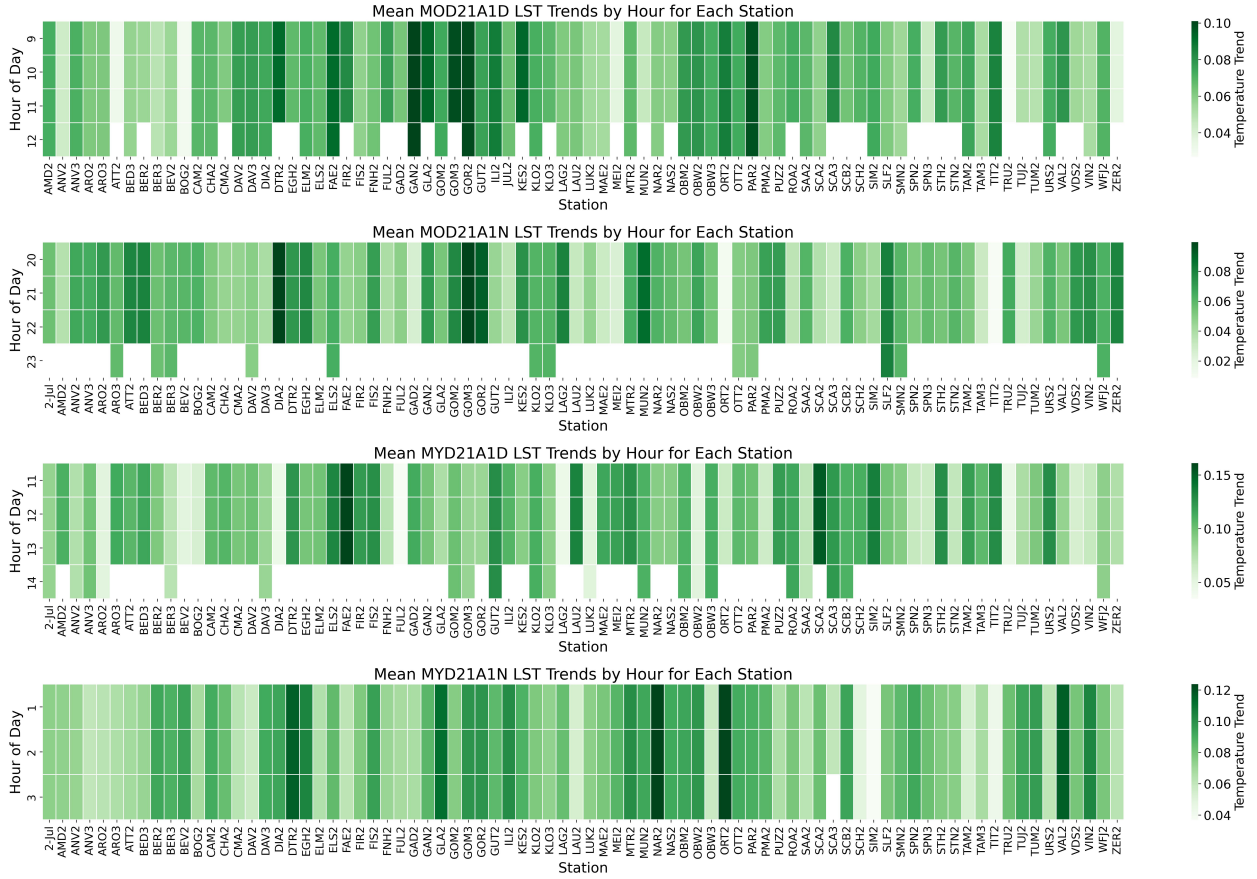

Figure 4.2: Color scale visualization of MOD21A1D, MOD21A1N, MYD21A1D, and MYD21A1N LST trends variations as a function of stations and hours of the day.

Given the heat maps is not enough to understand the variations that take place within the trends of both datasets, in addition to approaching a useful comparison between both data. For this reason, an additional step towards a clear comparison was taken by creating a scatter plot visualization for each of the available hours, comparing the trends of both datasets at the same time and location. In other words, the hours available in the MODIS datasets were considered in the IMIS datasets by station name, and all other hours were filtered out in addition to the incomplete or outlier data points. Then, metrics such as the MAD-2 and the PC, which are responsible for calculating the discrepancies and the strength of the linear relationship between the two data, respectively, were calculated. This approach helped to understand the differences in trend variations between IMIS and MODIS datasets, taking into account location and time.

However, for better understanding of overall trend variation, , a general comparison was made between the means of the two datasets. As the detailed analysis of the actual measurements was supported by a general means analysis, trend analysis is also supported similarly, where the means of trends of the MODIS observation time are plotted as MODIS versus IMIS data. For in-depth and well explained analysis, two different values are calculated, the Mean Absolute Error (MAE) and Standard Deviation were added, knowing that MAE is responsible for representing the error between the trends and the Standard Deviation represents the precision of the comparison. MAE is calculated using the following equation (Zhu et al., 2013):

$$\text{MAE} = \frac{1}{n} \sum_{i=1}^{n} \left| y_i^{\text{MODIS}} - y_i^{\text{IMIS}} \right| \tag{4.5}$$

where:

- n is the number of data points.
- y_i^{MODIS} is the temperature trend from MODIS for station i.
- y_i^{IMIS} is the temperature trend from IMIS for station i.
- $|\cdot|$ denotes the absolute value.

4.5 Trends at MODIS Observation Times Versus Overall Trend

Since the variation in the trends over different MODIS observation times was studied, the temporal accuracy has to be taken into account. For this purpose, a comparison was made between the IMIS LST trends over different MODIS observation times and the overall trend of the data over the entire time span.

Four different scatterplots were generated, each representing a MODIS observation time. The x-axis represents the names of the stations, and the y-axis represents the mean LST trend of each

station over the represented MODIS observation time during the entire period of the study. Pearson's correlation and MAD-2 values were added to improve the accuracy of the comparison. This approach will help to understand the representativeness of the IMIS LST trend at each MODIS observation time for the overall trend of data at each station over the entire period of the study.

4.6 Environmental and Sensor-related Influences on LST Changes

For the variability in LST trends, it was significant to identify the influences that may cause these variations and differences in the analyzed data. For IMIS data, it was used to understand the effect of elevation and aspect, while for MODIS data that was used to investigate any effect of the view angle.

4.6.1 Elevation Effect On LST Trends

To investigate the effect of elevation change on the LST trends, a Python code was written using two data sets, one containing LST trend means of each station, and the other containing the elevations of the stations in addition to some other related values. The LST trends' means and elevations were aligned according to the names of stations they represent and combined into one data frame; then a visualization using a scatterplot with the LST trends' means on the y-axis and the elevations on the x-axis was used to better understand the variation of LST trends as a function of elevation change.

4.6.2 Aspect Effect On IMIS Trends

In order to determine whether the variations in the topographic aspect have an effect on the LST measurements, a similar methodology to the one used to investigate the effects of elevation on these measurements was used. However, instead of using all aspects, bins were created due to the large number of aspects in addition to the variability between different stations and times.

Hence, each unit of the x-axis of the generated plot represents a bin of, for example, 50 °C, the first unit represents all data points of an aspect ranging from 0 to 50 °C, and so on. While, the y-axes represent the means of LST trends derived using the applied harmonic regression model.

4.6.3 View Angle Effect On MODIS Measurements

Studying view angle in MODIS data; especially there is a continuous daily orbital change, is necessary to determine any effect of the view angle on LST data for each observation time Thus, view angle was compared according to various observation times (MOD21A1D, MOD21A1N, MOY21A1D and MYD21A1N). For this purpose, we used a methodology similar to that used for the aspect investigation, where the x-axes of the generated plot represent bins of 15 view angles by each unit (e.g., one unit represents data points of view angle from -75 to -60), and the whole axes range between -75 and 75 °C, while the y-axes represent the mean of LST measurements. This method was repeated to create four different figures representing the four different MODIS

datasets of different observation times.

4.7 Landsat Implications

In addition to MODIS satellites, there is also an orbital change exists in Landsat and it enables adding more acquisition times (Figure 4.3(Gök et al., 2024)).

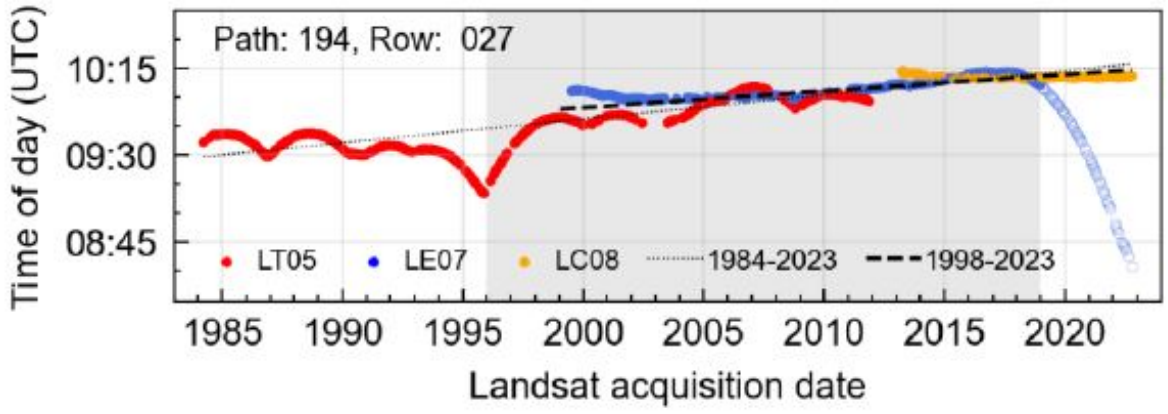

Figure 4.3: Figure 2. Acquisition times (UTC) of Landsat LT05 (red), LE07 (blue), and LC08 (orange) at path 194 and row 027. LE07's noticeable orbital drift after 2019 (hollow blue circles), causes a significant shift in revisit timing and has been excluded from the analysis. Linear regression lines (dotted and dashed) depict acquisition time trends, with and without abrupt LT05 orbit changes prior to 2000. The gray-shaded area indicates the time period for which IMIS station data exists, although with variable record length (Gök et al., 2024).

Figure 4.3 visualizes the change exits in the timing of different Landsat satellites over the studied Swiss Alpine Region, and it is important to mention the coverage of the IMIS LST data in the study is different from that shown in the figure. In this concern, the time span covered by different Landsat satellites is clearly between 8:45 and 10:30 a.m. in UTC (Coordinated Universal Time) which is 9:45 and 11:30 a.m in European time. This motivates us to make a comparison between the representativeness of the timing of Landsat and MODIS observations in order to come up with better implications.

The comparison is made by the creation of figure that visualizes the means and trends of LST IMIS data of all stations at all hours of the day. Then five-time widows were created; four representing the four MODIS observation times and one representing the Landsat satellite observation time. The statistical values result, where the overall mean of all LST means was calculated, and then the mean LST of each observation time of MODIS and Landsat (Time Window Mean). The mean difference between each observation time and the total was calculated and used in the comparison between the two data sources. In addition, a count-based representation was made, it calculates the percentage of data in each time window from the total data. This approach helped in understanding the representativeness of each time window of both MODIS and Landsat, and facilitated suggesting some implications regarding Landsat observation times.

5 Results

5.1 Change Analysis Between MODIS and IMIS Data

As resulted from the methodology, the analysis of change between MODIS and IMIS LST data was calculated over two levels, i.e., the analysis of the actual measurements and the analysis of the trends.

5.1.1 MODIS Versus IMIS LST Measurements

The first comparison was done between the measurements of the two datasets depended on three statistical values representing the variability of both datasets, which are the R-squared value that shows the proportion of variance explained by the model, the slope value revealing the rate of change between MODIS and IMIS measurement, and MAD-1 value that gives the median of the absolute difference between the two datasets. In addition, a histogram was performed to investigate the deviation that occurs between the datasets.

For this comparison, four figures representing four different MODIS observation times were created showing a clear similarity between night measurements of both Terra and Aqua satellites, and between day measurements of both satellites as well. In this regard, the observation time of MOD21A1D (Figure 5.1) R-squared value is 0.76 which shows a strong relationship and consistency between the two datasets, with a remaining 0.24 of variance that might be caused by a variety of reasons (e.g., cloud cover, solar radiation, etc.). MAD-1 value for the mentioned observation time is 3.60 °C, indicating a general agreement between the two datasets with a noticeable expected difference due to some factors and limitations of satellite data. Finally, the slope value is 0.94 and it indicates excellent linear relation between the two datasets with a slight difference that was clearly indicated by the other two comparison values.

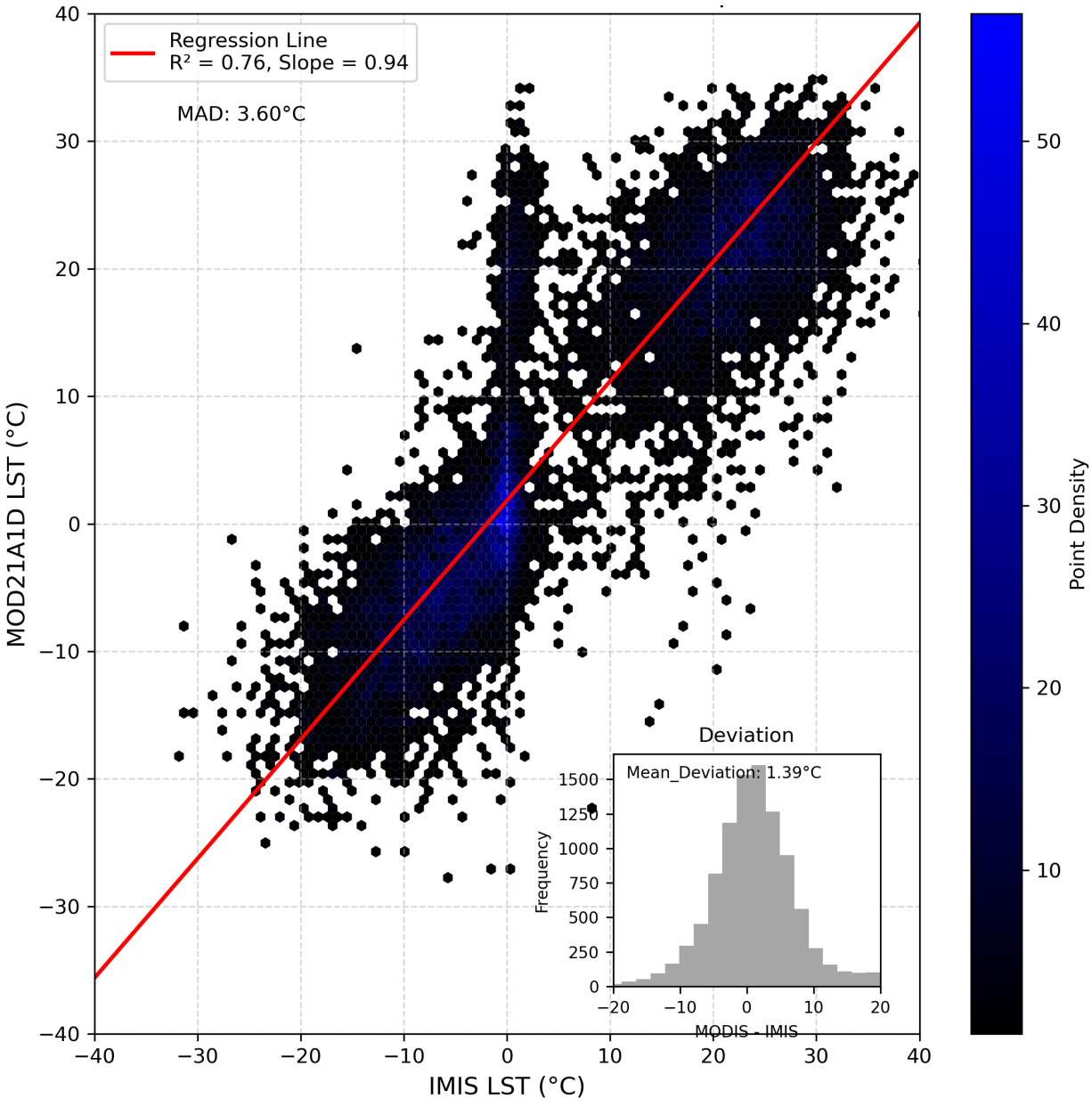

Figure 5.1: The comparison between MOD21A1D and IMIS data measurements with slope, R-squared and Mean Absolute Deviation values calrifying the deviation btween the two datasets represented in the histogram.

The values of MYD21A1D (Figure 5.2) observation times followed similar analysis where the R-squared value is 0.79 and it also represents a strong relationship and consistency between the two datasets with 0.21 remaining variance. In addition, MAD-1 value is 3.37 °C which also shows a general agreement between the two datasets with a clear difference of 3.37 °C, and finally the slope value is 0.89 indicating a strong linear relationship between the two datasets with a slightly stronger difference than the one in the MOD21A1D data.

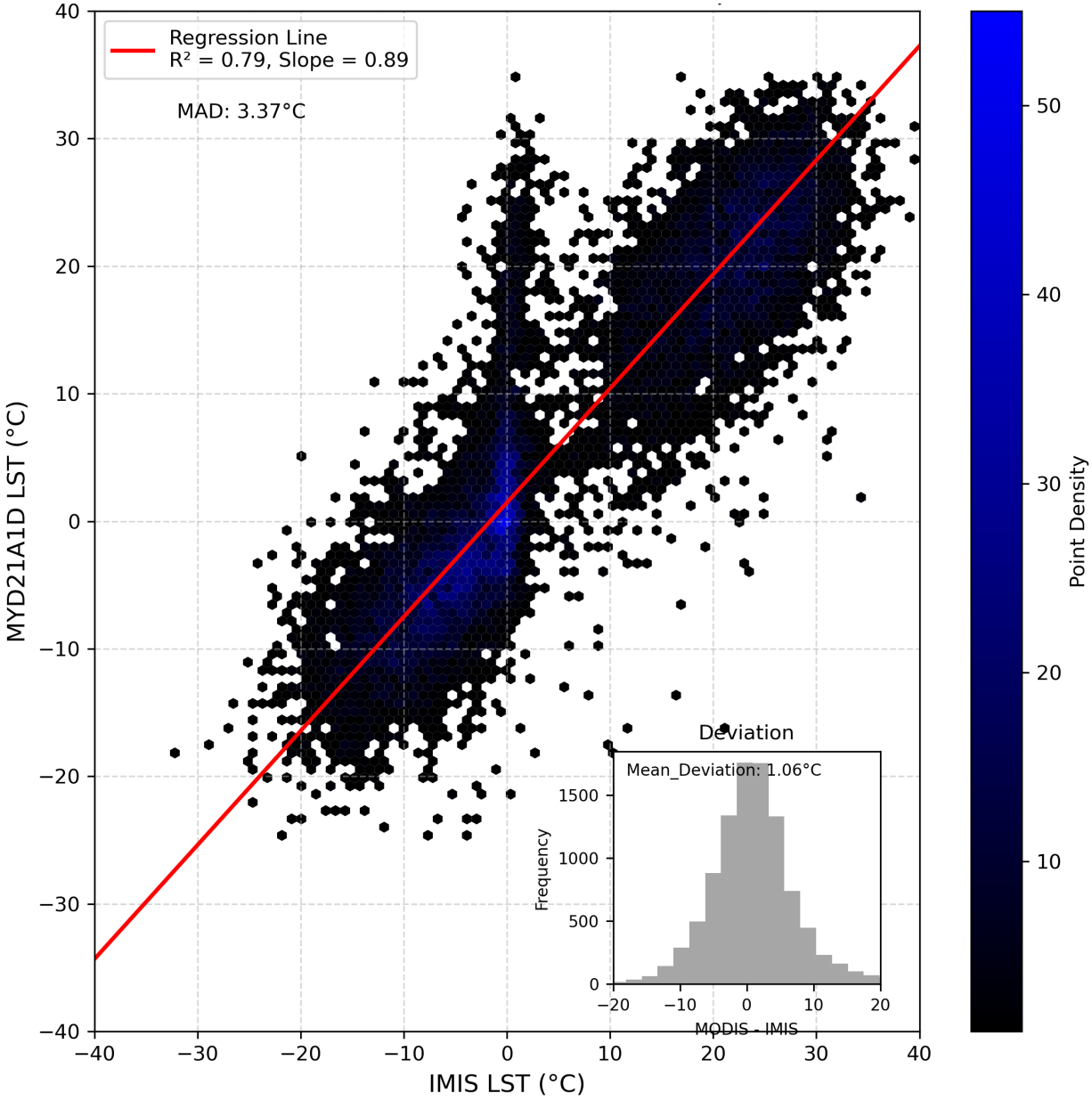

Figure 5.2: The comparison between MYD21A1D and IMIS data measurements with slope, R-squared and Mean Absolute Deviation values clarifying the deviation between the two datasets represented in the histogram.

In both MOD21A1D and MYD21A1D data with respect to IMIS LST, the measurements are spread across the Y-axes representing the MODIS measurements. The same phenomenon occurred in another study (Gök et al., 2024), when comparing IMIS LST with Landsat LST measurements, and it was attributed to differences in spatial resolution and the presence or absence of snow cover in the different measurement areas.

For the day time, scatter plots show two main clusters that separated by the absence of plots which can be attributed to the temperature climax during the mid-day from the MODIS measurements, but not the IMIS data which shows a continuation of plots as an elongated stretch. This might be attributed to the high reflection from sunlight observed by MODIS. However, this is not the case for the night time where no remarkable change in temperature exists. This contradicts the previous explanation of spatial resolution and the presence or absence of snow cover, which did not appear in the study examining Landsat data because all Landsat measurements were daytime measurements.However, the differences presented in the values between daytime and nighttime data were relatively small; and thus, for MOD21A1N (Figure 5.3), the R-squared value is 0.66 which means that the relationship and consistency represented by both daytime data sets was much better than the one presented here. However, MAD-1 value is 3.12 °C, which shows a better relationship with a smaller difference between IMIS and MODIS data, and finally the slope value is 0.89, which is almost similar to that of the daytime data with similar linear relationship between the two MODIS and IMIS data sets.

Similar to the day time data, night data also shows a clear similarity in their comparison values, where MYD21A1N (Figure 5.4) R-squared value is 0.67 representing the same relationship and consistency represented by the MOD21A1N data. In addition, MAD-1 value is 3.09 and the slope value is 0.85, meaning that both night data sets show similar results concerning the representativeness of MODIS data as a function of IMIS dataset.

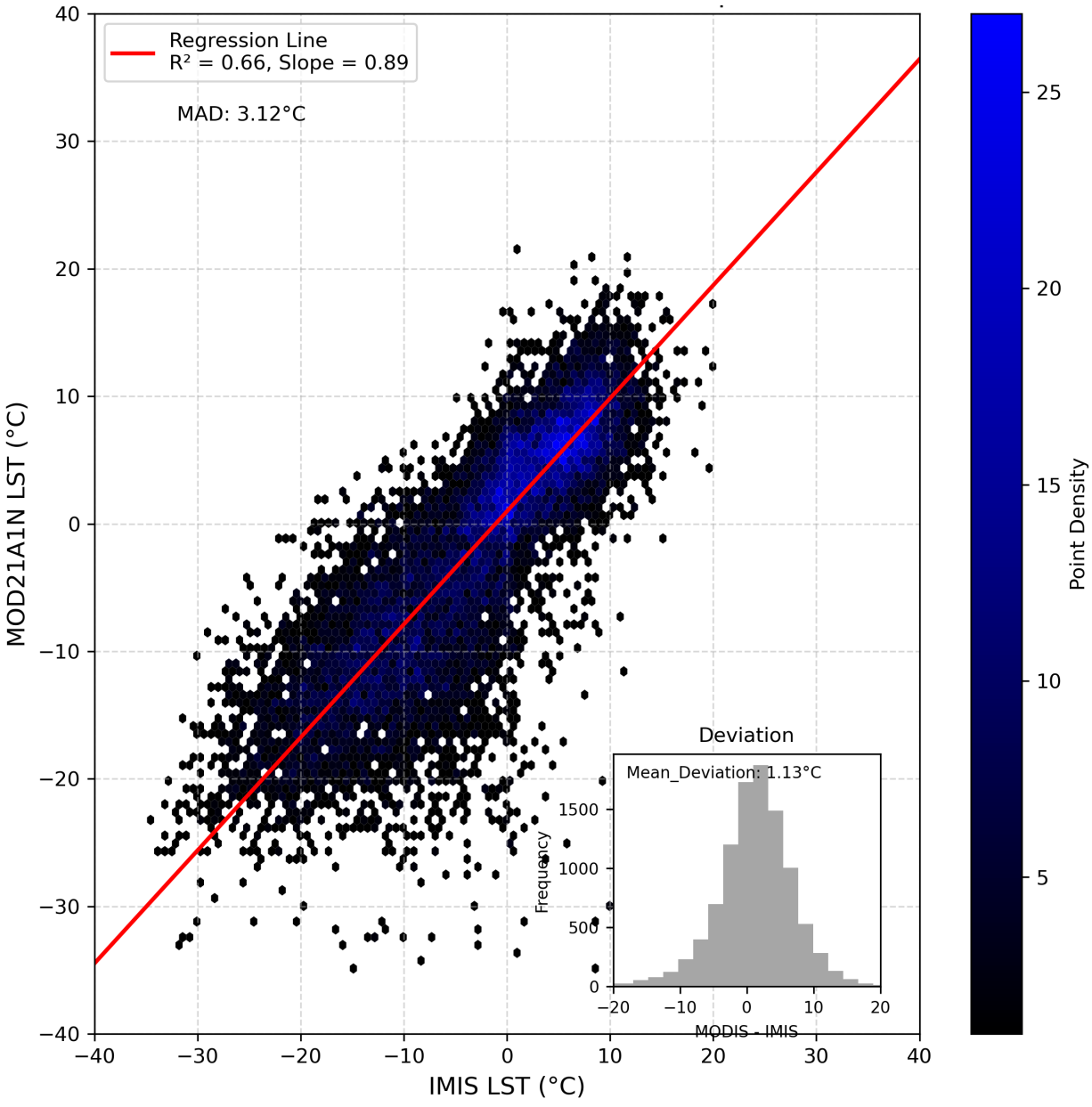

Figure 5.3: The comparison between MOD21A1N and IMIS data measurements with slope, R-squared and Mean Absolute Deviation values clarifying the deviation between the two datasets represented in the histogram.

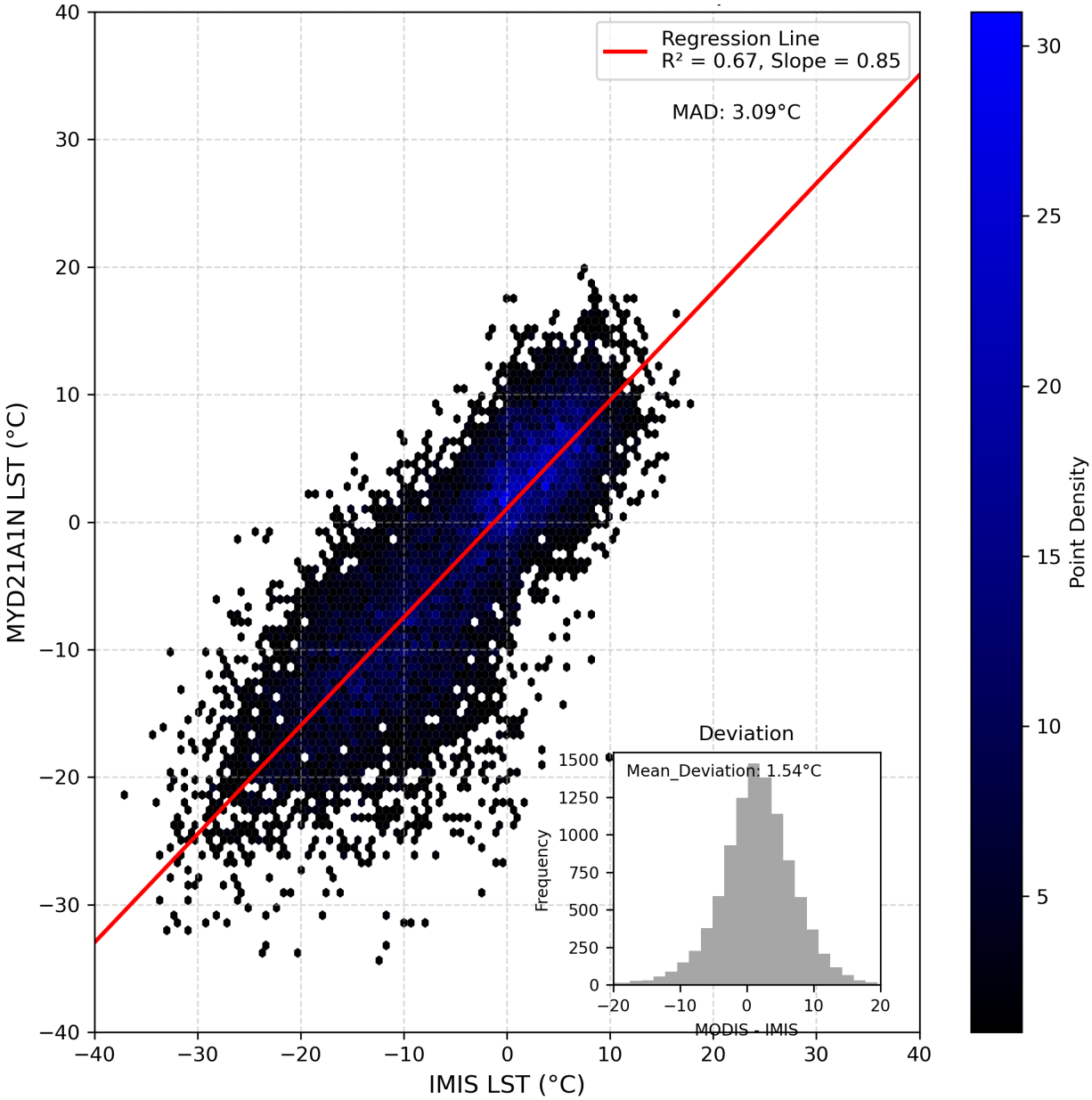

Figure 5.4: The comparison between MYD21A1N and IMIS data measurements with slope, R-squared and Mean Absolute Deviation values clarifying the deviation between the two datasets represented in the histogram.

The four figures (Figures 5.1−5.4) show a histogram with deviation occurs between both MODIS and IMIS datasets at the presented observation time; in addition, to the representation of the mean value of this deviation (Table 5.1), to the represented values, the mean deviation for the MOD21A1D observation time is 1.39 °C, while that is 1.06 °C for MYD21A1D. This means that the representativeness of the MYD21A1D data is slightly better than that MOD21A1D data. This is also clear from the R-squared and MAD-1 values explained earlier. Besides, the mean deviation of the MOD21A1N data is 1.13 °C less than that of MYD21A1N, which is 1.54 °C. Thus, MOD21A1N has better representativeness than MYD21A1N, but this is not clear in the comparison values where the R-squared and MAD-1 are so close, which is explained by the presence of some outliers

that could have affected the final mean deviation value.

Table 5.1: Comparison of Metrics for Different Observation Times (Degree Celsius)

	MOD21A1D	**MOD21A1N**	**MYD21A1D**	**MYD21A1N**
R-squared	0.76	0.66	0.79	0.67
MAD-1	3.60	3.12	3.37	3.09
Slope	0.94	0.89	0.89	0.85
Mean-Deviation	1.39	1.13	1.06	1.54

Results clearly showed good representativeness of MODIS data at the four different observation times of the IMIS ground station data, with some differences being represented by the mean deviation values. Although the representation was clear, yet it was necessary to compare the means of the data (Table 8.1) instead of the actual measurements in order to obtain well explained results. As mentioned in the methodology, four plots comparing the means of the MODIS and IMIS datasets at the four different observation times were created with two comparison values, i.e., the Pearson correlation and the MAD-2.

Figure 5.5 shows the plot and statistics of MODIS and IMIS means data of all stations at MOD21A1D observation time. It is clear from the Pearson's correlation value which is 0.86, that there exists a strong but not perfect positive linear correlation between the two datasets, meaning that whenever one of them changes, the other changes accordingly. However, MAD-2 value, which is represents the whole data over the projected time span is 8.45 °C, showing a unexpected difference between the two datasets, and that is clear also on the plot the existing difference in the visualized standard deviation of the two data.

The same results were presented in the second figure (Figure 5.6) which represents the data at MYD21A1D observation time. The Pearson's correlations value is 0.92 showing a stronger but also not perfect positive linear correlation. While, MAD-2 value is 8.38 °C which is almost similar to MOD21A1D time. The results of daytime observations indicate that the linear correlation of the two datasets is strong, whereas a cleardifference in measurements exists and that might be related to spatial resolution, calibration, viewing angle, or any other natural effects.

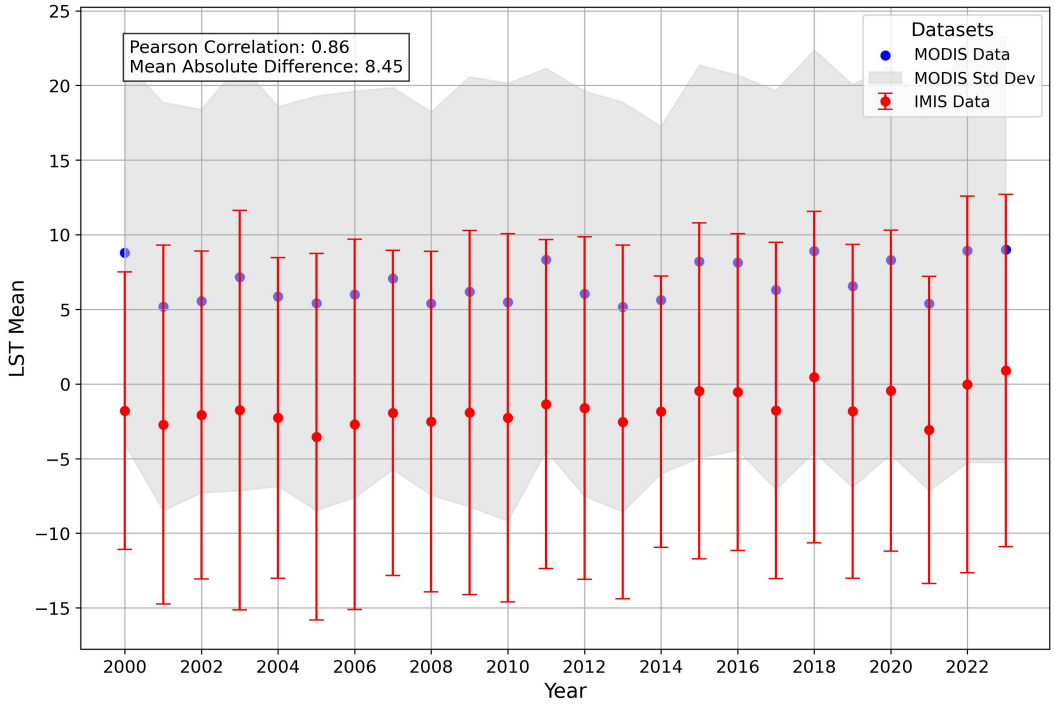

Figure 5.5: Comparison between MOD21A1D and IMIS data measurements' means with Pearson's correlation and mean absolute difference values clarifying the relation between the two datasets.

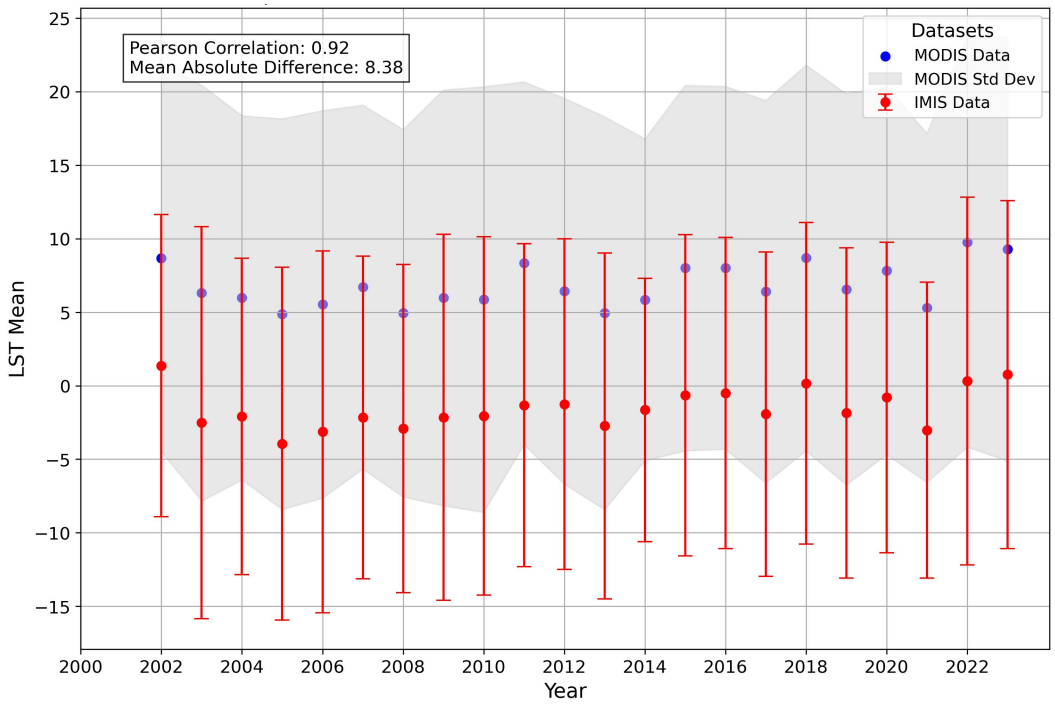

Figure 5.6: Comparison between MYD21A1D and IMIS data measurements' means with Pearson's correlation and mean absolute difference values clarifying the relation between the two datasets.

Nevertheless, the case is often different for data during the night observation times. At MOD21A1N time the results show an almost perfect positive linear correlation (Figure 5.7), where the value of Pearson's correlation is 0.93, which is very close to that of MYD21A1D, and both cannot be considered as a perfect correlation. On the other hand, MAD-2 value is very different, being 3.20 °C, indicating that the measurements from both IMIS and MODIS sources are more representative for each other at this time than in the daytime data.

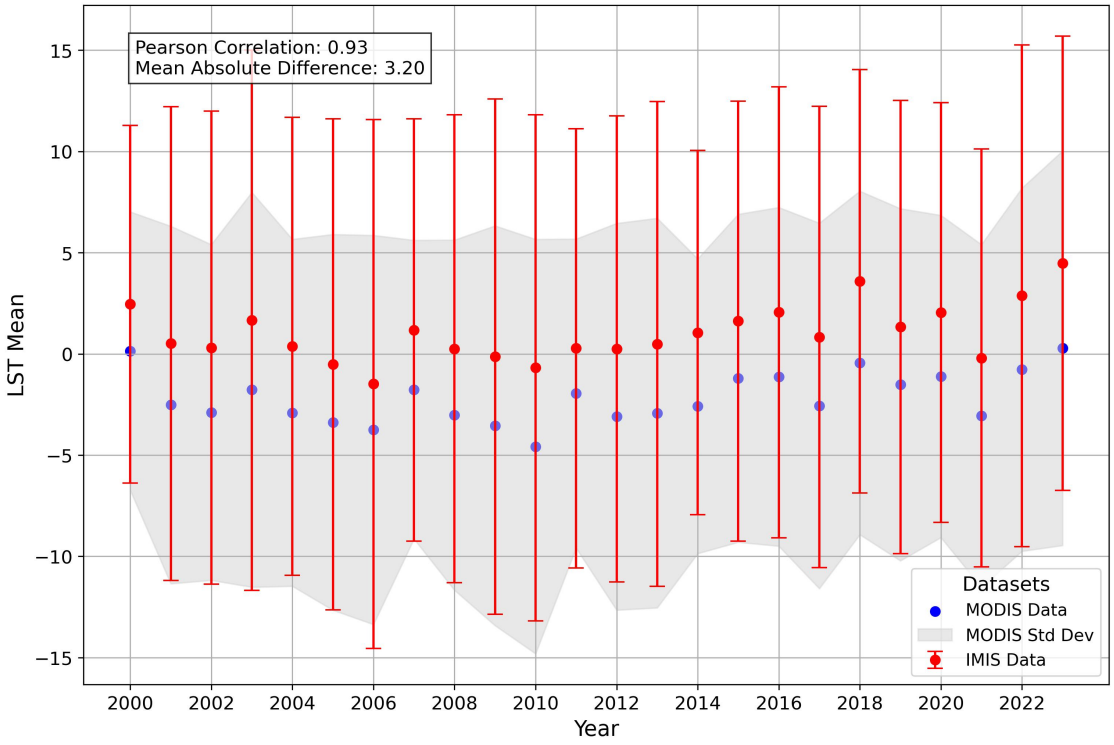

Figure 5.7: Comparison between MOD21A1N and IMIS data measurements' means with Pearson's correlation and mean absolute difference values clarifying the relation between the two datasets.

For MYD21A1N observation time indicative results have been reached (Figure 5.8). The Pearson correlation value is 0.97, which is the best value among all observation times, and it is the closest to a perfect positive linear correlation between IMIS and MODIS LST data. In addition, MAD-2 value is also the smallest among all others, where it is 1.45. This represents the specificity of the measurements between the two datasets and how representative they are for each other.

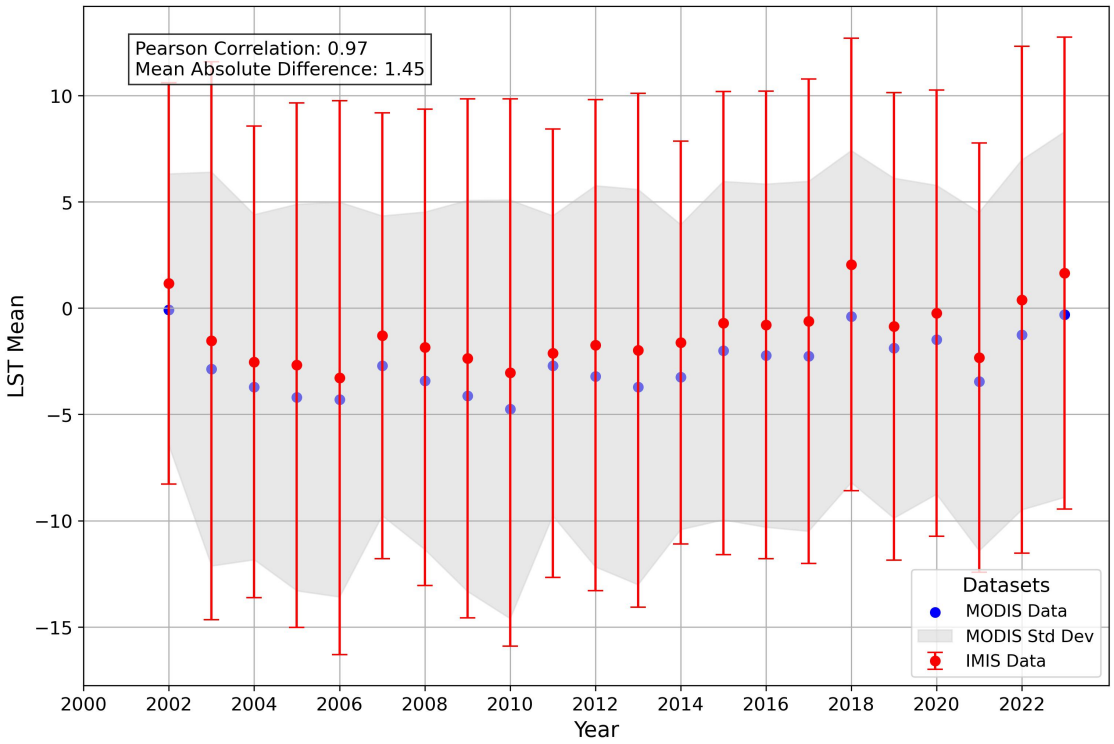

Figure 5.8: Comparison between MYD21A1N and IMIS data measurements' means with Pearson's correlation and mean absolute difference values clarifying the relation between the two datasets.

According to this observation, it is clear that the difference in LST data during the night time is much smaller and better than it during the day time. This suggests that the reason for the difference is natural and not technical, which could be related to the solar influence during the day or the rapid cooling that happens at night, but most likely it is due to atmospheric effects, where the solar radiation dominates, affecting the atmospheric content such as cloud cover, humidity, etc.. This dominance may in turn affect the acquisition of accurate LST; and therefore, by considering all these values (Table 5.2, Table 5.1) of the first and second comparisons, it can be concluded that MODIS and IMIS data have a good representativeness of each other, which is better at night times. With some differences that could be resulted due to atmospheric effects especially during daytime.

Table 5.2: Comparison of LST Means' Metrics for Different Observation Times

	MOD21A1D	**MOD21A1N**	**MYD21A1D**	**MYD21A1N**
Means' Pearson's Correlation	0.86	0.93	0.92	0.97
Means' MAD-2	8.45	3.20	8.38	1.45

5.1.2 MODIS Versus IMIS LST Trends

The analysis and visualization of the actual LST measurements clearly show that there have change during the studied time period. This change, called the LST trend, needs to be investigated and compared similarly to the actual measurements, which helps in approaching beneficial and clear implications.

For this purpose, the two procedures mentioned in the methodology were applied. The first one represents the visualization of the hourly trend of the day for each station as a color scaled figure (i.e., heat map), where each square represents the mean LST trend at each station at each time of the day for the IMIS data (Figure 4.1). The number of used measurements differs from one station to another depending on the availability of valid data but all ranges between 8640 to about 8750 measurements. For other figures representing the four MODIS datasets during their four different observation times (Figures 3.6).

The comparison between these figures was then made using a scatterplot visualization for the available hours considering the time rounding mentioned in the methodology comparing the trends of both datasets at the same time and location. Thus, only hours available in the MODIS data were considered for this comparison, which used MAD-2 and Pearson's correlation for specificity.

For MOD21A1D observation times, 10:00 AM is the first time visualized and compared (Figure 8.4 in the Appendix). It reveals that the Pearson correlation value at this time is 0.05, which is a very small value above zero, indicating that the relationship between the two data cannot be considered a good positive linear correlation nor a negative one. This means that the variations that occur in both data are not related. While, MAD-2 value is responsible to represent the difference between the two studied data is 0.03, which is also very small, representing that the two data are quite close with very small differences that could be caused by the represented outliers that could also be responsible for the small Pearson's correlation value.

In The observation times 11:00 AM and 12:00 PM (Figures 8.5, 8.6 in the Appendix) similar conclusions were reached, where at 11:00 AM the Pearson's correlation value is 0.03 and the MAD-2 is 0.04, while at 12:00 pm, the Pearson's correlation value is 0.14, which is a little higher than the previous two values, but it is still far from 1, leading to the same conclusion, with MAD-2 value of 0.04 °C. it is worth mentioning that not all stations are represented at 12:00 noon due to some reasons that prevented the measurements at that time, such as cloud cover. Having all the measurements and stations could affect the resulting values and the conclusion.

The second observation time of MYD21A1D starting at 11:00 AM (Figure 8.7), where the Pearson's correlation value is -0.14, indicating linear relationship between the trends of the two data as mostly neutral, but it is oriented in a negative direction due to the presence of the minus sign.

However, MAD-2 value is also 0.05, which confirms the neutral relationship between the two data and explains the Pearson's correlation value by the presence of outliers.

Similarly, the same explanation applies for the three other times, 12:00 pm 13: pmand 14:00 pm (Figures 8.8, 8.9, and 8.10 in the Appendix) where the Pearson's correlation values are -0.1, -0.09, and -0.03; respectively. MAD-2 values are also 0.05 for all three timings, confirming the existing neutral linear correlation between the trends of the two datasets.

The previous Figures were the daytime results from both the Aqua and Terra satellites. Regarding the nighttime Terra dataset(i.e., MOD21A1N), it starts at 8:00 PM (Figure 8.11 in the Appendix) when the Pearson correlation value is 0.08, which leads to the same conclusion as for MOD21A1D datasets, and the linear correlation is considered neutral, but positively skewed. In addition, MAD-2 value, which is 0.04, also indicates the similarity of both data, confirming that the neutrality represented by the Pearson correlation value is caused by the presence of outliers.

The same results also were presented at 9:00 pm (Figure (Figure 8.12) in the Appendix) and 10:00 pm (Figure (Figure 8.13) in the Appendix), where the Pearson's correlation value is 0.09 at both times, and MAD-2 value is also 0.04 °C at both times. This presents the same neutrality which is positively skewed and the similarity of the data.

A tiny difference was presented by the data at 11:-00 PM (Figure 8.14 in the Appendix) which leads to the same results with a difference and neutrality is negatively skewed. The Pearson's correlation value is -0.09 and MAD-2 value is the same as before 0.04 °C. This small difference might be due to the fact that not all stations are presented at this time, so that they appear at 11:00 PM after the rounding of time mentioned in the methodology, plus the cloud cover that might had played a role in the absence of measurements.

ForMYD21A1N starting at 1:00 AM(Figure (Figure 8.15) in the Appendix), the Pearson correlation value is 0.11, almost indicating neutral linear relationship, with positive skewness represented more by the higher PC value than in the previous data sets. However, MAD-2 value is still stable in its previous ranges, i.e. 0.04 °C, confirming the similarity of the data. Also, the results of the two other observation times are almost the same, and the Pearson's correlation value at 2:00 AM (Figure 8.16 in the Appendix) is 0.1 and at 3:00 AM (Figure 8.17 in the Appendix) is 0.14. Both values confirm the same neutrality and positive skewness. In addition, MAD-2 value at both times is 0.05 that also drives to the same conclusion of data similarity.

All values are represented in the following tables (Table 5.3), (Table 5.4), facilitating the comparison between the values of different observation times of different datasets. Where these values state a clear similarity between the trends taking place in MODIS data and that in IMIS, during the different observation times of MODIS satellites.

All LST (for IMIS and MODIS)metrics are presented in Tables 5.3 and 5.4 for facilitating the comparative analysis of different observation times from the two sources of datasets. The datasets of from these sources almost imply similarity between the trends in MODIS and IMIS LSTs during the different observation times of MODIS satellites.

Table 5.3: Comparison of LST Trends' Metrics for MOD21A1 Observation Times

	MOD21A1D			**MOD21A1N**			
	10 AM	**11 AM**	**12 PM**	**20 PM**	**21 PM**	**22 PM**	**23 PM**
Pearson's Correlation Value	0.05	0.03	0.14	0.08	0.09	0.09	-0.09
MAD-2 Value	0.03	0.04	0.04	0.04	0.04	0.04	0.04

Table 5.4: Comparison of LST Trends' Metrics for MYD21A1 Observation Times

	MYD21A1D				**MYD21A1N**		
	11 AM	**12 PM**	**13 PM**	**14 PM**	**1 AM**	**2 AM**	**3 AM**
Pearson's Correlation Value	-0.14	-0.1	-0.09	-0.03	0.11	0.1	0.14
MAD-2 Value	0.05	0.05	0.05	0.05	0.04	0.05	0.05

As the detailed analysis of the actual measurements was supported by a general means analysis, trend's analysis is also supported similarly. where the means of trends of the MODIS observation time are plotted as MODIS versus IMIS data. And for deeper and well explained analysis, two different values are calculated, the MAE which is the mean absolute error, that is responsible for the error estimation between the two data sets, and the other value is the precision which is calculated as the standard deviation of the data.

For the first observation time which is MOD21A1D (Figure 5.9), it shows that the MAE value at this time is 0.04. Compared to the examined trends, which lie somewhere between 0.00 and 0.1, this value is considered effective, which means a disagreement of about 40 percent between the two data sets. In addition, the value of the standard deviation is also 0.06, which also indicates some disagreement. The general indication of the values represented by the first observation time, shows a general agreement between the two datasets, with a clear and considerable disagreement, most likely caused by the presented outliers that reached high values (between 0.25 and 0.3) mainly in IMIS data, facing very low values represented by MODIS, which remained below 0.1. And knowing that MAE is very sensitive to extreme values (outliers), this could have played an important role in influencing it and the value of the standard deviation. This leads to the indication of the mentioned considerable discrepancy between the two datasets.

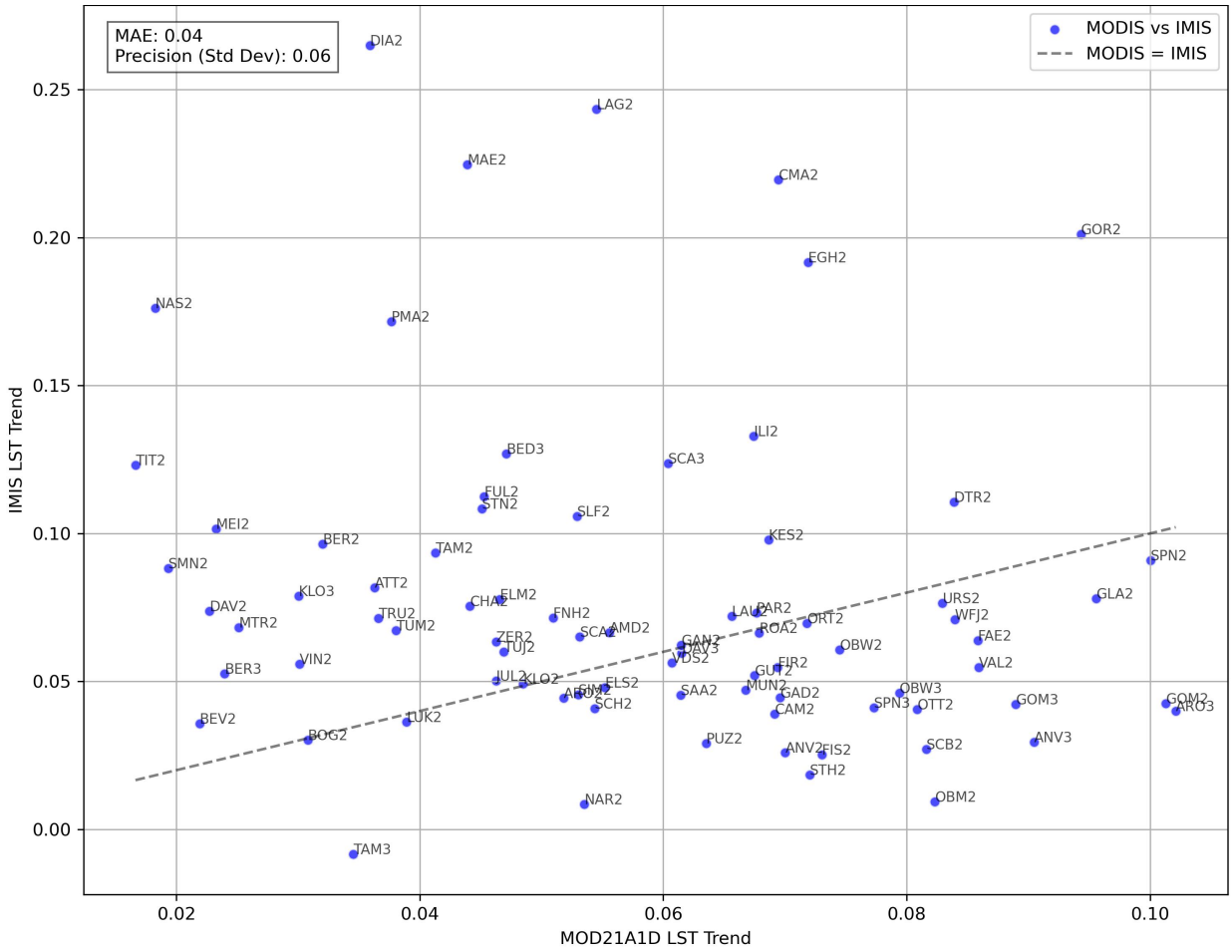

Figure 5.9: Comparison between MOD21A1D data trends' means with that of IMIS data including MAE and standard deviation values.

The results of the second observation time MYD21A1D (Figure 5.10) confirm the indication of the first observation time. So that the MAE value at the second time is 0.05 and the standard deviation is 0.07, this slight increase in the values came after the increase that appeared in the trends represented by the outliers, which exceeded the values of the first observation, reaching values above 0.3. This confirms that the general agreement that appears between the two data sets is correct and that the presented disagreement is a false implication given and modified by the presence and the change of some outliers.

The results of the second observation time MYD21A1D (Figure 5.24) confirm the indication of the first observation time. The MAE value at the second time is 0.05 and the standard deviation is 0.07, this slight increase in the values occurred after the increase in the trends represented by the outliers, which exceeded the values of the first observation by reaching values above 0.3. This confirms that the general agreement appears between the two datasets is correct, and the presented disagreement is a false implication given and modified by the presence and the change of outliers.

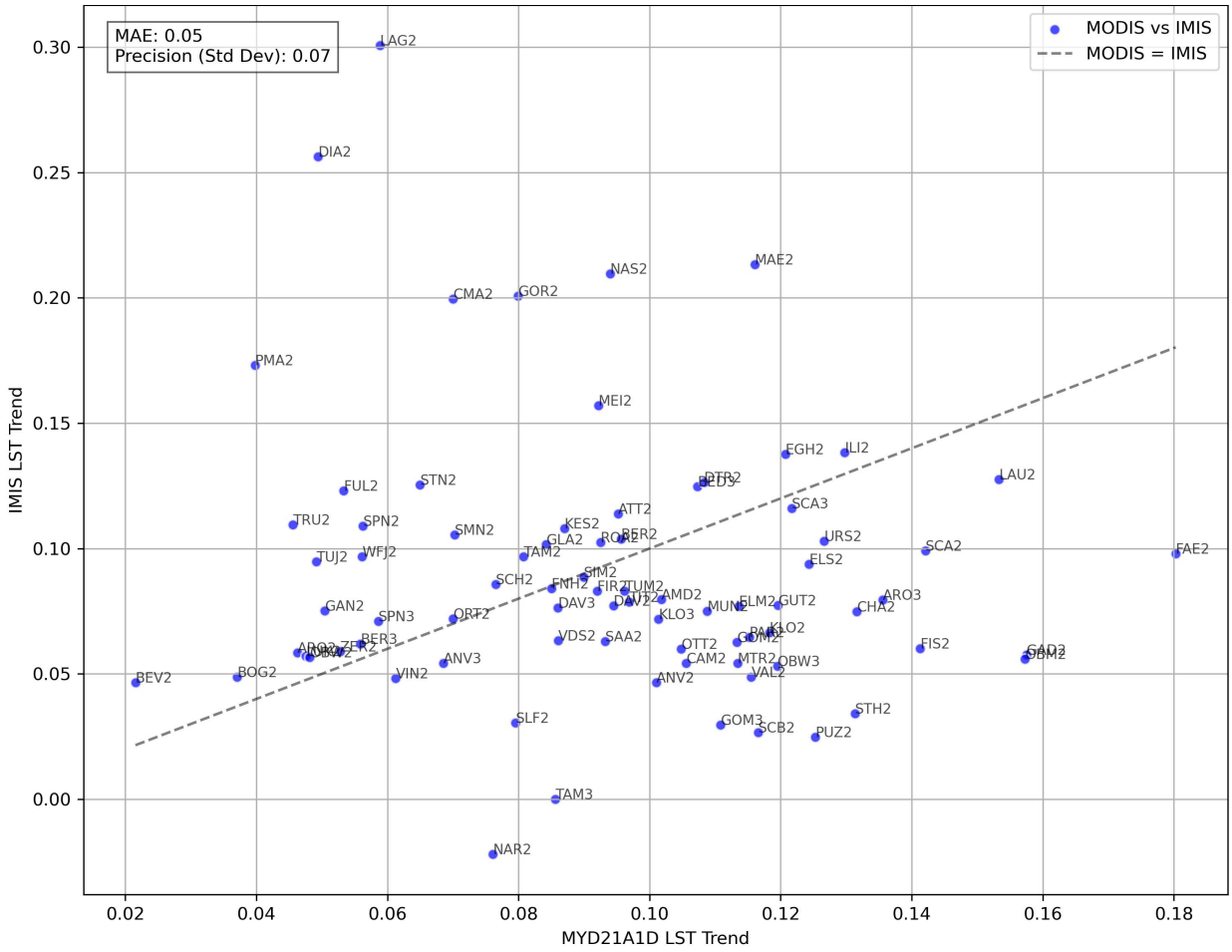

Figure 5.10: Comparison between MYD21A1D data trends' means with that of IMIS data including MAE and standard deviation values.

Similar results are presented in the night observation times. Where in MOD21A1N (Figure 5.11) the MAE value is 0.04 and the standard deviation is 0.05, with one outlier exceeding 0.3 in IMIS trends and the others mostly below 0.2. In addition, in the MYD21A1N (Figure 5.12), the MAE value is 0.05, and the standard deviation is 0.07, also with one outlier above 0.3 but with more of them above 0.2.

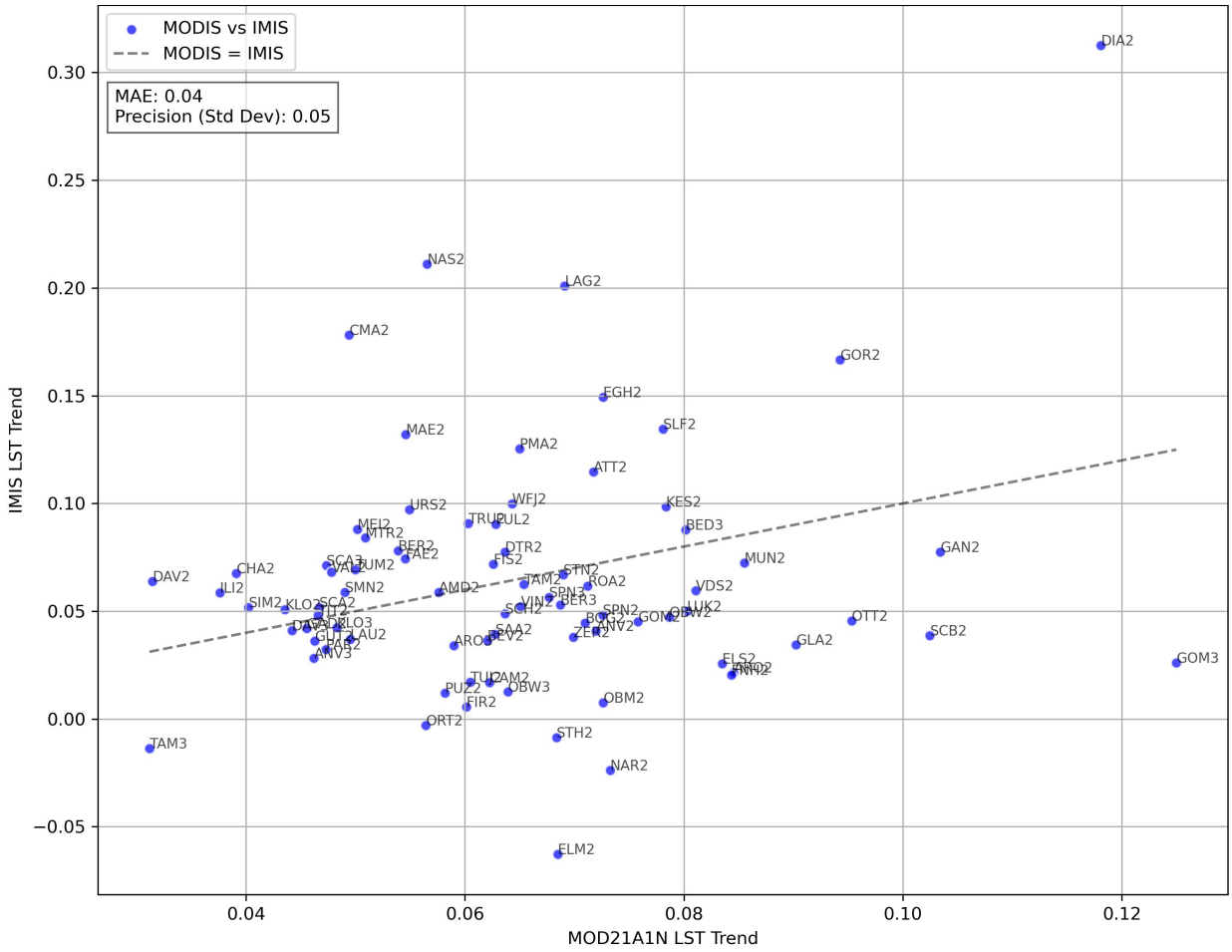

Figure 5.11: Comparison between MOD21A1N data trends' means with that of IMIS data including MAE and standard deviation values.

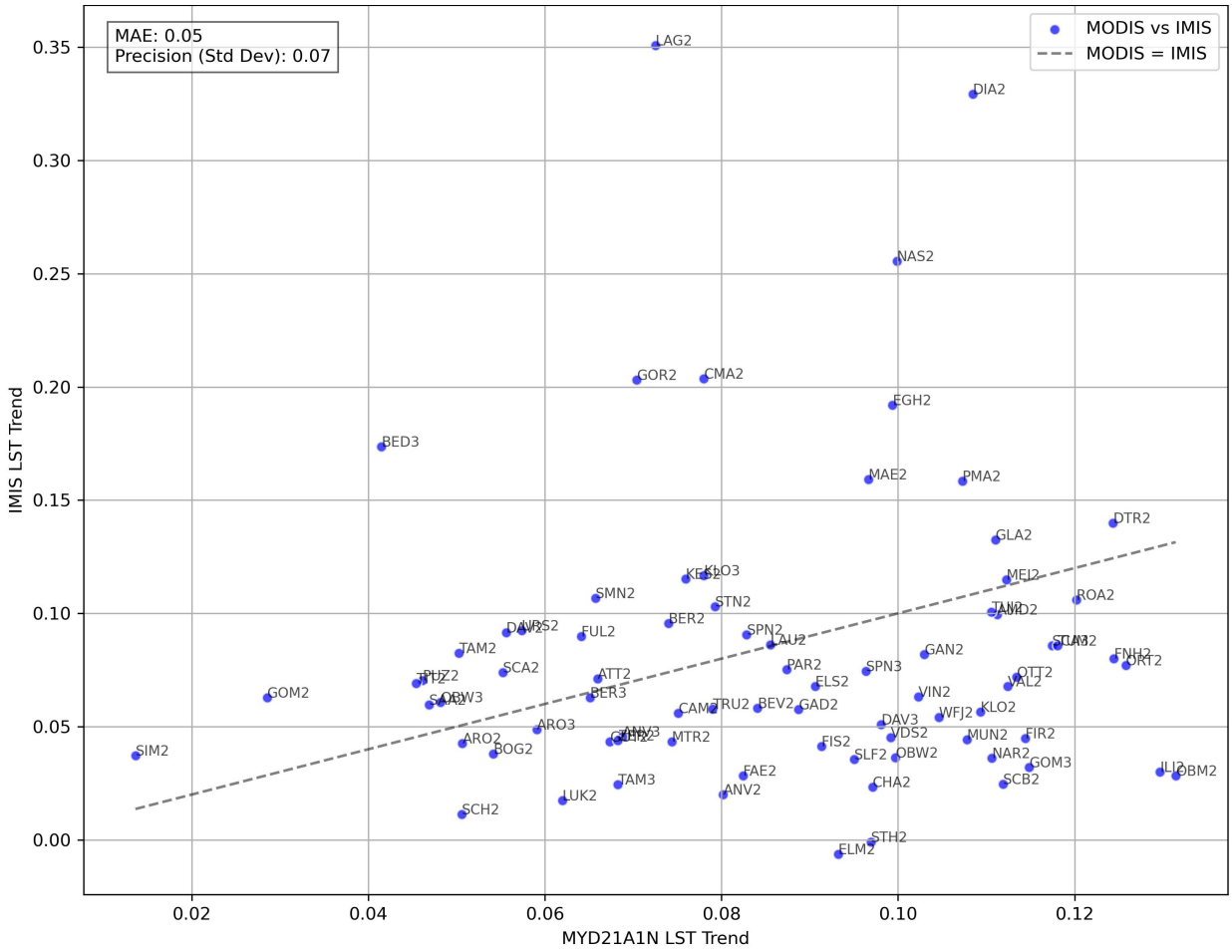

Figure 5.12: Comparison between MYD21A1N data trends' means with that of IMIS data including MAE and standard deviation values.

As an overall result taken for the MAE and standard deviation values (Table 5.5), there is a clear general agreement between the two data sets at all observation times. This agreement is affected by the presence of outliers that differ in their values from one observation time to another, leading to some disagreements represented by the MAE and the standard deviation values. The same final result could be applied as a result of the whole comparison of the trends, where the detailed hourly comparison and the general mean's comparison lead to the same mentioned conclusion.

Table 5.5: Comparison of LST Trends' Metrics for Different Observation Times

	MOD21A1D	**MOD21A1N**	**MYD21A1D**	**MYD21A1N**
MAE Value	0.04	0.04	0.05	0.05
Standard Deviation Value	0.06	0.05	0.07	0.07

5.2 Trends at MODIS Observation Times Versus Overall Trend

Since there are LST trend changes between different times, it is preferred to represent the overall trend with respect to the trend of each observation time(Figure 8.1). This approach was used to find out the most representative observation time for overall trends occurring in the data.

MOD21A1D dataset, which represents the day observation time of the Terra satellite, seems to be in good agreement with the overall trend (Figure 5.13). It shows a small difference. Thus, trends at MOD21A1D time appear to be slightly higher than those represented by the overall curve. However, the Pearson's correlation value is 0.91, which indicates perfect correlation between the two data with almost small difference mentioned. This is also represented by MAD-2 value (0.03). Overall, LST trends at MOD21A1D time has a good representation for the entire trend of the data.

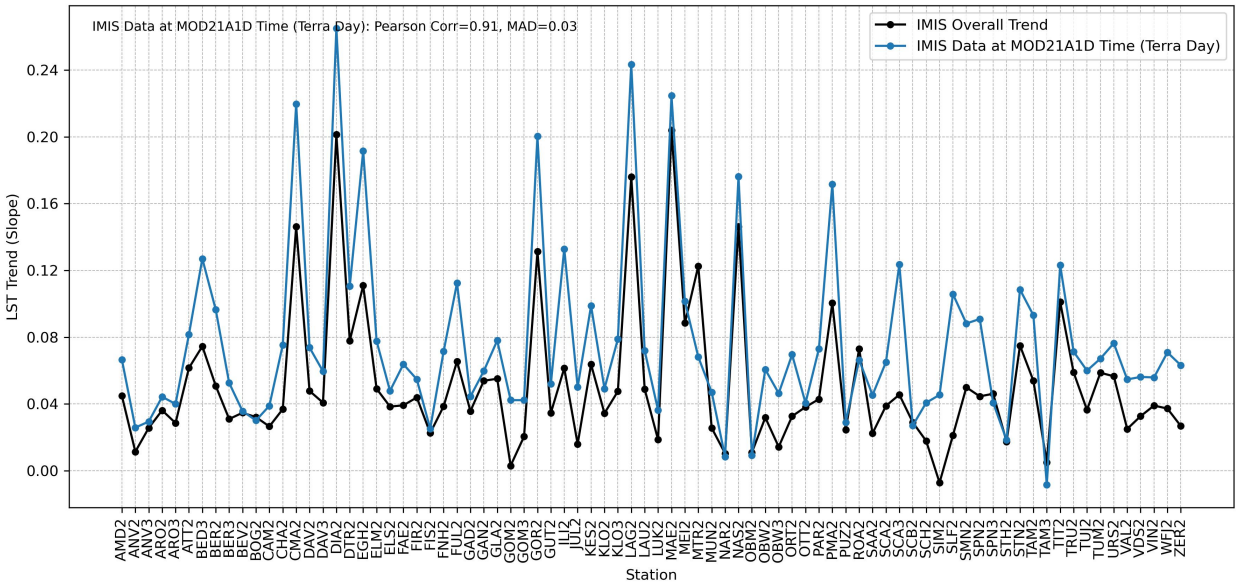

Figure 5.13: Representativeness of IMIS LST trend at MOD21A1D times for the overall trend of the data over the whole study period including MAD-2 and Pearson's correlation values.

MOD21A1N and MYD21A1N (Figures 5.14 and 5.15) represent the night observation time of MODIS Terra and Aqua satellite; respectively; however, they do not seem to agree with the overall trend. There is a clear difference between the two datasets and the overall trend, where the curves seem to have different variation. In addition, troughs and peaks in the data at MODIS observation times curves do not appear in the overall trend. Moreover, Pearson's correlation value, which is 0.35 for both MOD21A1N and MYD21A1N figures, shows a very low value that indicates a clear disagreement between the represented datasets. With the MAD-2 value, which is 0.04 for MOD21A1N and 0.05 for MYD21A1N shows a slight disagreement.

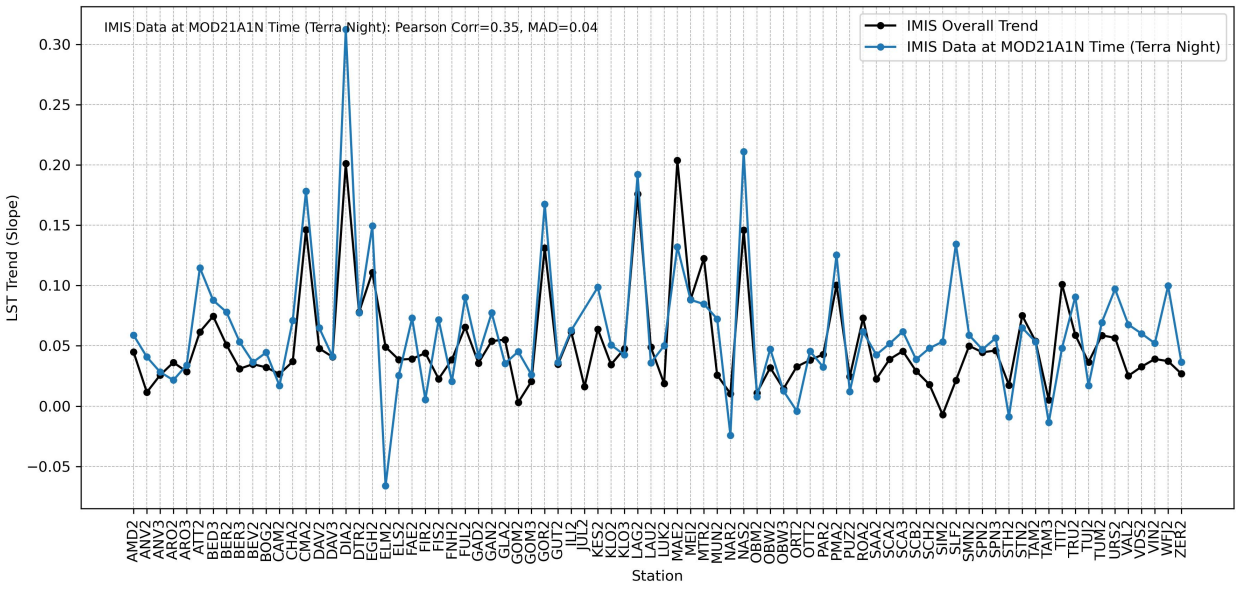

Figure 5.14: Representativeness of IMIS LST trend at MOD21A1N times for the overall trend of the data over the whole study period including MAD-2 and Pearson's correlation values.

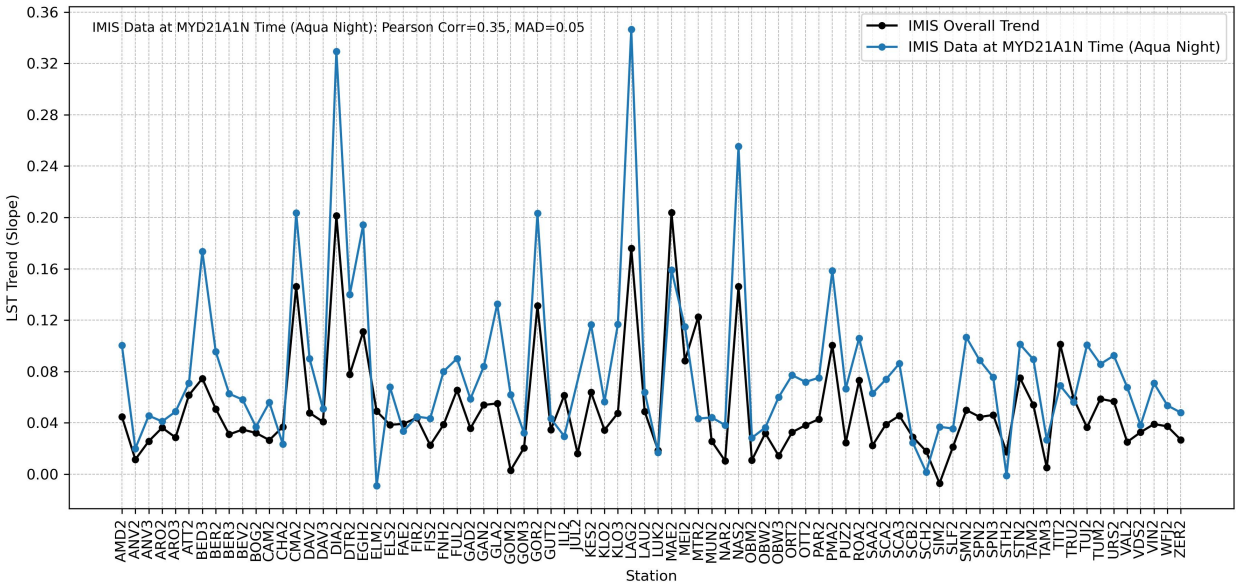

Figure 5.15: Representativeness of IMIS LST trend at MYD21A1N times for the overall trend of the data over the whole study period including MAD-2 and Pearson's correlation values.

Similarly, the trend of MYD21A1D represents the day observation time of MODIS Aqua satellite, and it disagrees with the overall trend (Figure 5.16). Also, the difference between the two datasets is clear where MYD21A1D curve appears to be higher than that of the overall trend with some fluctuations. The Pearson's correlation value is 0.39 which is also considered as low values indicating disagreement between the two datasets. The MAD-2 value is 0.05 which is a bit considerable in comparison with the overall trends' values represented by the data.

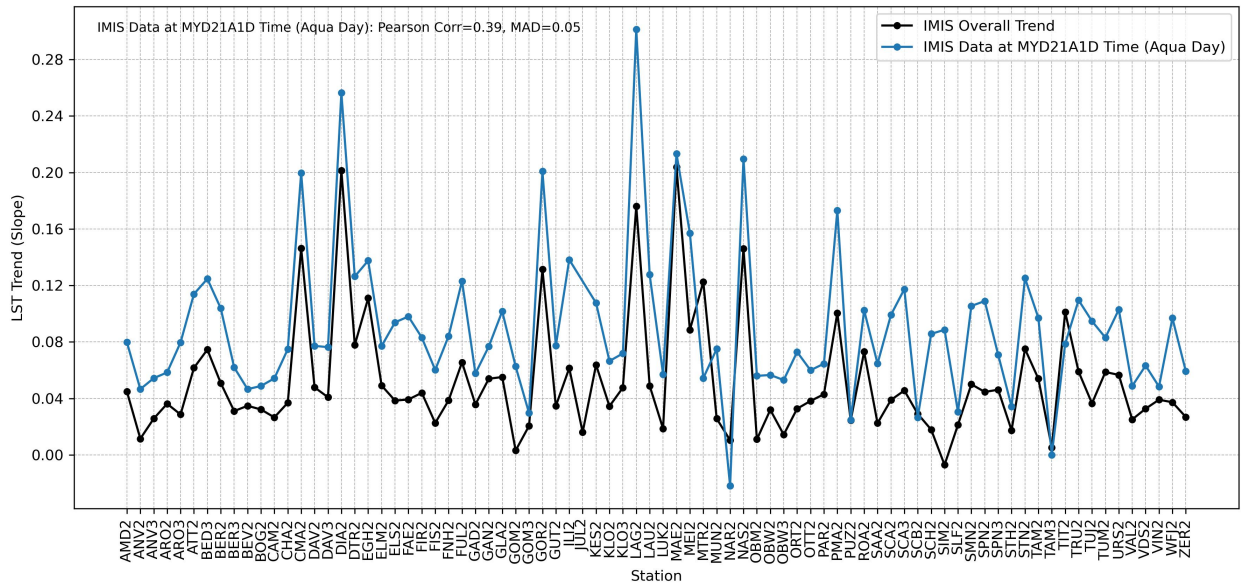

Figure 5.16: Representativeness of IMIS LST trend at MYD21A1D times for the overall trend of the data over the whole study period including MAD-2 and Pearson's correlation values.

Resulted values (Table 5.6) of applied the comparison reveals that the best representative trend for the overall trend of the whole data is the trend of the time limits of the MOD21A1D dataset, which is the daytime dataset of the MODIS Terra satellite. The Pear-son's correlation values is the highest (0.91) and MAD-2 value is the lowest (0.03).

Table 5.6: Comparison of Metrics of LST Trends at Different Observation Times Versus Overall Trend

	MOD21A1D	**MOD21A1N**	**MYD21A1D**	**MYD21A1N**
Pearsons' Corellation Value	0.91	0.35	0.39	0.35
MAD-2 Value	0.03	0.04	0.05	0.05

5.3 Environmental and Sensor-related Influences on LST

There are variables (i.e., influences) that might cause change in the LST measurements and trends. These influences must be identified in order to determine their impact of the calculated LST data.

5.3.1 Elevation Effect

Elevation above sea level is one of the most attractive variables that could influence LSTs notably that air temperature decreases with altitude. The approach mentioned in the methodology was applied to investigate if elevation has any effect on LST. This was analyzed in the scatter plot (Figure 5.17) which represents the variation of the mean LST trends as a function of the changes in station's altitude. Results does not show any relation between the elevation of various IMIS stations and the LST trend means. However, there is clear density of plots below 0.05 LST trend means between 2000 and 2800 m elevation (Figure 5.17). .

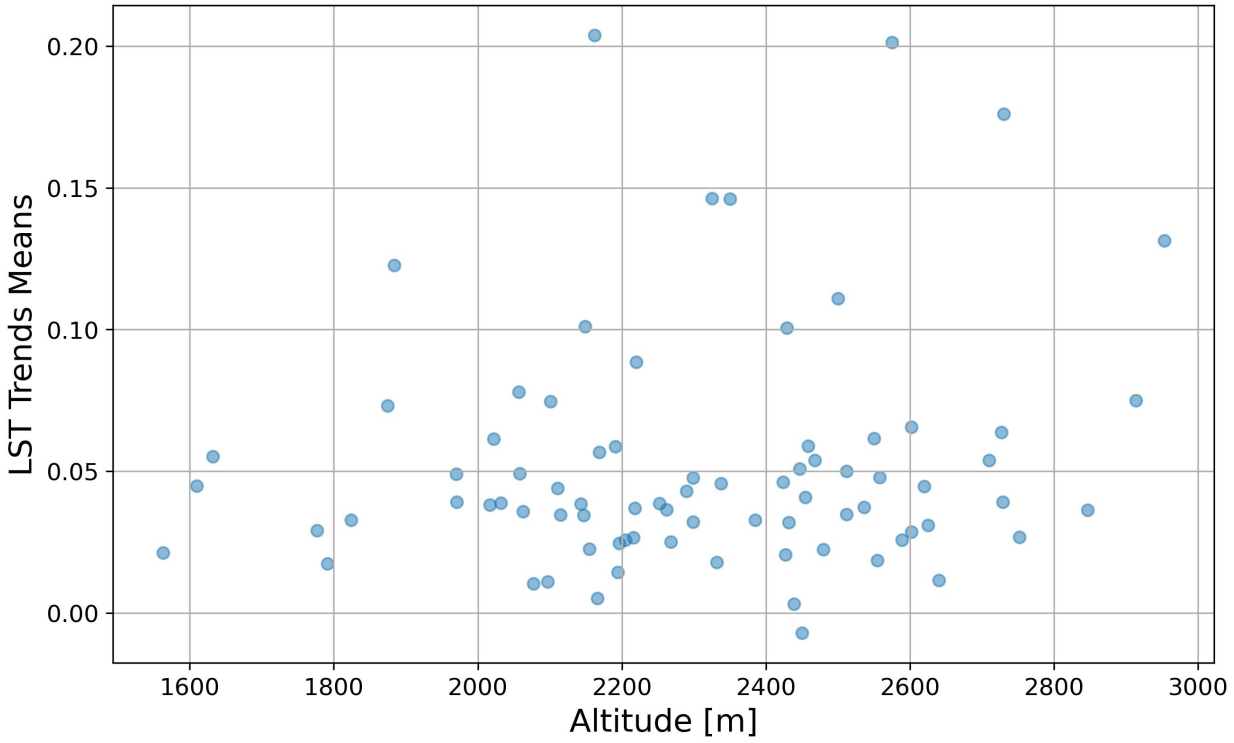

Figure 5.17: Change of mean LST trends as a function of station's elevation variation.

5.3.2 Aspect Effect

The topographic aspect is also considered as one of the causes that impacts LST trends. The same graphical comparison (scatter plot) made with elevation was also made between LSTs' trends and aspects (Figure 5.18), with the difference that the aspects are combined as bins on the x-axes due to their random distribution among different stations. The resulted curve does not show any

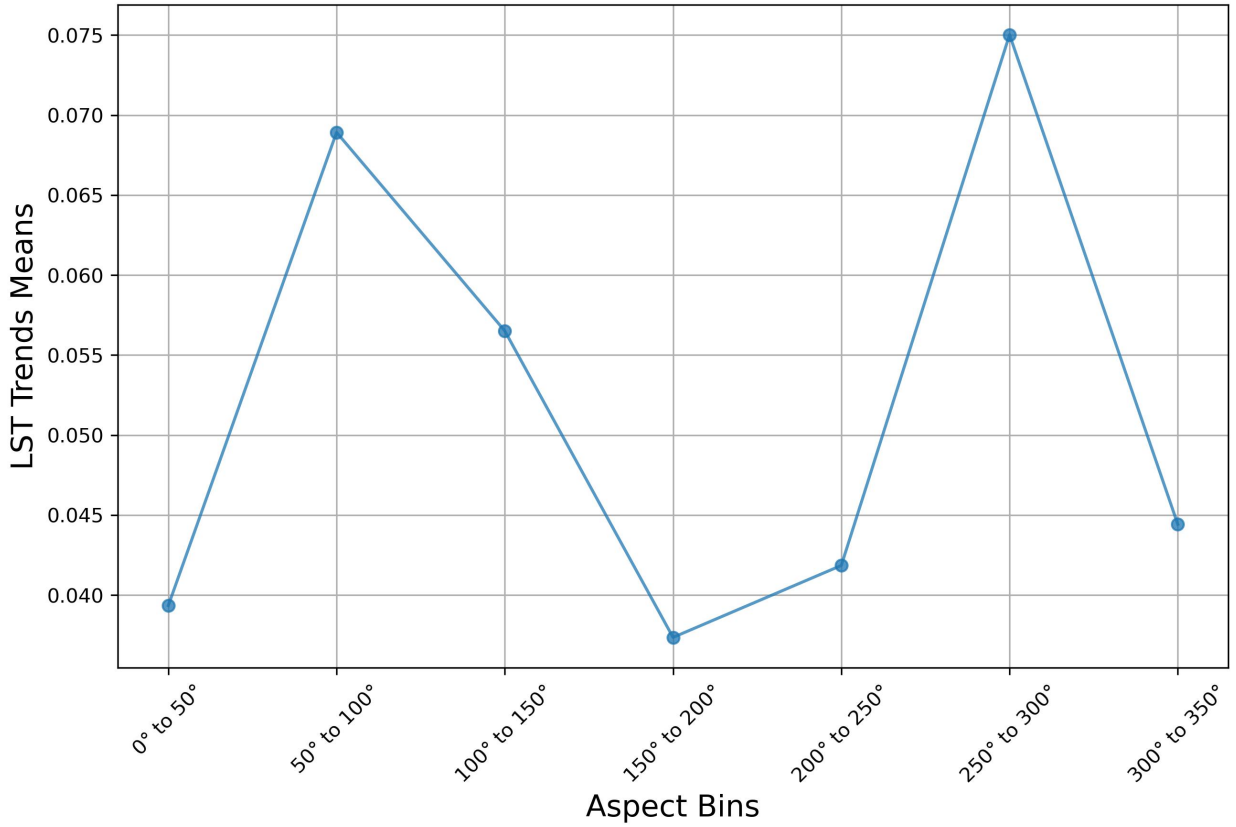

Figure 5.18: Change of mean LST trends as a function of station's aspect variation.

relationship between the change in LST s' trends and the change in station aspect. This may be attributed to the fact that the influence of the other relevant factors can make much impact that minimize the aspect impact.

5.3.3 View Angle Effect

For the retrieved MODIS LST data, and due to the orbital change, it is not feasible to get the trends of each location at each observation time with the same view angle. For this reason, the different view angles may give erroneous results and this will actual MODIS LST measurements. Therefore, scatter plots were generated for each station (e.g. AMD2 in Table 8.2 and at different observation times). In addition, the same scatterplot was generated for the means' average of all stations (Figure 5.19, 5.20, 5.21, and 5.22), which helps to draw a general and comprehensive conclusion.

Therefore, scatterplot show the following results for various observation times, LST and the view

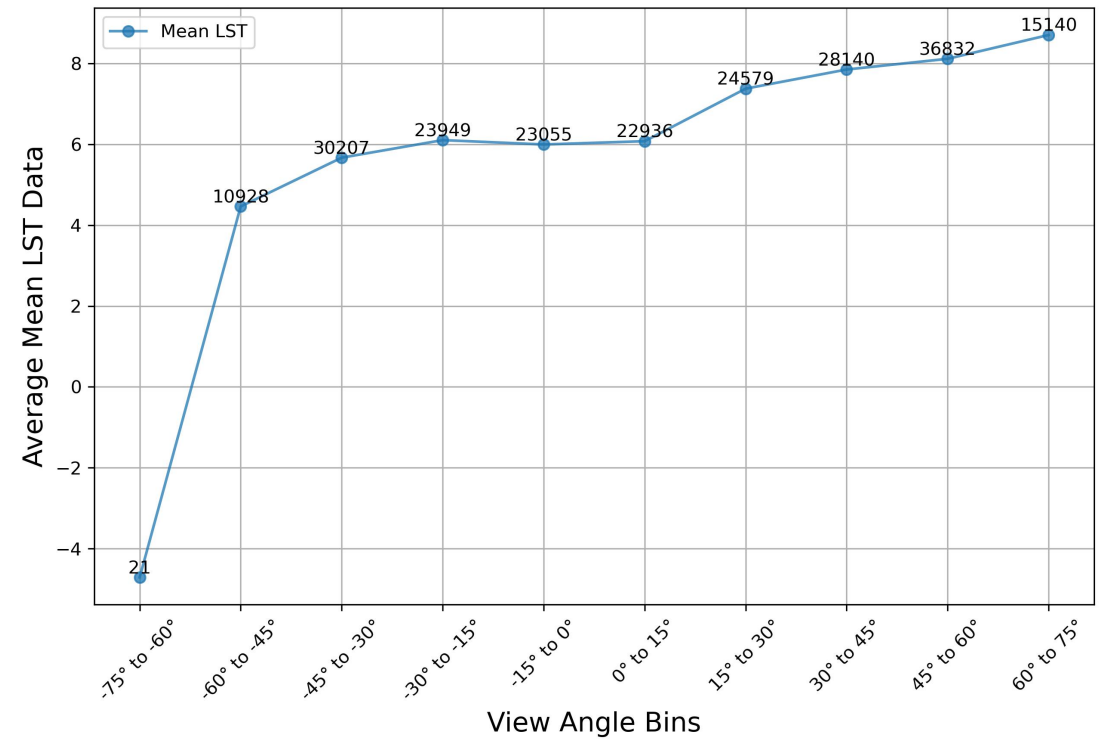

Figure 5.19: Change of LST as a function of view angle variation at all stations at MOD21A1D observation time, showing the nubmber of observations at each view angle.

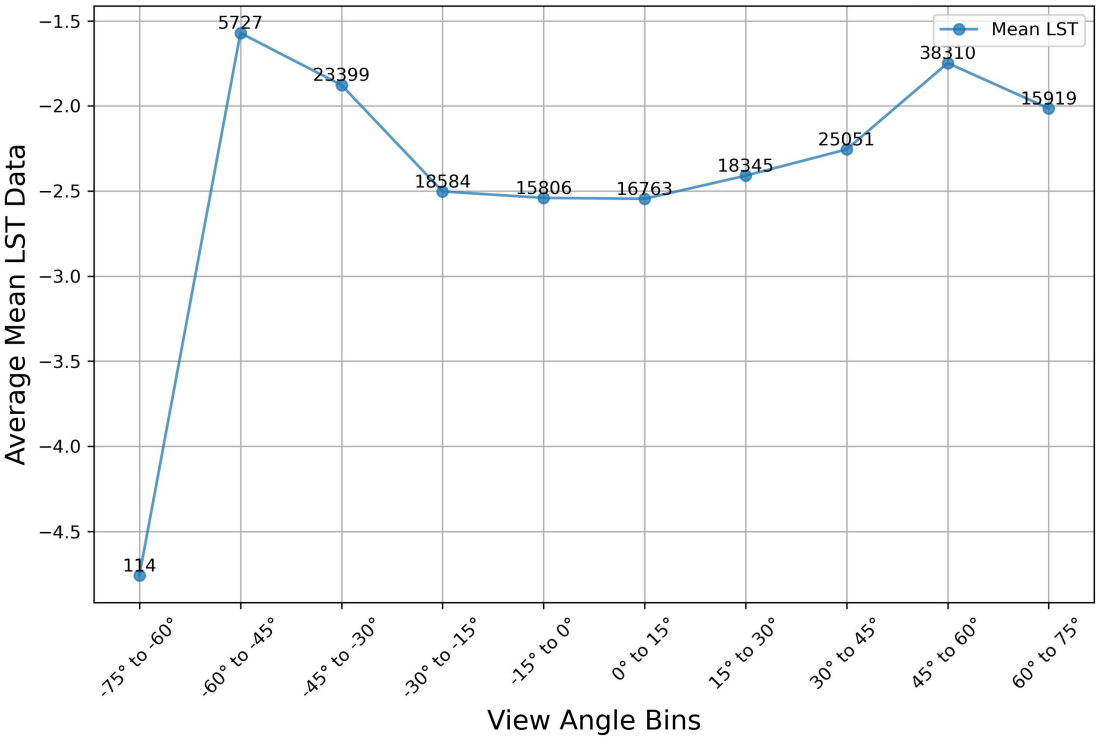

Figure 5.20: Change of LST as a function of view angle variation at all stations at MOD21A1N observation time, showing the nubmber of observations at each view angle.

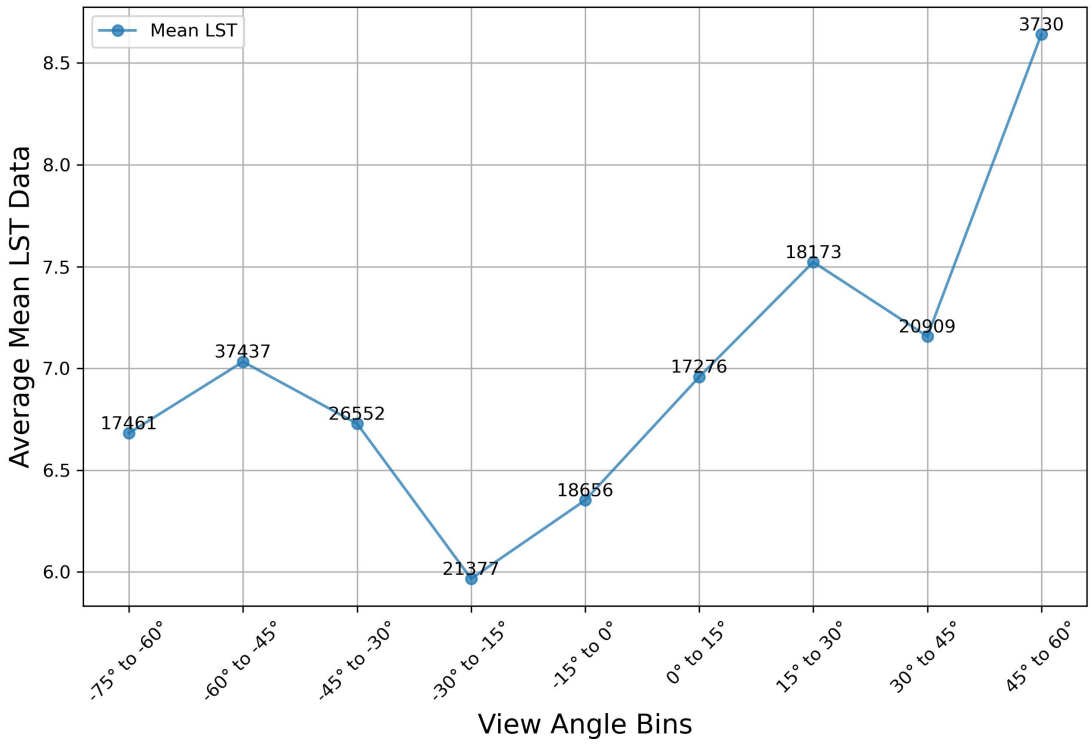

Figure 5.21: Change of LST as a function of view angle variation at all stations at MYD21A1D observation time, showing the nubmber of observations at each view angle.

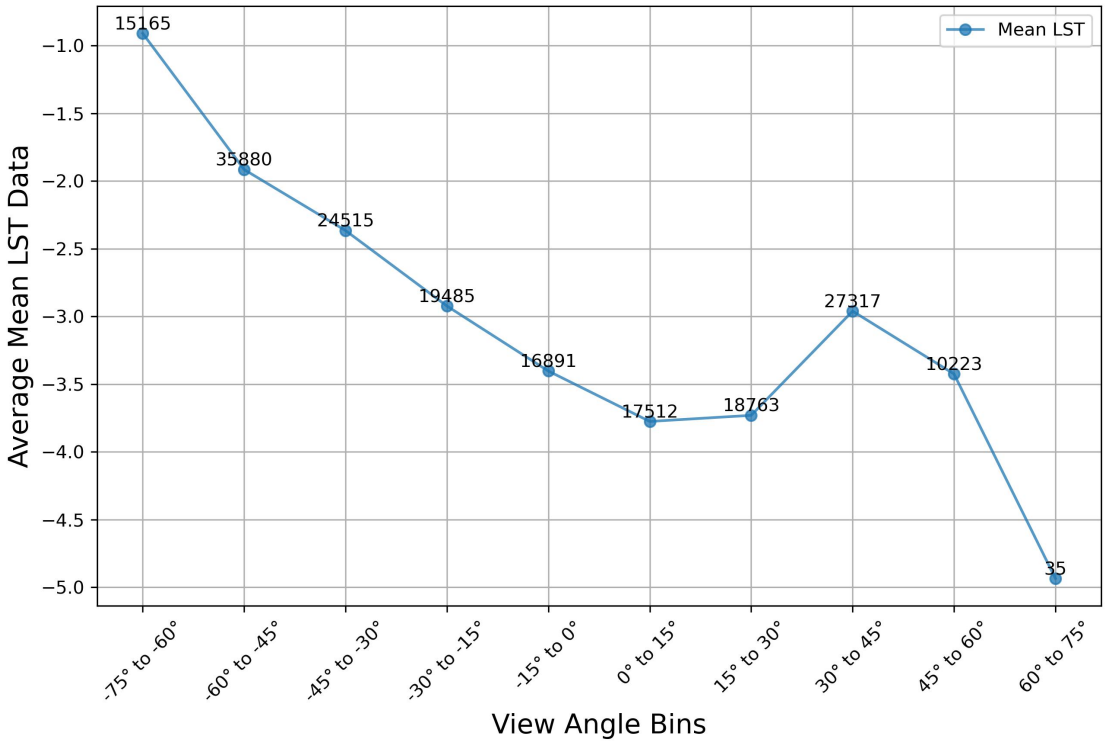

Figure 5.22: Change of LST as a function of view angle variation at all stations at MYD21A1N observation time, showing the nubmber of observations at each view angle.

angles:

- MOD21A1D: Sharp increase (about 3°) in LST with positive view angle (0° to 75°), beside a decrease (about 2°) with negative view angle (0° to -75°).
- MOD21A1N: Slight increase (about 0.5°) in LST with positive view angle, and slight increase (< 1°) with negative view angle.
- MYD21A1D: There is no define behavior between LST and the view angle.
- MYD21A1N: Sharp increase (> 3°) in LST with negative view angle, besides undefined trend of LST with positive view angle.

5.4 Landsat Implications

As mentioned in the methodology, a statistical and visualization process was applied to understand the representativeness of the Landsat observation time of the total IMIS LST measurements compared to that of MODIS. The five observation times were visualized on a plot representing the mean LST at all hours of the day taken from the IMIS measurements. It (Figure 5.23) shows that MOD21A1D observation time is from 9 AM to 12 PM, MOD21A1N from 8 PM to 11 PM, MYD21A1D from 11 AM to 2 PM, MYD21A1N from 1 AM to 3 AM, and Landsat from 9:45 AM to 11:30 AM, taking into account the time rounding mentioned in the previous methods.

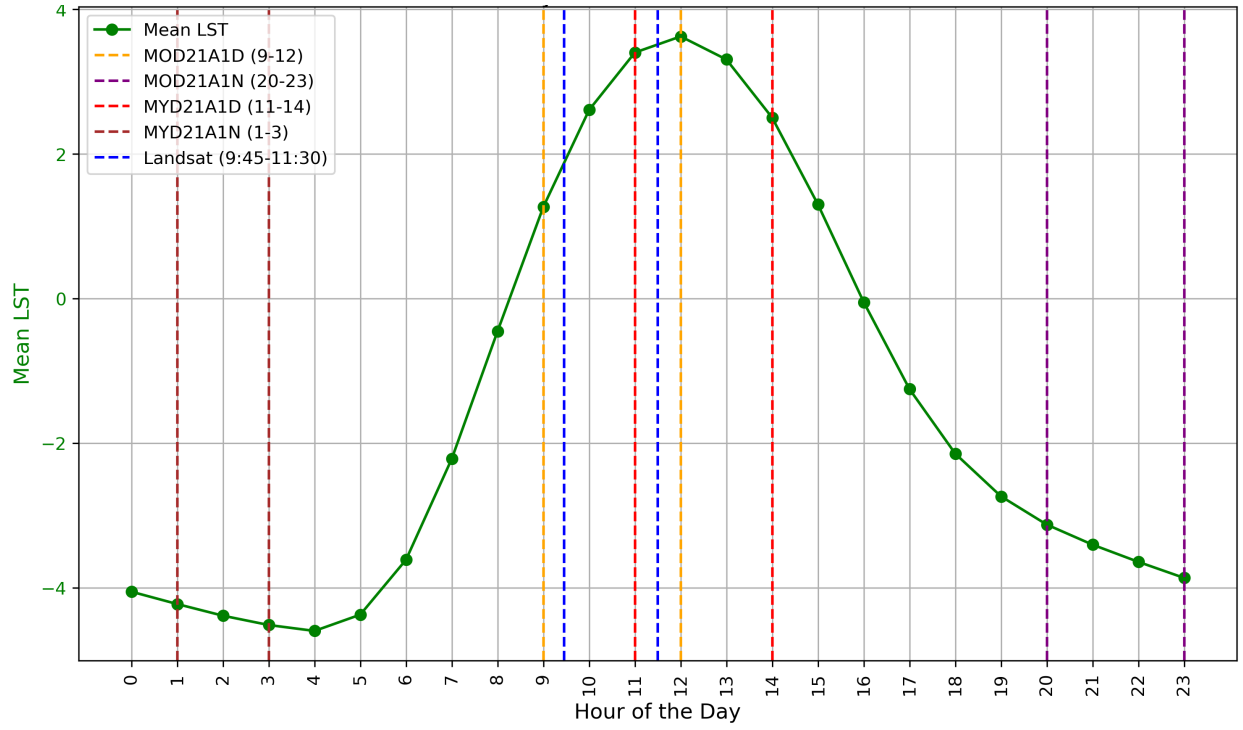

Figure 5.23: IMIS mean LST during hours of the day of all stations over the whole study period with MODIS and Landsat observation times marked with respect to the IMIS curve.

The overall mean of IMIS data was then calculated and found to be -1.14 °C. In addition, the statistics (Table 5.7 and Table 5.8) included the time window means that include the means of IMIS

data during the five observation times, as well as the mean difference between each observation time and the overall mean; in addition to the count based representation that shows the percentage of data included in each time window from the total data.

	MOD21A1D 9-12	MOD21A1N 20-23	MYD21A1D 11-14
Time Window Mean	2.43	-3.39	3.45
Mean Difference with Overall (-1.14 °C)	3.87	1.95	4.89
Count-Based Representation (%)	12.5	12.5	12.5

Table 5.7: Representativeness of different MODIS observation times for the overall LST mean of all stations during the daytime hours over the whole study period in IMIS data.

	MYD21A1N 1-3	Landsat 9:45-11:30
Time Window Mean	-4.31	3.01
Mean Difference with Overall (-1.14 °C)	2.86	4.45
Count-Based Representation (%)	8.33	8.33

Table 5.8: Representativeness of different MYD21A1 and Landsat observation times for the overall LST mean of all stations during the daytime hours over the whole study period in IMIS data.

The time window mean is 2.43 °C for MOD21A1D observation time, with a difference of 3.87 °C from the overall mean, and its count-based representation value is 12.5% from the overall measurement count. The mean of MOD21A1N observation time is -3.39, with a mean difference of 1.95 from the overall mean, and its count-based representation value is similar to that of MOD21A1D, which is 12.5%. For the MYD21A1D observation time, the time window mean is 3.45 °C, resulting in a mean difference of 4.89 °C for the overall mean; and similarly, the count-based representation value of MYD21A1D is 12.5%.

The different count-based representation values were calculated for the remaining two observation times. Thus, the mean LST of the MYD21A1N observation time is -4.31 °C with a mean difference of 2.86 °C from the total, but the count-based representation values are 8.33%. The statistics of the Landsat observation time shows that its mean is 3.01 °C with a mean difference of 4.45 °C, and a count-based representation value similar to that of MYD21A1N which is 8.33%. All statistics were helpful for understanding the representativeness of the five different satellite observation times for overall IMIS measurements.

6 Discussion

Recently, there is significant dependence on remote sensing platform for broader implications in acquiring geospatial data, such as CHIRPS, TRMM, GPM, ERA5, etc. This is less time-consuming and can provide data which is lacking into the available records, data with uncertainty, or data with difficulty to be measured. However, the acquired data from remote sensing must be credible to be utilized for further analysis, and this data is often compared with data taken from ground-based stations to assure its certainty, like the case in this study where the main objective is to investigate the correspondence between satellite data (i.e. MODIS LST) and the datasets retrieved from IMIS ground-based stations for the Swiss Alps, the majority of this work implies a comparative analysis between the two data sources. The positive agreement will motivate the use of satellite data; especially where ground stations are absent or where rugged topography dominates. The analytical methods used in this research can be extended to other types of satellite imagery with more distinctive spatial signatures.

Within the context of the results from this study, LST is not the same as the air temperature which is mentioned in the daily weather reports, and it varies throughout the year. Thus, LST is monitored because the warmth rising off Earth's landscapes influences weather and climate patterns. In addition, LST is a key indicator of the Earth surface energy budget, and its implications are required for hydrology, meteorology, and climatology. It has fundamental importance to the net radiation budget at the Earth surface and to monitoring the state of crops and vegetation, as well as an important indicator of both the greenhouse gases (GHGs) effect and the energy flux between the atmosphere and ground (Becker and Li, 1995).Many studies investigate the trends' variations exist in LST ground stations data, which is usually a key information for studying many relevant topics. For instance, Wei et al., 2021 analyzed the LST variation in the agricultural pastoral ecotone of northern China from 2003 to 2020, and Xing et al., 2020 examined the year-to-year variations of LST under clear-sky conditions for the whole world based on ATC model" (Li et al., 2022). While many researchers have used MODIS LST products to investigate temperature trends, only a few have evaluated the reliability of these trends (Xu, 2023).

6.1 MODIS Versus IMIS Data Comparisons

Results showed a similarity between MODIS Terra and Aqua whether for nighttime or daytime measurements when compared with IMIS data. However, the spread shape shows a clear spread of the MODIS data with highest LST, which might be attributed to temperature climax and differentiation during the day, but this was not marked during the night time when temperature difference is often limited. This shape also appeared in a similar comparison between the same IMIS data and different Landsat LST observations during a different study period (Gök et al., 2024) ; and this was explained in relation to differences in spatial resolution and the existence of snow cover with dissipated snow patches due to differential melting between sun-exposed and shaded snow areas.

Given that Landsat do not have nighttime measurements; therefore, the spread shape did not appear in the nighttime scatter plots, and this indicates that the spread is not due to the coarse spatial resolution of MODIS, but more likely due to the effect of solar radiation on MODIS measurements during daytime. With the fact that the coarse spatial resolution of MODIS (i.e., 1km) reduces the matching with IMIS measurements at a specific node. Thus, traditional LST measurements are obtained from ground-based stations. However, these measurements do not represent the spatial distribution of LST since they are point-based measurements (Becker and Li, 1995). This raises a challenge in assessing spatial representativeness of ground stations, because validating LST products with a spatial resolution of hundreds or thousands of meters with ground based measurements will result error from the scale mismatch with land cover type (LCT) making the validation less reliable and hinder the process (Yu et al., 2017).

The comparison between IMIS and MODIS data at the four different observation times depends more on the meaning of the calculated values that were represented in the results. Therefore, all values in the MOD21A1D and MYD21A1D comparison indicates a good compatibility between the datasets at these times. This has negligible effect of outliers on the mean deviation values that differs slightly. Also, the comparison between the day and night time representativeness was performed using small values with slight differences due to the higher temperature difference during data time. These results can be reanalyzed due to the small difference (weak accuracy) in values between data sets, and due to the appearance of the unexpected features in some observation times and absence in another, such as the speared of MODIS data at IMIS LST 0 °C.

The means comparison and the difference between the day and night observation times is clear, and it obviously confirms the accuracy of the night observation times with day observations. This is also confirmed by the calculated values that indicated the significant difference between the means of the MODIS and IMIS data during the day observation times, which was absent in the nighttime observations.

Nighttime values indicate relatively positive linear correlation between MODIS and IMIS data at night times, with a minor difference. The results assure the accuracy of MODIS nighttime data over daytime data with respect to IMIS data. In addition, many studies have shown that MODIS daytime LST presents obviously lower levels of validation accuracy than nighttime LST due to high levels of daytime LST heterogeneity (Wang et al., 2008,Coll et al., 2009). In the daytime, hill shadows within pixels can produce considerable LST heterogeneities, while at night, the ground surface becomes cool and more homogeneous, when it is free of solar heating uncertainties (Wang et al., 2008).

6.2 MODIS Versus IMIS Trends Comparisons

Considering the hourly trends, the Pearson's Correlation values that have slight difference between each other, indicated the absence of any correlation between the MODIS and IMIS data. However, the shapes of the two curves at all times show clear correlation whether positive or negative between the data. This concludes that low Pearson's Correlation values are caused by the presence of outliers the affected the shape and calculation of the right correlation. Therefore, it is not reliable to depend only on Pearson's Correlation to investigate the relation between these two datasets where in-depth analysis could be achieved using robust statistical measurement that might be more comprehensive and avoid the effects of outliers. Hence, current guidelines recommend using robust methods to identify outliers, such as those relying on the median as opposed to the mean (Leys et al., 2019), and this is makes the necessity of using MAD-2. In addition, there is significance in using the scatter plots which played a role in understanding the effect of outliers on the statistical values.

For means comparison, the slightly affective MAE values indicted that the compared datasets are a bit different and lack strong compatibility. Although the results were not expected according to the values presented, it is obvious that Terra data is slightly more compatible with the IMIS data than that of Aqua. Knowing that a clear correlation was presented by the actual measurements, reanalysis and assessment of the MAE values results is necessary, since they could be affected by the outliers. In addition, the high standard deviation values, indicated that MAE values increase as the standard deviation values between the Terra and Aqua data increase.

However, the scatter plots showed that these high values were caused by the presence of outliers, and this confirms the compatibility of the datasets retrieved by the actual measurements. In a statistical context, there are concerns about the disproportionate influence of outliers on statistical analyses, based on sample means and variance.

Studies provided evidence on the effect of outliers resulted in inflation of Type I error rates (Zimmerman, 1994,Wilcox, 1998,Liao et al., 2016).

6.3 Limitations of Environmental and Sensor-related Influences on LST

Based on the analysis (scatterplots) of the studied influences, elevation and aspect of ground station did not show remarkable effect on the trend measurements. While, LST measurements from MODIS satellites vary with viewing angle at different observation times.

Using the means of all MODIS actual measurements instead of trends helped to identify different effects of the view angle on satellite's LST measurements which showed an impact of observation times of the view angle on LST. This effect increases the differences between satellite LST products; and thus, increasing the challenge of using multi-sensor and multi-decadal data to provide harmonized LST datasets suitable for long-term climate observations (Ermida et al., 2017). This could be caused by the effect of the viewing angle (obliqueness) on the pixel size, and it was noted that the pixel size varies with the viewing angle if the instantaneous field of view (IFOV) remains constant for all viewing directions (Ren et al., 2015).

These influences made it difficult to determine the exact effect of the satellite's pointing angle (i.e. nadir) on LST measurements, and this has several branches that need to be resolved before reaching a final conclusion. In addition, considering daytime and nighttime data separately for such comparison might come up with different conclusions concerning the view angle effect. Thus, many biases may exist according to the observation time; especially that the quality of MODIS data has a Root Mean Square Error (RMSE) of 2.44 K and 3.70 K at nighttime and daytime, respectively (Xu, 2023). In addition, there is different climatic conditions between day and night which may also affects the quality of LST between day and night time observations; while, the observed dependencies of nighttime biases on view angle agree with results reported for night-time LST from the AVHRR and SEVIRI LST (Trigo et al., 2021). In contrast, at daytime, the differences were considerably larger and asymmetric with respect to nadir; and this suggests that these differences are linked to illumination geometry and reflect the viewing geometry dependence of shadow and sunlit areas in the sensor's field of view (Pérez-Planells et al., 2023).

In order to reach better clarification of the effect of elevation and aspect on LST measurements, it would be better to compare it to the ground-based LST measurements instead of its comparison with trends. This step is responsible for increasing the number of data points used, providing better explanation of any change. In this respect, the elevation and aspect play a role in LST measurement notably that elevation is linked with air temperature, and the aspect with sunlight orientation increases air temperature; however, this effect will evenly influence all ground stations and space-borne measurements, which makes it as a constant variable on the resulted LST values. It is worth mentioning that there are other factors that could emerge and impact IMIS diurnal trend patterns, such as climatic conditions (e.g., wind speed, humidity), type of surficial materials that capture heat (e.g., clayey soil, bare rock, etc.), as well as rapid dynamics of clouds-masking that prevent sunlight to reach terrain surface.

6.4 Landsat Implications

In reference to the presented results, it is obvious that the MOD21A1N observation time data has the best mean deference (1.95 °C) from the over all (-1.14 °C) and count based representation values 12.5%. This means that the MOD21A1N observation time has a higher representativeness than all the other times, including those of Landsat 5, 7, and 8, which are shown earlier (Figure 4.3). The concluded results states that this is a limitation for Landsat measurements. Therefore, using only LST values from a single Landsat scene to represent a season or a whole year shows some limitation of the LST value representativeness (Dang et al., 2020) which would have higher accuracy during night time specially if they have similar observation time as that of MO21A1N. Therefore, consisting of two platforms launched in a similar time period as Landsat 7 ETM+ (although the Aqua platform was released in 2002), MODIS products can provide high accurate LST data (Burnett and Chen, 2021).

The processing of additional type of satellite images would be helpful for validation and regulating some issues that might existed in MODIS data. This is the case for Landsat images which have higher spatial resolution. In this respect, the comparison of observation time was carried out, and it has been resulted that MOD21A1N observation time data has the best mean deference (1.95 °C) from the overall (-1.14°C) and count based representation values 12.5%. This means that the MOD21A1N observation time has a higher representativeness than all the other times, including those of Landsat 5, 7, and 8, which are shown earlier (Figure 4.3). This is a limitation for Landsat measurements. Therefore, using only LST values from a single Landsat scene to represent a season or a whole year shows some limitation of the LST value representativeness (Dang et al., 2020); while it has higher accuracy during night time specially if they have similar observation time as that of MO21A1N. Therefore, with two platforms launched in a similar time period as Landsat 7 ETM+ (although the Aqua platform was released in 2002), MODIS products can provide high accurate LST data (Burnett and Chen, 2021).

Based on the aforementioned discussion, the explicit unexpected results in this study must be acknowledged, such as MODIS LST spread of data, absence of aspect effect, etc. These results might have different causes that could enhance cloud correction methods to reduce residual contamination affecting LST accuracy. In addition, the general compatibility that appeared between datasets, which provide credibility of using LST measurements directly from satellite data with a special emphasis to MODIS Terra and Aqua sensors. This will motivate performing similar research studies to calculate LST over different time periods, notably LST of drought indices can be used for assessing climate change regime and identifying its geographic and temporal dimensions.

7 Conclusion

The novelty of this study is represented mainly by the use of MODIS data, which has not been used for measuring LST in Swiss Alps before. The presence of similar study done by Gök et al., 2024, but using another satellite image types (Landsat), was helpful and it was used as a reference line for the workflow in this study, which has been implemented in synergy with the primarily identified research questions which have been responded as follows:

- There is similarity in the LST measurements acquired and calculated form MODIS and IMIS ground stations at different observation times in the Swiss Alps, but they have a preference for night time observations that showed higher similarity than day time data.
- IMIS ground-based stations proved to be creditable reference for validation of LST data acquired from MODIS satellite images. Thus, results showed a similarity between MODIS and IMIS trends, which was indicated in the scatter plots, where a preference of night time observation exists in the trends' means comparison.
- MODIS LST trends, at different observation times, represent the overall trend at all time and this was evidenced by the similarity between the obtained trends, where IMIS data trend at MOD21A1D (Terra daytime observation) is the best representative of the IMIS overall trend.
- A number of factors resulted in different LST trends at different observation times. Thus, LST showed different behavior with the view angle at various observation times, even that it was not defined for MYD21A1D. In addition, there was a remarkable effect of the elevation above 2000 m on the LST as resulted from the scatterplots. Nevertheless, no clear effect of aspect on LST has been reported.
- The implications of the comparison between MODIS and Landsat LST observation has been viewed from the complementary of characteristics between both satellites. Thus, MODIS is characterized by short revisit time, day and night observations, but with relatively low spatial resolution (1 km). Besides, the high spatial resolution (60 m in the thermal bands) in Landsat serves for accurate LST data, but it is hindered by the individual daytime observation and the longer revisit time (16 days). Hence, the implication of using both satellite includes the utility from the advantages present in each satellite.

The existed challenges in the study were addressed by analytical methods required to guarantee reliable comparison of MODIS satellites LST measurements IMIS data, this will assure optimal results when similar approaches are applied for researches on climate change, evapotranspiration,

and urban heat managements, etc.

As a matter of concern, the absence of both elevation and aspect effects raises questions regarding the unexpected results; especially elevation was found to have an impact in many studies using MODIS LST, particularly those conducted over a large area where the terrain is variable (Phan et al., 2018). For example, in air temperature (Ta) estimation using MODIS LST data, along with ground LST, elevation was considered one of the most impactful variables effecting the results of Ta estimation" (Gawuć and Strużewska, 2016, Chen et al., 2016,Huang et al., 2017,Phan et al., 2018). This makes it questionable if such an effect would appear when the number of used stations and LST measurements are increased.

In this regards, questions have been raise: Should the LST measurements be used instead of trends to figure out the effect of these variables on IMIS measurements? While the accuracy of the measurements is essential for these obvious variations, so what other influences on LST measurements might be studied for better understanding of the existing trends over such a long-time span? Considering that analysis of different possible influences is crucial to explain the changes taking place within the data, and these influences may differ between regions.

Given that MOD21A1D appeared to be the most representative of the overall in IMIS data trends, is it convenient to rely on it to understand long-term variations of IMIS LST trends? All these questions open the door to many significant ideas and complications that would be extremely beneficial if solved.

This study did not only brought up and responded to a lot of key questions, but also expressed different methodologies for achieving a comprehensive approach in LST measurements studies. While, the lack of long-term LST records in the past has hindered the application of satellite LST in several climate studies, and only a few studies have examined the role of LST datasets in climate variations (Trigo et al., 2008,Jiménez-Muñoz et al., 2013). The study sheds the light on different gaps created a facility for more in-depth studies to understand LST measurements and their implications.

Based on the findings of this study, it can be concluded that MODIS datasets for measuring LST have good reliability for calculating the temperature of land surface with various LCU components and over different time periods. During the implementation of this study, there are challenges raised and they need to be addressed in-depth for selected pilot areas where long time series data with high accuracy is available to perform distinctly comparative analysis between MODIS LST data and data from ground stations. If these areas include mountainous (as the Swiss Alps) and flat terrain, more precision in data comparison can be reached.

In addition, the variety of land characteristics (e.g., elevation, aspect, etc.) must be strictly studies

to appraise the influence of these characteristics on data accuracy; which means that the terrain characteristics should be categorized according to their interaction with heat received from sunlight radiation. Moreover, this must be integrated with the validation of technical influences (e.g., view angle) that often resulted from the space-borne sensors. In addition, down-scaling between various satellite images can be utilized; specially to integrate the short revisit time of MODIS images with high-resolution thermal images (e.g., Aster, Landsat, etc.), but with relatively long revisit time.

The study concludes that MODIS datasets for measuring LST are useful tool that can be adopted to assess heat fluxes and differentiate various surface heat radiation; and this in turn can be applied in serval themes with a special emphasis to study drought indices induced by climate change, identifying heat islands for further innovative cooling shelter, soil dryness/moisture for agricultural purposes, regional heat flow dynamics, indicative hydrological clues (e.g., paleodrainages, wet horizons, etc.); porous rocks and lineaments, as well as this can extend to agriculture in defining vegetation health and crop-water requirement.

Bibliography

Abbas, A., Q. He, L. Jin, J. Li, A. Salam, B. Lü, and Y. Yasheng (2021). "Spatio-temporal changes of land surface temperature and the influencing factors in the Tarim Basin, Northwest China." *Remote Sensing* 13.19, p. 3792.

Abunnasr, Y. and M. Mhawej (2023). "Fully automated land surface temperature downscaling based on RGB very high spatial resolution images." *City and Environment Interactions* 19, p. 100110.

Al-Faisal, A., A. Al Kafy, F. Rahman, A. Al Rakib, K. Akter, V. Raikwar, D. Amir Jahir, J. Ferdousi, and M. Kona (2021). "Assessment and prediction of seasonal land surface temperature change using multi-temporal Landsat images and their impacts on agricultural yields in Rajshahi, Bangladesh." *Environmental Challenges* 4, p. 100147.

Andronis, V., V. Karathanassi, V. Tsalapati, P. Kolokoussis, M. Miltiadou, and C. Danezis (2022). "Time series analysis of Landsat data for investigating the relationship between land surface temperature and forest changes in Paphos forest, Cyprus." *Remote Sensing* 14.4, p. 1010.

Balas, D. (2023). "Impact of land surface temperature (LST) and ground air temperature (Tair) on land use and land cover (LULC): An investigative study." *International Journal of Environment and Climate Change* 13.10, pp. 3117–3130.

Bassett, G. W. and R. Koenker (1978). "Asymptotic theory of least absolute error regression." *Journal of the American Statistical Association* 73.363, p. 618.

Becker, F. and Z. Li (1995). "Surface temperature and emissivity at various scales: Definition, measurement and related problems." *Remote Sensing Reviews* 12.3-4, pp. 225–253.

Burnett, M. and D. Chen (2021). "The impact of seasonality and land cover on the consistency of relationship between air temperature and LST derived from Landsat 7 and MODIS at a local scale: A case study in Southern Ontario." *Land* 10.7, p. 672.

Chen, Y., J. Quan, W. Zhan, and Z. Guo (2016). "Enhanced statistical estimation of air temperature incorporating nighttime light data." *Remote Sensing* 8.8, p. 656.

Coll, C., Z. Wan, and J. M. Galve (2009). "Temperature-based and radiance-based validations of the v5 MODIS land surface temperature product." *Journal of Geophysical Research: Atmospheres* 114.D20.

D'Agostino, V. and A. Zelenka (1992). "Supplementing solar radiation network data by co-kriging with satellite images." *International Journal of Climatology* 12.7, pp. 749–761.

Dang, T., P. Yue, F. Bachofer, M. Wang, and M. Zhang (2020). "Monitoring land surface temperature change with Landsat images during dry seasons in Bac Binh, Vietnam." *Remote Sensing* 12.24, p. 4067.

Dutta, C. K., A. Mahanta, D. Roy, S. Devi, J. Das, I. Ahmed, P. J. Borah, K. Nath, and A. Chutia (2022). "A GIS based study of river bank erosion and its impact in land use and land cover of Dibru-Saikhowa National Park during 2010–2020." *Int J Basic Appl Sci* 11.2, pp. 9–15.

Ermida, S., C. DaCamara, I. Trigo, A. Pires, D. Ghent, and J. Remedios (2017). "Modelling directional effects on remotely sensed land surface temperature." *Remote Sensing of Environment* 190, pp. 56–69.

Fontana, F., C. Rixen, T. Jonas, G. Aberegg, and S. Wunderle (2008). "Alpine Grassland Phenology as Seen in AVHRR, VEGETATION, and MODIS NDVI Time Series - a Comparison with In-Situ Measurements." *Sensors* 8.4, pp. 2833–2853.

Foppa, N. and G. Seiz (2012). "Inter-annual variations of snow days over Switzerland from 2000–2010 derived from MODIS satellite data." *The Cryosphere* 6, pp. 331–342.

Gawuć, and J. Strużewska (2016). "Impact of MODIS quality control on temporally aggregated urban surface temperature and long-term surface urban heat island intensity." *Remote Sensing* 8.5, p. 374.

Guo, F., D. Hu, and U. Schlink (2022). "A new nonlinear method for downscaling land surface temperature by integrating guided and Gaussian filtering." *Remote Sensing of Environment* 271, p. 112915.

Guo, X., L. Zhang, and Z. Li (2021). "Interpolation of IMIS LST data to synchronize with MODIS LST observations." *Journal of Remote Sensing Integration* 10.2, pp. 123–135.

Gök, D. T., D. Scherler, and H. Wulf (2024). "Land surface temperature trends derived from Landsat imagery in the Swiss Alps." *The Cryosphere* 18.11, pp. 5259–5276.

Hidalgo, D. and J. Arco (2022). "Modeling the Surface Urban Heat Island (SUHI) to study its relationship with variations in the thermal field and with the indices of land use in the metropolitan area of Granada (Spain)." *Sustainable Cities and Society* 87, p. 104166.

Huang, F., W. Ma, B. Wang, Z. Hu, Y. Ma, G. Sun, and Y. Lin (2017). "Air temperature estimation with MODIS data over the northern Tibetan Plateau." *Advances in Atmospheric Sciences* 34.5, pp. 650–662.

Huber, P. J. and E. Ronchetti (2009). *Robust Statistics*. Wiley Series in Probability and Statistics.

Jiménez-Muñoz, J. C., J. A. Sobrino, C. Mattar, and Y. Malhi (2013). "Spatial and temporal patterns of the recent warming of the Amazon forest." *Journal of Geophysical Research: Atmospheres* 118.11, pp. 5204–5215.

Journée, M., R. Müller, and C. Bertrand (2012). "Solar resource assessment in the Benelux by merging Meteosat-derived climate data and ground measurements." *Solar Energy* 86.12, pp. 3561–3574.

King, M. D. (1999). "Land surface temperature as an essential climate variable: NASA's perspective." *Proceedings of the First International Symposium on Land Surface Climatology (ISLSC)*, pp. 15–18.

Leys, C., M. Delacre, Y. Mora, D. Lakens, and C. Ley (2019). "How to classify, detect, and manage univariate and multivariate outliers, with emphasis on pre-registration." *International Review of Social Psychology* 32.1.

Li, S., Z. Qin, S. Zhao, M. Gao, S. Li, Q. Liao, and W. Du (2022). "Spatiotemporal variation of land surface temperature in Henan Province of China from 2003 to 2021." *Land* 11.7, p. 1104.

Liao, H., Y. Li, and G. Brooks (2016). "Outlier impact and accommodation methods: Multiple comparisons of type I error rates." *Journal of Modern Applied Statistical Methods* 15.1, pp. 452–471.

Liu, Y., Y. Yamaguchi, and C. Ke (2007). "Reducing the discrepancy between ASTER and MODIS land surface temperature products." *Sensors* 7.12, pp. 3043–3057.

Mariati, N. P. A. M., I. N. Budiantara, and V. Ratnasari (2020). "Combination estimation of smoothing spline and Fourier series in nonparametric regression." *Journal of Mathematics* 2020, pp. 1–10.

Martin, M. A., D. Ghent, A. C. Pires, F. M. Göttsche, J. Cermak, and J. J. Remedios (2019). "Comprehensive in situ validation of five satellite land surface temperature data sets over multiple stations and years." *Remote Sensing* 11.5, p. 479.

Measurement, I. and I. S. IMIS (2023). *IMIS measuring network*.

Mohammadi, A., B. Mashhoodi, A. Shamsoddini, E. Pishgar, and R. Bergquist (2025). "Land surface temperature predicts mortality due to chronic obstructive pulmonary disease: a study based on climate variables and impact machine learning." *Geospatial Health* 20.1.

Moharir, K., C. Pande, V. Gautam, S. Dash, A. Mishra, K. Yadav, H. Darwish, M. Pramanik, and M. Elsahabi (2025). "Estimation of land surface temperature and LULC changes impact on groundwater resources in the semi-arid region of Madhya Pradesh, India." *Advances in Space Research* 75.1, pp. 233–247.

Muro, J., A. Strauch, S. Heinemann, S. Steinbach, F. Thonfeld, B. Waske, and B. Diekkrüger (2018). "Land surface temperature trends as indicator of land use changes in wetlands." *International Journal of Applied Earth Observation and Geoinformation* 70, pp. 62–71.

Nega, W. and A. Balew (2022). "The relationship between land use land cover and land surface temperature using remote sensing: systematic reviews of studies globally over the past 5 years." *Environmental Science and Pollution Research* 29, pp. 42493–42508.

Oh, S. J., D. H. Lee, M. Park, K. H. Park, J. Lee, and B. K. Kim (2015). "Enhancement of viewing angle properties of a single-domain fringe-field switching mode using zero pretilt alignment." *Journal of Physics D: Applied Physics* 48.40, p. 405502.

Owe, M., R. d. Jeu, and T. Holmes (2008). "Multisensor historical climatology of satellite-derived global land surface moisture." *Journal of Geophysical Research: Earth Surface* 113.F1.

Pal, S. and S. Ziaul (2017). "Detection of land use and land cover change and land surface temperature in English Bazar urban centre." *The Egyptian Journal of Remote Sensing and Space Science* 20.1, pp. 125–145.

Phan, T., M. Kappas, and T. Tran (2018). "Land surface temperature variation due to changes in elevation in Northwest Vietnam." *Climate* 6.2, p. 28.

Pérez-Planells, L., D. Ghent, S. Ermida, M. Martin, and F. Goettsche (2023). "Retrieval consistency between LST CCI satellite data products over Europe and Africa." *Remote Sensing* 15.13, p. 3281.

Rahman, M., A. Aldosary, and M. Mortoja (2017). "Modeling Future Land Cover Changes and Their Effects on the Land Surface Temperatures in the Saudi Arabian Eastern Coastal City of Dammam." *Land* 6.2, p. 36.

Ren, H., G. Yan, R. Liu, Z. Li, Q. Qin, F. Nerry, and Q. Liu (2015). "Determination of optimum viewing angles for the angular normalization of land surface temperature over vegetated surface." *Sensors* 15.4, pp. 7537–7570.

Roy, D., B. Das, P. Singh, et al. (2025). "Assessing the accuracy of multi-model approaches for downscaling land surface temperature across diverse agroclimatic zones." *Scientific Reports* 15, p. 10824.

Shaikh, S., J. Gala, A. Jain, S. Advani, S. Jaidhara, and M. M. Roja (2021). "Analysis and prediction of COVID-19 using regression models and time series forecasting." *2021 11th International Conference on Cloud Computing, Data Science Engineering (Confluence)*, pp. 989–995.

Sismanidis, P., I. Keramitsoglou, B. Bechtel, and C. Kiranoudis (2016). "Improving the downscaling of diurnal land surface temperatures using the annual cycle parameters as disaggregation kernels." *Remote Sensing* 9.1, p. 23.

Thakur, P., S. Samant, and R. Verma (2023). "Spatiotemporal changes of forest cover and land surface temperature using geo-spatial techniques in Talra Wildlife Sanctuary, Shimla, North-Western Himalaya." *Preprint*.

Thakur, S., D. Maity, I. Mondal, G. Basumatary, B. Ghosh, P. Das, and K. De (2021). "Assessment of changes in land use, land cover, and land surface temperature in the mangrove forest of Sundarbans, northeast coast of India." *Environment, Development and Sustainability* 23.2, pp. 1917–1943.

Tom, N., T. Wu, E. Baltsavias, and K. Schindler (2022). "Recent Ice Trends in Swiss Mountain Lakes: 20-year Analysis of MODIS Imagery." *Journal of Photogrammetry, Remote Sensing and Geoinformation Sciences* 90.4, pp. 1–19.

Toomey, M., D. A. Roberts, C. J. Still, M. L. Goulden, and J. P. McFadden (2011). "Remotely sensed heat anomalies linked with Amazonian forest biomass declines." *Geophysical Research Letters* 38.19, n/a–n/a.

Torres, A., J. Filho, A. Rocha, R. Gondim, and J. Souza (2017). "Outlier Detection Methods and Sensor Data Fusion for Precision Agriculture." *Proceedings of the Brazilian Symposium on GeoInformatics (SBCUP)*, pp. 928–937.

Trenberth, K. E., R. A. Anthes, B. Alan, O. B. Brown, T. Habermann, T. R. Karl, and B. A. Wielicki (2013). "Challenges of a sustained climate observing system." *Climate Science for Serving Society*, pp. 13–50.

Trigo, I. F., S. L. Ermida, J. P. Martins, C. M. Gouveia, F. Göttsche, and S. C. Freitas (2021). "Validation and consistency assessment of land surface temperature from geostationary and polar orbit platforms: SEVIRI/MSG and AVHRR/METOP." *ISPRS Journal of Photogrammetry and Remote Sensing* 175, pp. 282–297.

Trigo, I. F., I. T. Monteiro, F. Olesen, and E. Kabsch (2008). "An assessment of remotely sensed land surface temperature." *Journal of Geophysical Research: Atmospheres* 113.D17.

Veraverbeke, S., W. Verstraeten, S. Lhermitte, R. Van der Kerchove, and R. Goossens (2012). "Assessment of post-fire changes in land surface temperature and surface albedo, and their relation with fire burn severity using multitemporal MODIS imagery." *International Journal of Wildland Fire* 21.3, pp. 243–256.

Wang, F., Z. Qin, C. Song, L. Tu, A. Karnieli, and S. Zhao (2015). "An improved mono-window algorithm for land surface temperature retrieval from Landsat 8 thermal infrared sensor data." *Remote Sensing* 7.4, pp. 4268–4289.

Wang, W., S. Liang, and T. P. Meyers (2008). "Validating MODIS land surface temperature products using long-term nighttime ground measurements." *Remote Sensing of Environment* 112.3, pp. 623–635.

Wang, Y., B. Samset, F. Stordal, A. Bryn, and D. Hessen (2023). "Past and future trends of diurnal temperature range and their correlation with vegetation assessed by MODIS and CMIP6." *Science of The Total Environment* 904, p. 166727.

Wei, B., Y. Bao, S. Yu, and S. Yin (2021). "Analysis of land surface temperature variation based on MODIS data: A case study of the agricultural-pastoral ecotone of northern China." *International Journal of Applied Earth Observation and Geoinformation* 100, p. 102342.

Weng, Q. and P. Fu (2014). "Modeling annual parameters of clear-sky land surface temperature variations and evaluating the impact of cloud cover using time series of Landsat TIR data." *Remote Sensing of Environment* 140, pp. 267–278.

Wilcox, R. R. (1998). "How many discoveries have been lost by ignoring modern statistical methods?" *American Psychologist* 53.3, pp. 300–314.

Xing, Z., Y. Yu, S. Duan, Z. Li, M. Gao, P. Leng, and G. Shang (2020). "Modeling year-to-year variations of clear-sky land surface temperature using Aqua/MODIS data." *IEEE Access* 8, pp. 114541–114553.

Xiong, X. and W. Barnes (2006). "An overview of MODIS radiometric calibration and characterization." *Advances in Atmospheric Sciences* 23.1, pp. 69–79.

Xu, S. (2023). "Assessing the reliability of the MODIS LST product to detect temporal variability." *IEEE Geoscience and Remote Sensing Letters* 20, pp. 1–5.

Yang, Y., T. Onishi, and K. Hiramatsu (2015). "Impacts of different spatial temperature interpolation methods on snowmelt simulations." *Hydrological Research Letters* 9.2, pp. 27–34.

Yao, R., L. Wang, X. Huang, L. Sun, R. Chen, and X. Wu (2021). "A Robust Method for Filling the Gaps in MODIS and VIIRS Land Surface Temperature Data." *IEEE Transactions on Geoscience and Remote Sensing* 59.12, pp. 10738–10752.

Yu, W., M. Ma, Z. Li, J. Tan, and A. Wu (2017). "New scheme for validating remote-sensing land surface temperature products with station observations." *Remote Sensing* 9.12, p. 1210.

Zhao, X., H. Xia, L. Pan, H. Song, W. Niu, R. Wang, and Y. Qin (2021). "Drought monitoring over Yellow River Basin from 2003–2019 using reconstructed MODIS land surface temperature in Google Earth Engine." *Remote Sensing* 13.18, p. 3748.

Zhu, W., A. Lü, and S. Jia (2013). "Estimation of daily maximum and minimum air temperature using MODIS land surface temperature products." *Remote Sensing of Environment* 130, pp. 62–73.

Zhu, X., S. Duan, Z. Li, W. Zhao, H. Wu, and B. Leng (2021). "Retrieval of Land Surface Temperature with Topographic Effect Correction from Landsat 8 Thermal Infrared Data in Mountainous Areas." *IEEE Transactions on Geoscience and Remote Sensing* 59.8, pp. 6674–6687.

Zimmerman, D. W. (1994). "A note on the influence of outliers on parametric and nonparametric tests." *The Journal of General Psychology* 121.4, pp. 391–401.

8 Appendices

8.1 Code

The code can be accessed at `https://github.com/asheib/AS_Master_Thesis_Code.git`.

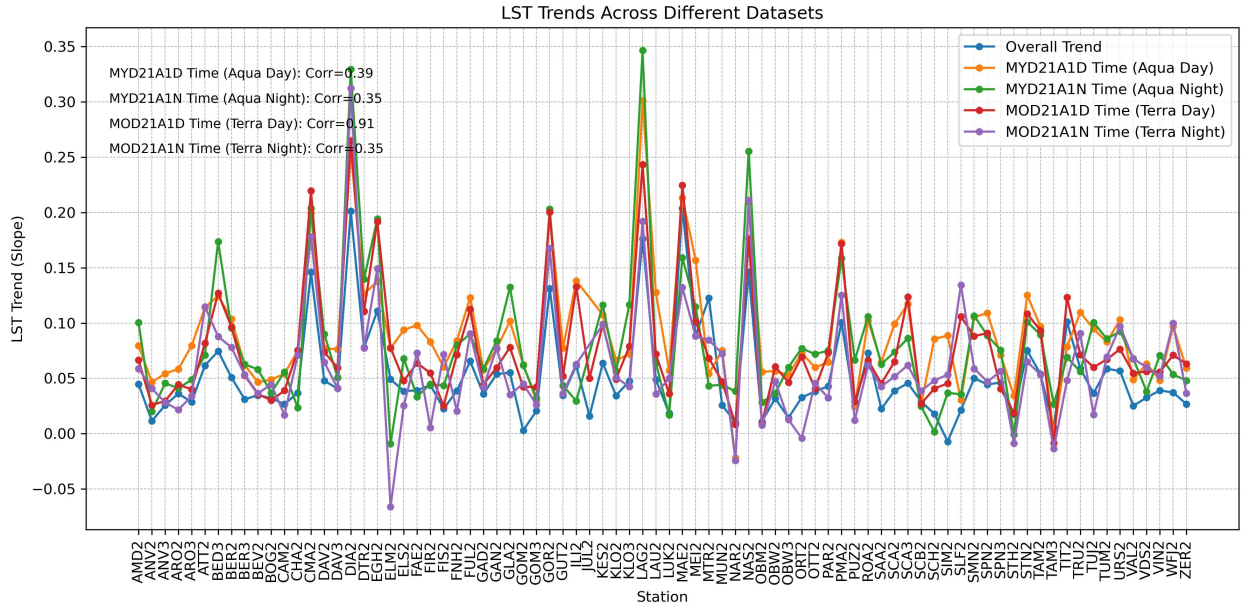

Figure 8.1: The IMIS LST trends at all MODIS observation times versus the overall trend of the data.

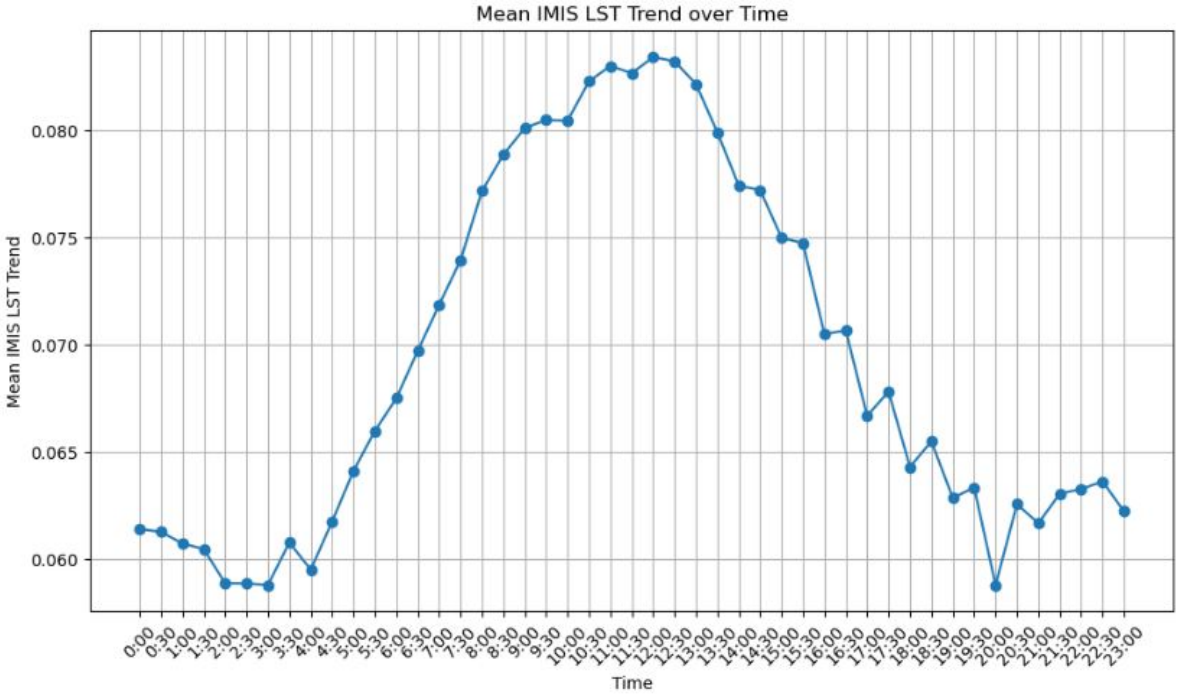

Figure 8.2: The Overall IMIS LST daily trend at all hours of the day

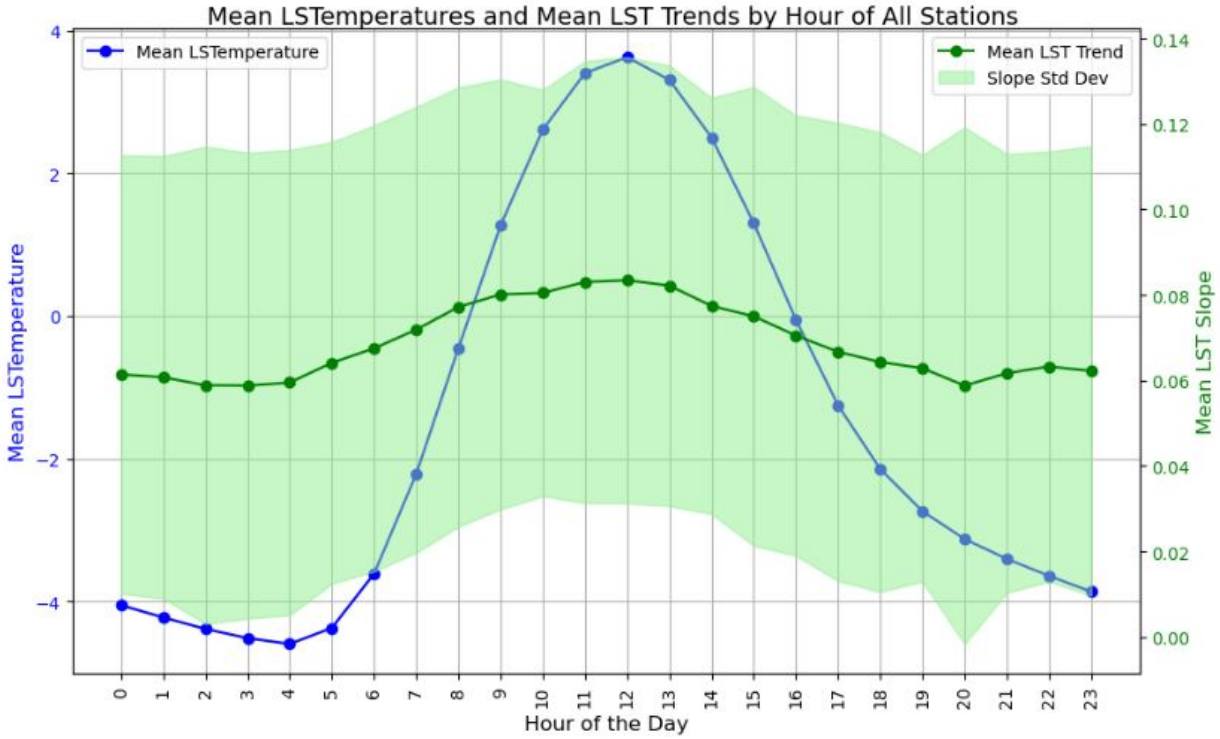

Figure 8.3: The Overall IMIS LST daily trend at all hours of the day versus the daily overall mean of actual measurements.

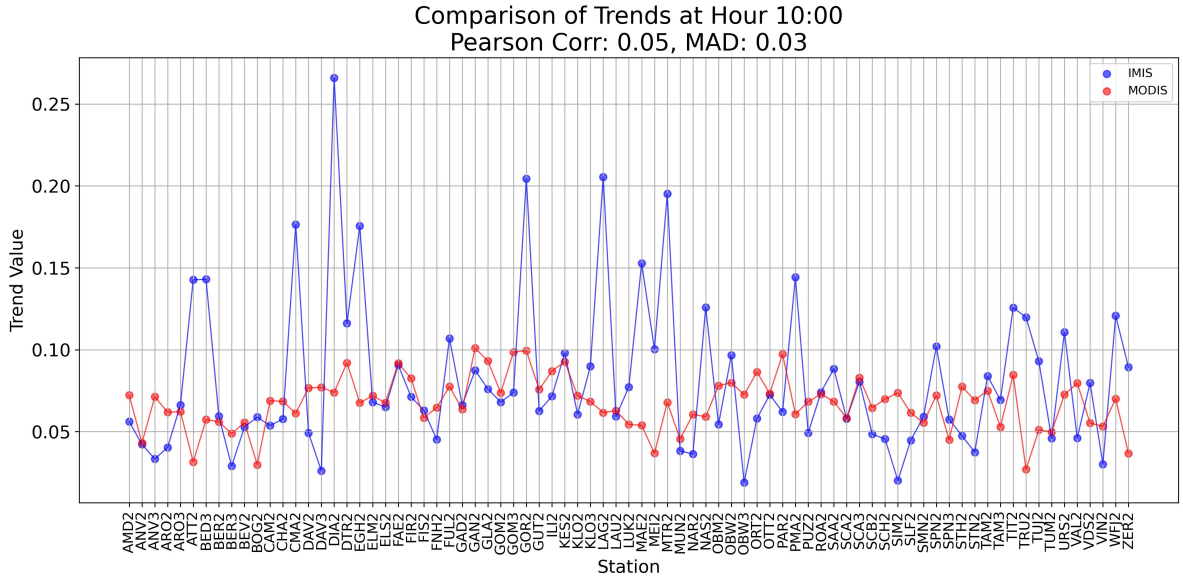

Figure 8.4: Comparison between MOD21A1D data trends with that of IMIS data at 10 am.

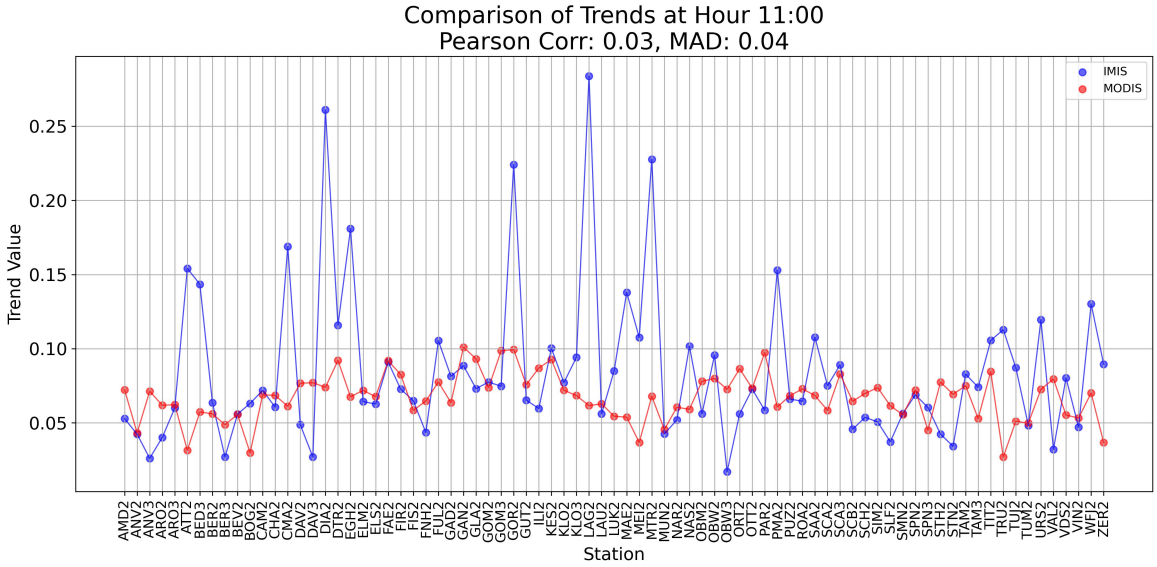

Figure 8.5: Comparison between MOD21A1D data trends with that of IMIS data at 11 am.

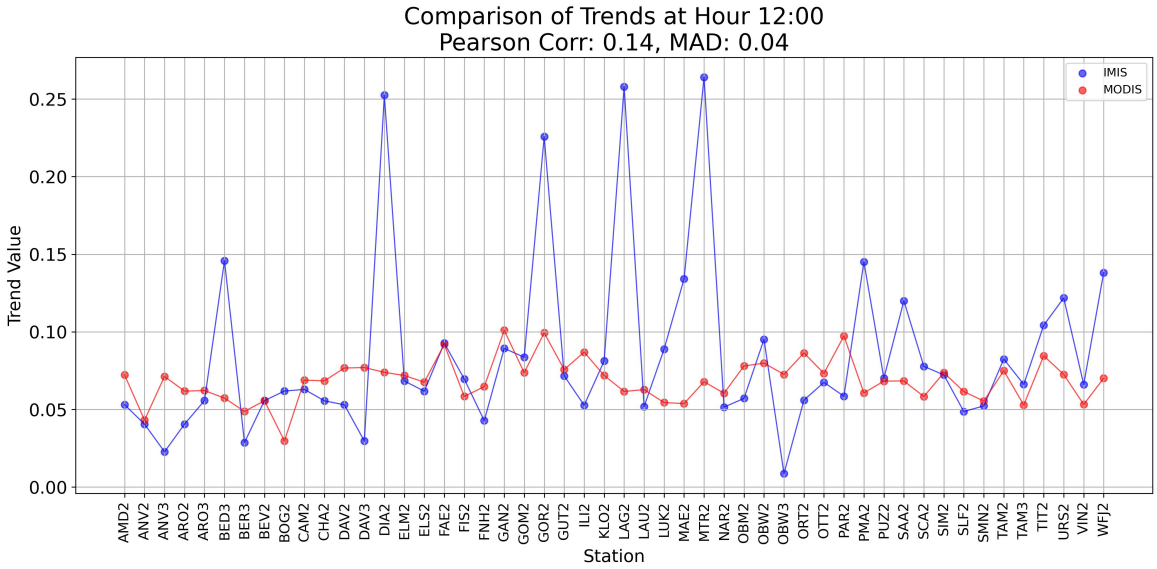

Figure 8.6: Comparison between MOD21A1D data trends with that of IMIS data at 12 am.

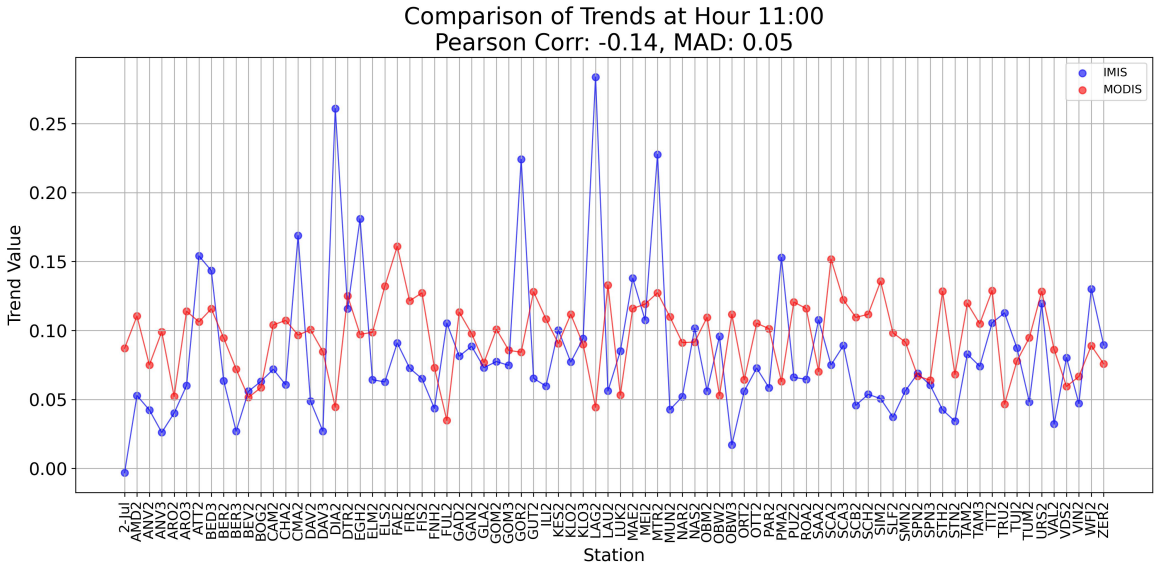

Figure 8.7: Comparison between MYD21A1D data trends with that of IMIS data at 11 am.

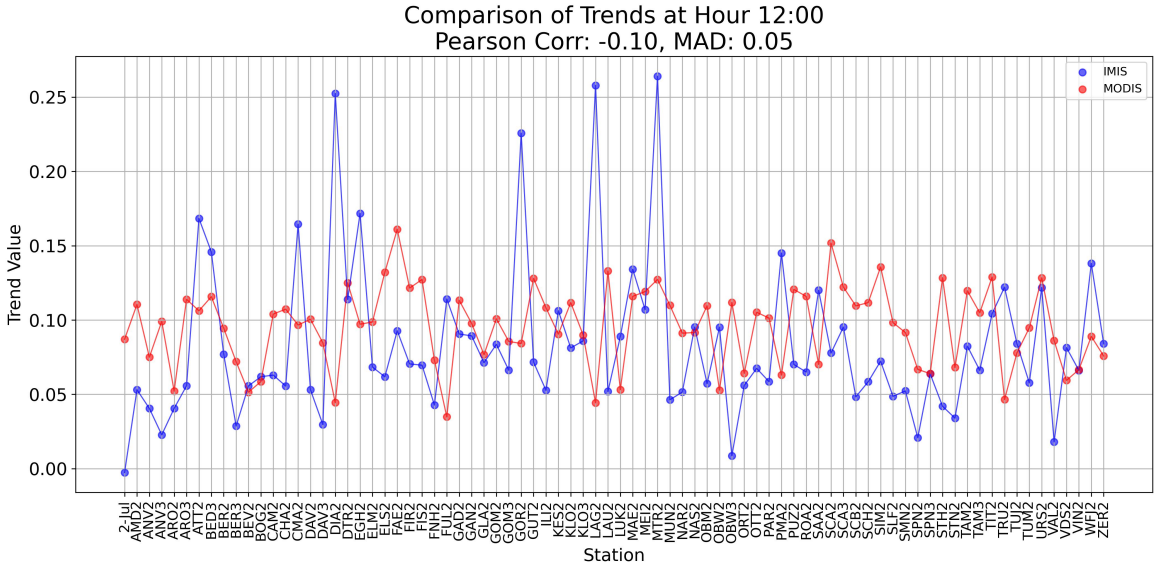

Figure 8.8: Comparison between MYD21A1D data trends with that of IMIS data at 12 pm.

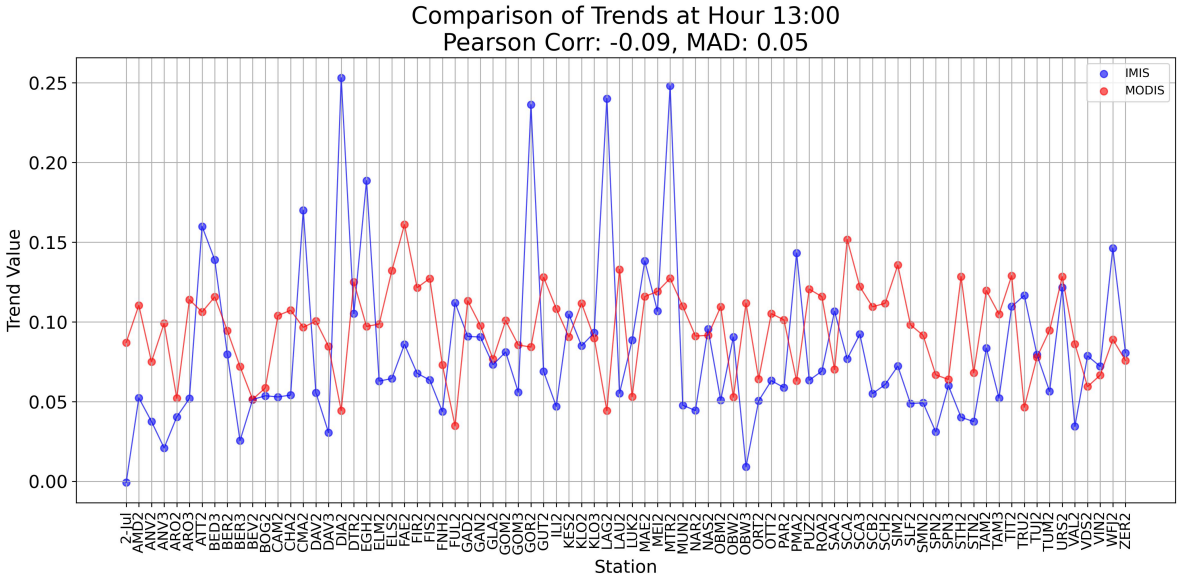

Figure 8.9: Comparison between MYD21A1D data trends with that of IMIS data at 13 pm.

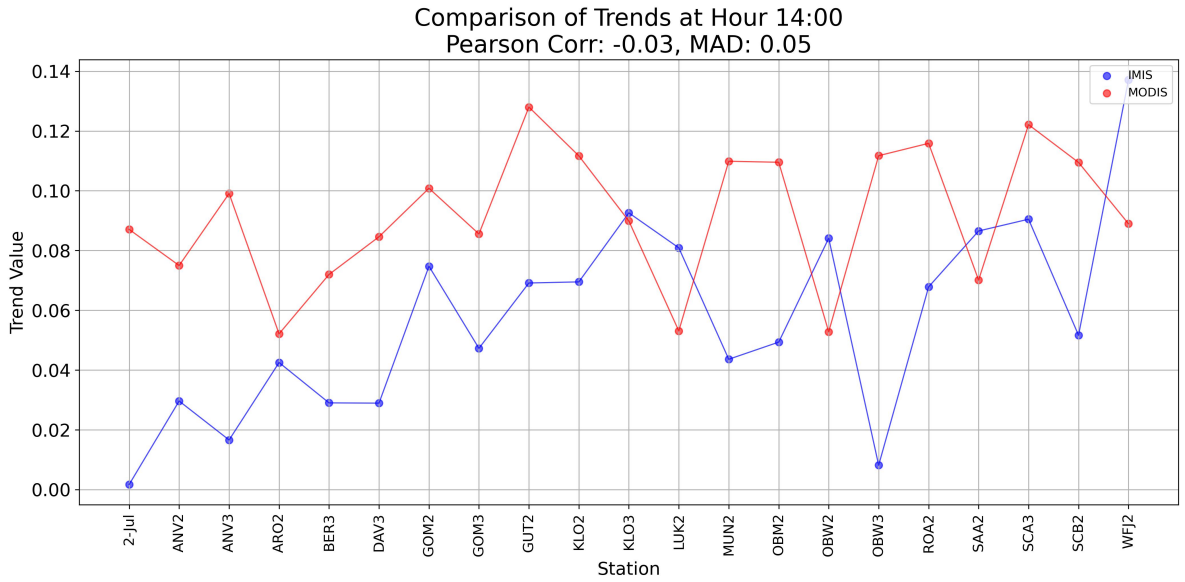

Figure 8.10: Comparison between MYD21A1D data trends with that of IMIS data at 14 pm.

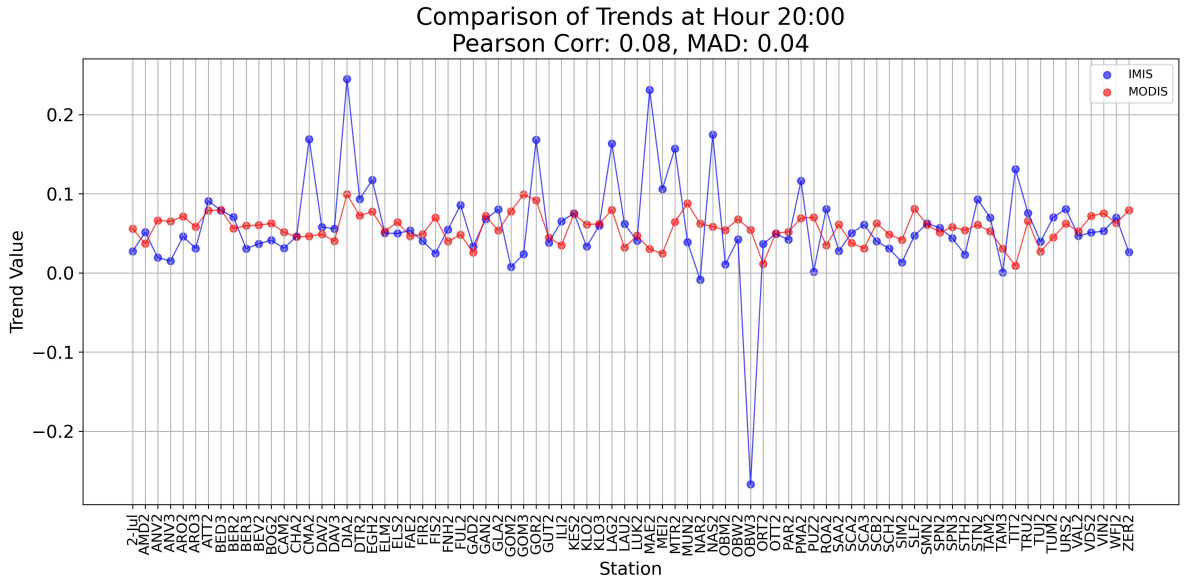

Figure 8.11: Comparison between MOD21A1N data trends with that of IMIS data at 20 pm.

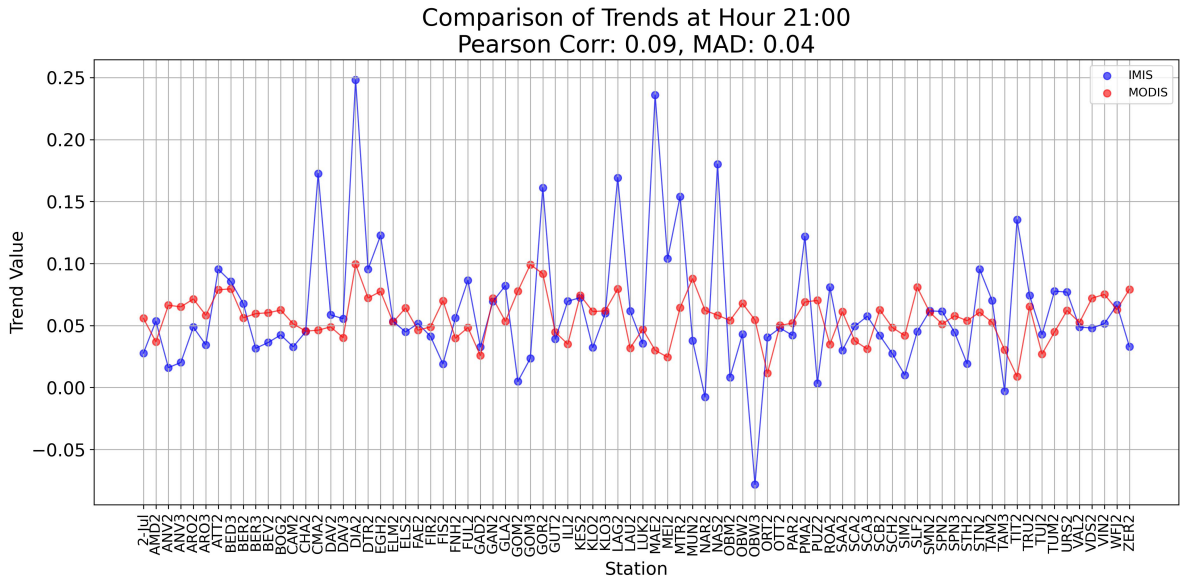

Figure 8.12: Comparison between MOD21A1N data trends with that of IMIS data at 21 pm.

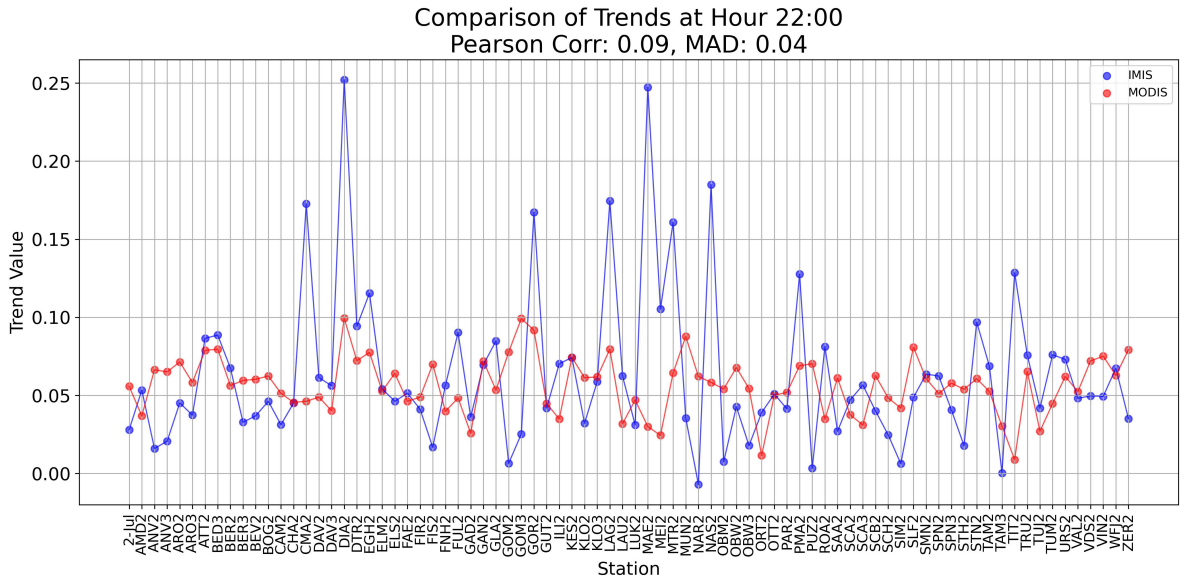

Figure 8.13: Comparison between MOD21A1N data trends with that of IMIS data at 22 pm.

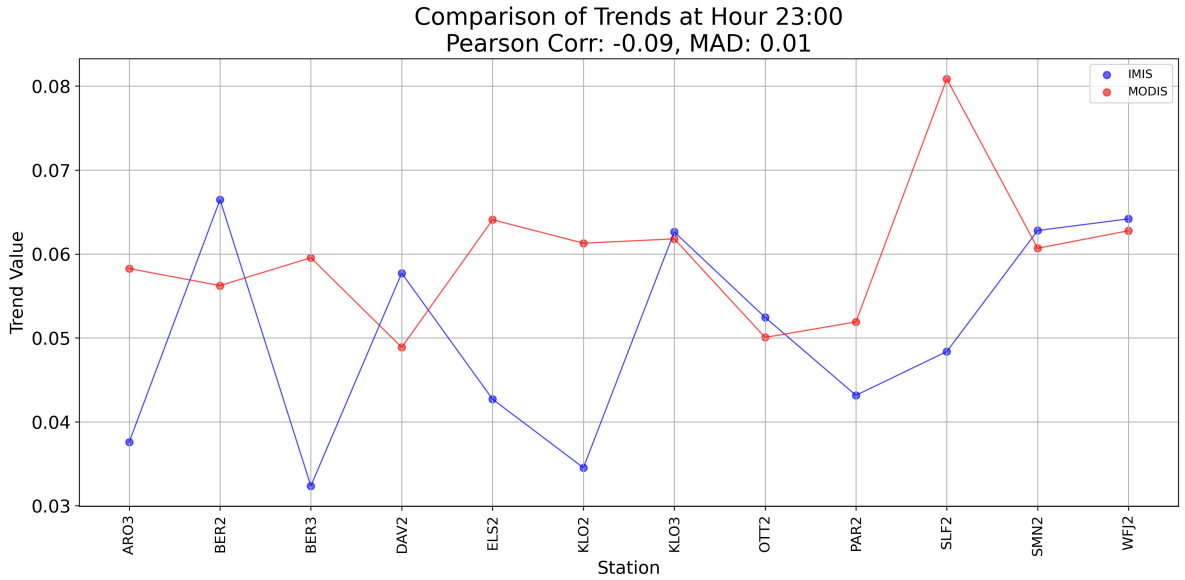

Figure 8.14: Comparison between MOD21A1N data trends with that of IMIS data at 23 pm.

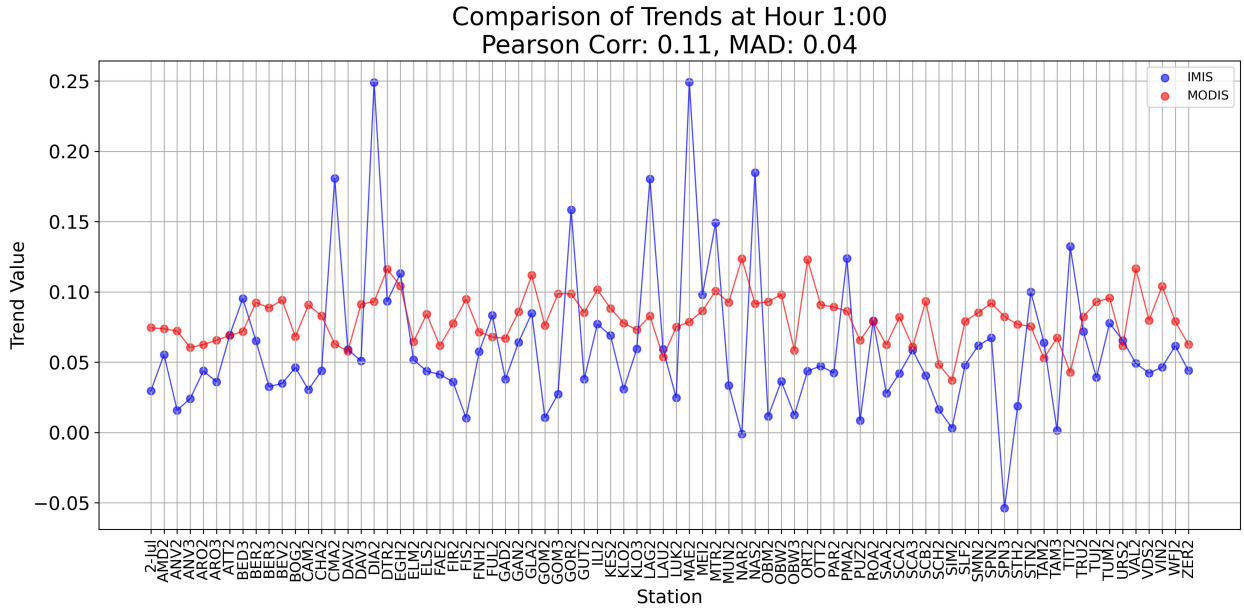

Figure 8.15: Comparison between MYD21A1N data trends with that of IMIS data at 1 am.

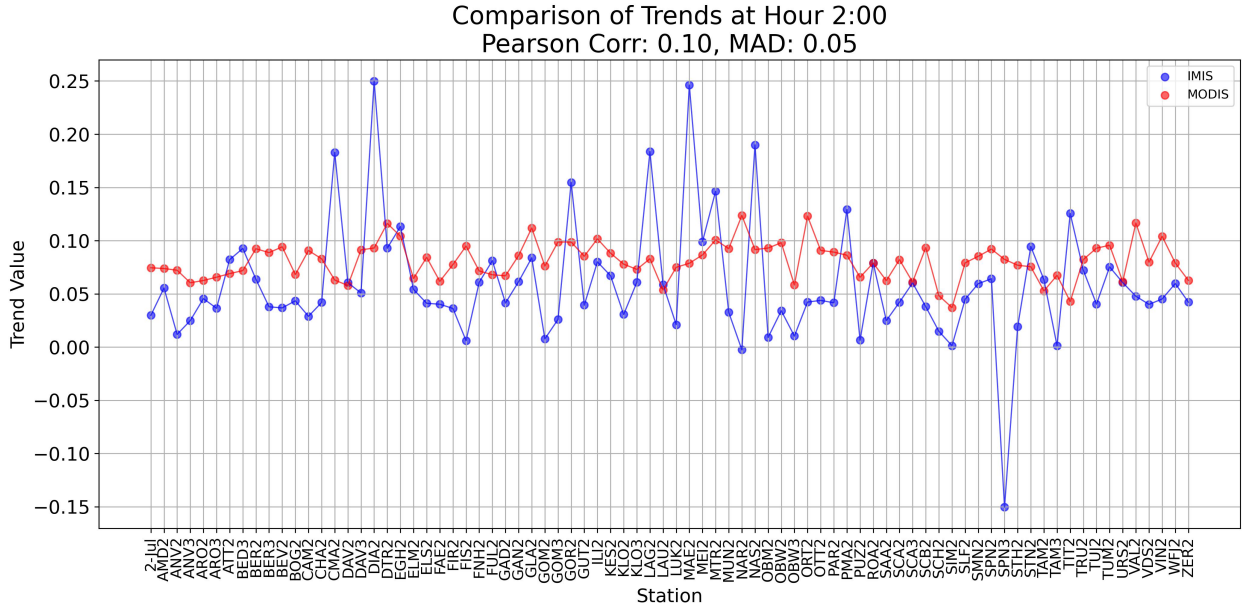

Figure 8.16: Comparison between MYD21A1N data trends with that of IMIS data at 2 am.

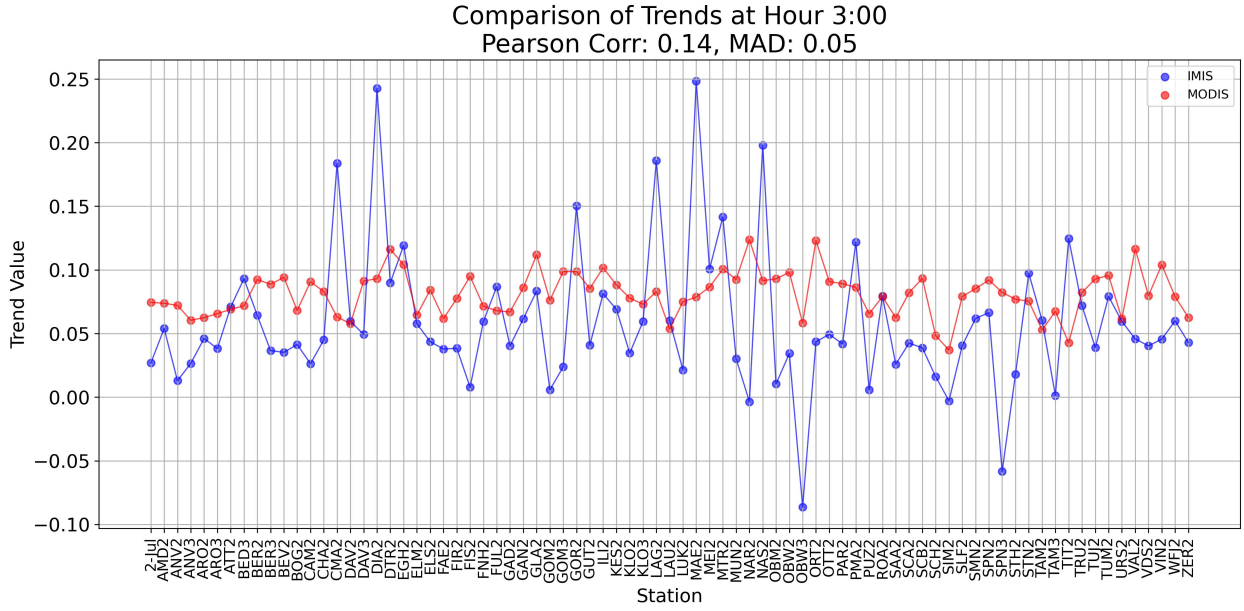

Figure 8.17: Comparison between MYD21A1N data trends with that of IMIS data at 3 am.

Table 8.1: Average LST (°C) of all stations from IMIS (at all times of the day) and the four MODIS times datasets through the whole study period

Station	IMIS Average (°C)	MOD21A1D Average (°C)	MOD21A1N Average (°C)	MYD21A1D Average (°C)	MYD21A1N Average (°C)
AMD2	3.01	11.66	-6.78	6.51	-6.66
ANV2	-3.91	6.88	5.38	10.76	3.75
ANV3	-2.58	3.19	-3.97	6.87	-5.89
ARO2	-4.67	3.02	-7.24	3.78	-6.31
ARO3	-2.62	3.64	-7.63	3.15	-8.29
ATT2	-2.83	4.49	-5.67	4.04	-5.63
BED3	-0.99	2.71	-1.36	6.31	-1.23
BER2	-2.27	6.22	-2.94	4.84	-3.27
BER3	-2.59	3.24	-6.38	6.85	-6.66
BEV2	-3.05	3.15	-6.83	4.06	-8.20
BOG2	-0.65	4.19	-5.60	5.00	-7.41
CAM2	-1.26	4.45	-4.34	3.58	-4.54
CHA2	-0.79	8.19	-2.52	5.79	-4.73
CMA2	-1.05	3.25	1.68	5.55	1.54
DAV2	-3.31	3.16	-4.62	4.49	-5.16
DAV3	-2.94	6.07	-7.23	3.17	-6.44
DIA2	-2.76	1.82	-3.20	6.85	-4.32
DTR2	0.73	11.36	-3.21	2.10	-4.79
EGH2	-1.93	10.34	-2.77	11.57	-2.69
ELM2	-0.53	6.79	-4.34	8.33	-5.21
ELS2	-0.24	8.86	2.66	6.11	0.32
FAE2	0.50	10.02	1.91	8.64	1.43
FIR2	0.02	9.26	0.63	8.20	1.77
FIS2	-0.99	9.48	0.05	10.05	-1.00
FNH2	-0.71	8.55	0.54	10.44	1.39
FUL2	-1.75	6.05	1.24	9.02	-1.79
GAD2	-1.74	7.54	-1.65	5.17	-0.80
GAN2	1.16	1.51	-0.14	7.75	2.63

Station	IMIS Average (°C)	MOD21A1D Average (°C)	MOD21A1N Average (°C)	MYD21A1D Average (°C)	MYD21A1N Average (°C)
GLA2	0.43	14.17	-4.56	0.90	-5.05
GOM2	-1.49	2.14	4.17	12.81	0.31
GOM3	-1.30	12.08	-6.03	3.21	-6.67
GOR2	-0.63	6.95	-1.79	9.41	-2.51
GUT2	1.20	10.45	-7.60	6.77	-8.11
ILI2	-0.88	8.27	-1.12	8.97	2.96
JUL2	-0.35	6.10	0.91	6.79	-0.04
KES2	1.29	1.77	-7.24	2.05	-8.11
KLO2	-2.04	9.14	-2.32	8.13	-1.52
KLO3	-1.60	2.71	-2.54	4.05	-3.79
LAG2	1.84	2.41	-7.74	2.99	-8.76
LAU2	-3.45	8.00	2.09	7.64	2.99
LUK2	-2.40	3.24	-5.92	3.84	-6.88
MAE2	-3.31	7.61	2.94	9.45	3.57
MEI2	0.70	7.78	-1.55	8.06	-0.76
MTR2	-3.84	13.52	2.39	14.16	3.85
MUN2	-3.48	11.60	-1.03	10.84	-1.87
NAR2	-1.37	10.03	-0.97	10.18	-1.66
NAS2	-0.57	8.66	-5.83	8.07	-6.12
OBM2	-0.71	9.42	3.47	8.16	1.98
OBW2	-1.75	8.62	-1.98	7.11	-2.92
OBW3	-1.74	3.54	-2.27	4.52	-0.23
ORT2	1.16	12.90	0.87	10.23	-1.81
OTT2	0.43	13.74	2.01	11.35	0.41
PAR2	-1.49	2.55	-2.95	4.52	-4.43
PMA2	-1.30	7.18	-3.53	7.77	-4.88
PUZ2	-0.63	5.73	-2.15	7.84	-2.03
ROA2	1.20	13.76	4.40	11.51	2.57
SAA2	-0.88	5.52	-3.97	6.88	-6.13

Station	IMIS Average (°C)	MOD21A1D Average (°C)	MOD21A1N Average (°C)	MYD21A1D Average (°C)	MYD21A1N Average (°C)
SCA2	-0.35	5.49	-1.32	6.39	0.80
SCA3	-2.30	6.27	-4.48	4.09	-3.53
SCB2	1.29	12.81	6.13	12.89	3.25
SCH2	-2.04	4.36	-1.18	4.59	-1.00
SIM2	-1.60	7.39	0.32	6.54	0.91
SLF2	1.84	11.53	-0.99	11.83	-1.75
SMN2	-3.45	3.33	-6.17	4.34	-6.34
SPN2	-2.40	5.48	-5.50	4.11	-5.68
SPN3	-3.31	3.97	-3.42	5.41	-6.77
STH2	0.70	8.78	3.95	9.48	4.22
STN2	-3.84	1.07	-8.47	1.08	-9.49
TAM2	-3.48	1.64	0.01	2.62	0.26
TAM3	-1.37	6.70	-0.85	8.84	0.07
TIT2	-0.57	-2.57	-0.76	-0.32	-1.46
TRU2	-3.01	13.12	-0.92	10.13	-4.73
TUJ2	-0.47	7.34	-1.45	7.48	-2.22
TUM2	-0.01	10.19	-2.49	7.81	-3.32
URS2	-0.41	5.05	-3.50	7.84	-3.14
VAL2	-1.17	12.56	-3.90	9.72	-2.70
VDS2	-1.99	7.05	-2.85	6.45	-3.73
VIN2	-3.84	5.68	-4.19	6.11	-6.32
WFJ2	-2.96	5.00	-3.40	5.41	-4.11
ZER2	-4.01	5.30	-7.57	4.78	-8.34

Table 8.2: Metadata Of Used IMIS ground stations (**IMIS2023**)

Station Abr.	Station number	station name	Station location	East Coordinates	North Coordinates
AMD	2	Amden	Bärenfall	729500	225840
ANV	2	Anniviers	Orzival	607468	115206
ANV	3	Anniviers	Tracuit	616833	107764
ARO	2	Arolla	Les Fontanesses	600558	97471
ARO	3	Arolla	Breona	609546	103997
ATT	2	Les Attelas	Lac des Vaux	586953	105990
BED	3	Bedretto	Cassinello	683169	149445
BER	2	Bernina	Motta Bianca	799121	144312
BER	3	Bernina	Puoz Bass	790343	146291
BEV	2	Bever	Valetta	783955	157064
BOG	2	Bosco Gurin	Hendar Furggu	679538	131902
CAM	2	Campolungo	Fontane	698228	146844
CHA	2	Chaussy	Pierres Fendues	578868	136214
CMA	2	Crap Masegn	La Fuorcla	733073	189894
DAV	2	Davos	Barentalli	782062	174726
DAV	3	Davos	Hanengretji	778292	184616
DIA	2	Les Diablerets	Tsanfleuron	584900	129200
DTR	2	Dotra	Preda	709714	155619
EGH	2	Eggishorn	Flesch	650210	140815
ELM	2	Elm	Chuebodensee	729279	199678
ELS	2	Elsige	Elsige	615575	153165
FAE	2	Farmel	Farmel	604344	152125
FIR	2	First	Schmidigen-Bidmeren	647887	168807
FIS	2	Fisi	Fisi	618068	146709
FNH	2	Finhaut	L'Ecreuleuse	563303	105584
FUL	2	Fully	Grand Cor	573059	115974
GAD	2	Gadmen	Gschletteregg	673273	177447
GAN	2	Gandegg	Gandegg	624748	142041

Station Abr.	Station number	station name	Station location	East Coordinates	North Coordinates
GLA	2	Glärnisch	Guppen	721610	206302
GOM	2	Goms	Bodmerchumma	661029	141320
GOM	3	Goms	Treichbode	660649	148952
GOR	2	Gornergrat	Gornergratsee	626731	92906
GUT	2	Guttannen	Homad	665114	170140
ILI	2	Val d'Illiez	Les Collines	552841	115728
JUL	2	Julier	Vairana	773049	149949
KES	2	Kesch	Porta d'Es-cha	788351	166289
KLO	2	Klosters	Madrisa	785499	198213
KLO	3	Klosters	Gatschiefer	790141	190813
LAG	2	Piz Lagrev	Tscheppa	777150	147050
LAU	2	Lauenen	Truttlisbergpass	595482	141633
LUK	2	Lukmanier	Lai Verd	703037	162315
MAE	2	Männlichen	Itramen	638674	163168
MEI	2	Meiental	Laucheren	685005	177555
MTR	2	Matro	Predanass	713717	140779
MUN	2	Mund	Chiematte	637466	131413
NAR	2	Nara	Bassa di Nara	709823	147852
NAS	2	Naluns	Schlivera	814920	188734
OBM	2	Ober Meiel	Obere Meiel	582760	141183
OBW	2	Oberwald	Jostsee	667290	155257
OBW	3	Oberwald	Mallige	670293	151138
ORT	2	Ortstock	Ortstock Matt	715769	197452
OTT	2	Ottere	Ottere	609435	154275
PAR	2	Parsenn	Kreuzweg	780436	191675
PMA	2	Piz Martegnas	Colms da Parsonz	760854	160907
PUZ	2	Puzzetta	Ils Plauns	709039	164889
ROA	2	Rotschalp	Rotschalp	642412	180499
SAA	2	Saas	Seetal	634036	113469

Station Abr.	Station number	station name	Station location	East Coordinates	North Coordinates
SCA	2	Schachental	Seewli	697589	185439
SCA	3	Schachental	Alpler Tor	702186	194253
SCB	2	Schonbuel	Schonbuel	650770	181126
SCH	2	Schilthorn	Turliboden	630363	158481
SIM	2	Simano	Piano del Simano	718450	147400
SLF	2	SLF	Davos Stilli (SLF)	783879	187447
SMN	2	Samnaun	Ravaischer Salaas	820671	204667
SPN	2	Simplon	Ze Seewe	652382	120004
SPN	3	Simplon	Wenghorn	646837	114241
STH	2	Stockhorn	Vorderstocken	606198	170095
STN	2	St. Niklaus	Oberer Stelligletscher	624091	112974
TAM	2	Taminatal	Wildsee	748557	203769
TAM	3	Taminatal	Schaftali	753894	195299
TIT	2	Titlis	Titlisboden	674132	182107
TRU	2	Trubelboden	Trubelboden	611306	135519
TUJ	2	Tujetsch	Culmatsch	698313	171100
TUM	2	Tumpiv	Val Miez	720868	182318
URS	2	Urseren	Giltnasen	682405	160066
VAL	2	Vallascia	Vallascia	690126	155980
VDS	2	Vallee de la Sionne	Donin du Jour	594521	130015
VIN	2	Vinadi	Alpetta	828725	202232
WFJ	2	Weissfluhjoch	Versuchsfeld Weissfluhjoch	780849	189231
ZER	2	Zermatt	Triftchumme	622354	99001

Acknowledgements

First of all, I would like to express my full appreciation and thanks to my supervisor, Dr. Hendrik Wulf, for all the support and efforts he has provided throughout the project, as well as his constructive and insightful advice and guidance, full of useful information that is beyond evaluation.

Also, many thanks to Professor Dr. Livia Piermattei for her eagerness to follow up on the details of the work, in addition to her fruitful advice and guidance, which played a major role in motivating me to complete the work successfully.

And great appreciation and thanks to my Professor Dr. Amin Shaaban for following up my work and guiding me, in addition to dedicating some of his time to review my work and give me feedback, which played a fundamental role in completing my project and presenting it in its final form.

In addition, I would like to express my sincere gratitude to my family and friends who have provided and continue to provide me with all kinds of support.

Finally, Special thanks to Deniz Gök for his help in comparing some of my work results with his, which uses a similar approach with different data.

Ali Sheib

8.1.1 AI Use

During the preparation of the thesis, I used Open AI (ChatGPT) to help in generating Python code under my guidance and according to my instructions, and to help with the computational work.

Personal Declaration

I hereby declare that the submitted thesis is the result of my own, independent work. All external sources are explicitly acknowledged in the thesis.

Date
April 22, 2025

Signature
Ali Sheib